528732

Western Australian Telecommunications Research Institute
(WATRI)

EQUALISATION FOR CARRIERLESS AMPLITUDE AND PHASE MODULATION

Jason Gao

This thesis is presented for the Degree of
Doctor of Philosophy
of
Curtin University of Technology

December 2002

Declaration

This thesis contains no material which has been accepted for the award of any other degree or diploma in any university.

To the best of my knowledge and belief this thesis contains no material previously published by any other person except where due acknowledgment has been made.

Signature: .....

Date: 05/12/02

To my parents, sister and dear wife Li Xiao-Ying

ACKNOWLEDGMENTS

I would like to thank many people who have helped me in writing this thesis. Among them, first and foremost person is my supervisor Dr Yee Hong Leung to whom I am truly indebted. It is his expertise, willingness to help, enthusiasm and patience in guiding me throughout the entire course of my research that has made all this possible.

I am forever grateful to my associate supervisor Professor Antonio Cantoni who has provided me many, many invaluable suggestions on the research project which this thesis is based on. It is his advice that have ultimately shaped my thesis and transform me from an undergraduate to a researcher. I feel very privileged to be able to learn from him.

Many thanks go to these people who have offered me their expertise and experience, as well as provided me many technical discussions on issues arising from my research work. They are Professor Sven Nordholm, Dr Hans-Jürgen Zepernick and Dr Zhuquan Zang.

I would also like to thank Mrs Désirée Oorloff-De Domenico, Mrs Marilyn Green, all the other supporting staff, and my peers who have helped me in more ways than they can imagine. They have made my life at ATRI more enjoyable. At least, I am not alone in this cause. Over the past a few years, I have had some very memorable times in my life.

I would also like to thank my parents for their kindness and understanding of their son's pursuit of a dream, my sister who in her already rather busy schedule, takes over my share of duty of looking after my parents.

My very special thanks are reserved for my wife Li Xiao-Ying who is my true friend and life companion. It is her love that has been a source of constant support which I can always rely on. With her love, I know I can reach the other end of this long journey.

ABSTRACT

Carrierless amplitude and phase (CAP) modulation is generally regarded as a bandwidth efficient two-dimensional (2–D) passband line code. It is closely related to the pulse amplitude modulation (PAM) and quadrature amplitude modulation (QAM) schemes. CAP has been proposed for various digital subscriber loop (DSL) systems over unshielded twisted pairs of copper wires. In this thesis, our main focus is on the minimum mean-square error (MMSE) performance of the ideal (i.e., infinite length) linear and non-linear (decision feedback) CAP receivers/equalisers in the presence of additive, coloured Gaussian noise, and/or data-like cross-talks. An in-depth analysis is given on the performance of both receiver structures.

In the case of the *linear* receiver, one possible view of the overall CAP transceiver system which includes both data and cross-talk transmission paths is that it is a linear multiple-input multiple-output (MIMO) system. Accordingly, the existing MMSE results for a general MIMO system are applicable also to CAP systems. However, up to date, this approach was shown to be unsuccessful in the sense that the derived MMSE expressions are too complex and offer little insights. In our analysis, in order to find a more incisive MMSE expression, we reconsider the problem of minimisation of the MSEs at slicers. By exploiting the Hilbert transform pair relationship between the impulse responses of the inphase and quadrature transmit shaping filters, we are able to obtain an elegant and more meaningful MMSE expression, as well as the corresponding transfer functions of the optimum linear receive filters.

In the case of the *nonlinear*, or decision feedback equaliser (DFE), receiver, we start our analysis with the receiver structure of a generic multi-dimensional (≥ 3) CAP-type system. This receiver consists of a bank of analog receive filters, the number of which equals the dimension of the CAP line code, and a matrix of cross-connected, infinite-length, baud-spaced feedback filters. It is shown that the optimum filters and the corresponding MMSE of the DFE receiver require the factorisation of a discrete-time channel spectral matrix. This mathematically intractable step can be avoided, however, when the DFE results are specialised to a standard 2–D CAP system where we are able to again exploit the Hilbert transform pair relationship to derive a further and more useful MMSE expression.

Three sets of numerical studies are given on the MMSE performance of the CAP receivers. In the first set of studies, we model the sum of all cross-talks as an additive, Gaussian noise source and select three test transmission channels over which we compare the MMSE performance of the linear and DFE receiver structures. In the second set of studies, we compare the performance of the two receiver structures, but in a data-like cross-talk environment. The results demonstrate the importance of NEXT equalisation in the design of CAP receivers operating in a NEXT dominant environment. In the final set of studies which follows from the second set of studies, we investigate the relationship between the MMSE performance of the DFE receiver and system parameters which include excess bandwidth, data rate, CAP scheme, and relative phase between the received signal and the NEXT signal. The results show that data-like cross-talks can be effectively suppressed by using a large excess bandwidth ($\alpha > 1$ in the case of a RC transmit shaping filter) alone. The relative phase also affects the receiver performance, but to a lesser degree.

In addition to the MMSE performance analysis, implementation issues of an adaptive linear CAP receiver are also considered. We propose a novel linear receiver by appending two fixed analog filters to the front-end of the existing adaptive linear receiver using fractionally-spaced equalisers (FSE). We show that if the analog filters are matched to the transmit shaping filters, then inphase and quadrature finite-length FSEs in the proposed receiver have the same MMSE solution. We further propose a modified least-mean-square (LMS) algorithm which takes advantage of this feature. The convergence analysis of the proposed LMS algorithm is also given. We show that the modified LMS algorithm converges approximately twice as fast as the standard LMS algorithm, given the same misadjustment, or alternatively, it halves the misadjustment, given the same initial convergence rate.

TABLE OF CONTENTS

LIST OF TABLES

LIST OF FIGURES

GLOSSARY

2B1Q	Two-Binary One-Quaternary
ADSL	Asymmetric Digital Subscriber Line
ANSI	American National Standards Institute
ATM	Asynchronous Transfer Mode
BER	Bit Error Rate
CAP	Carrierless Amplitude and Phase (Modulation)
CCI	Co-Channel Interference
CDMA	Code Division Multiple Access
DFE	Decision Feedback Equaliser
DMT	Discrete Multitone
DSL	Digital Subscriber Line
FB	Feedback
FDM	Frequency Division Multiplexing
FEXT	Far-End Cross-Talk
FF	Feedforward
FIR	Finite Impulse Response
FSE	Fractionally-Spaced Equaliser
HDSL	High Speed Digital Subscriber Line
IA	Independence Assumption
ISI	Inter-Symbol Interference
ITU	International Telecommunications Union

LAN	Local Area Networks
LMS	Least Mean Square
MCM	Multi-Carrier Modulation
MF	Matched Filter
MFB	Matched Filter Bound
MIMO	Multiple-Input Multiple-Output
ML	Maximum Likelihood
MLSD	Maximum Likelihood Sequence Detector
MMSE	Minimum Mean Square Error
MSE	Mean Square Error
NEXT	Near-End Cross-Talk
NRZ	Non-Return-to-Zero
ODMA	Orthogonality Division Multiple Access
PAM	Pulse Amplitude Modulation
PR	Perfect Reconstruction
PR-4	Partial Response Type–4
PSTN	Public Switched Telephone Networks
QAM	Quadrature Amplitude Modulation
RC	Raised Cosine
RRC	Root-Raised Cosine
SCM	Single Carrier Modulation
SISO	Single-Input Single-Output
SHDSL	Single-Loop High Speed Digital Subscriber Line
UTP	Unshielded Twisted Pair
VDSL	Very High-Speed Digital Subscriber Line

CHAPTER 1
INTRODUCTION

1.1 Digital Subscriber Lines

Over the past a few decades, the explosive growth of the Internet has created a pressing need for higher throughputs in data communication networks. Apart from the efforts in pushing up the data rates of existing voiceband (analog) modems, new technologies such as fixed wireless access, broadband satellites, and coax cable modems, etc., have been considered to address this problem. Another possible solution is to use the existing installed telephone network base, but with the family of newly emerged digital subscriber line technologies known collectively as xDSL. Compared to the other solutions, xDSL is more practical and cost-effective. It has been estimated that there are 790 million copper pair loops installed around the world, and this copper infrastructure represents one of the key assets owned by various telecommunication companies. Therefore, it would be sensible to re-use them as much as possible.

The term xDSL encompasses *digital subscriber line* (DSL), *high-speed* DSL (HDSL), *asymmetric* DSL (ADSL), and *very high-speed* DSL (VDSL). Modems using xDSL technologies differ dramatically from traditional voiceband modems in terms of the bandwidth utilised, and hence transmission throughput. Typical voiceband modems are limited to frequencies ranging from 300 Hz to 3.4 kHz, whereas xDSL modems utilise channel bandwidth of up to 30 MHz. As a result, ADSL modems for instance, can operate at up to

8 Mb/s, depending on the length of the transmission cables, whereas the latest generation V.90 voiceband modem specified by the International Telecommunication Union (ITU) can reach speeds of up to 56 kbps only. In order to achieve such high data rates, there are new challenges which need to be solved by telecommunication researchers and engineers alike.

The total channel impairment of a (subscriber) loop plant includes cable power loss, cross-talks, additive noise, and some impulsive effects. In particular, cross-talks which can be categorised as *near-end cross talk* (NEXT) or *far-end cross talk* (FEXT) are often the limiting factors in the speeds of xDSL modems. However, this is not the case for voiceband modems, because below the maximum 3.4 kHz, cross-talk channel loss is relatively high and hence presents no real threat to symbol detections. For frequency bands where xDSL modems operate, the research for suitable techniques to minimise the interference of cross-talks is central to the design of cross-talk resistant xDSL modems.

In relation to line codes, besides the traditional bandwidth efficient line codes such as *quadrature amplitude modulation* (QAM) and *pulse amplitude modulation* (PAM), various other line codes have been proposed for xDSL. Notably among them are *discrete multitone* (DMT) modulation, a multi-carrier line code that has been adopted by the ADSL ANSI standard [1], and carrierless amplitude and phase (CAP) modulation, a single carrier line code. DMT uses a frequency-division multiplexing (FDM) scheme, where the total transmission channel is divided into many parallel independent subchannels over which data are transmitted. The basic idea of the subchannel transmission is to take advantage of the fact that individual subchannels can be approximated by an ideal channel such that no equalisation is required. In contrast, the 'standard' 2–D CAP[1] may be considered to be a special form of QAM, but

[1]For the rest of the thesis, we simply refer to the standard 2–D CAP as CAP

without an explicit carrier. It uses two parallel transmit shaping filters whose impulse responses form a *Hilbert transform* pair. The outputs of these filters are combined, before entering the transmission channel. The comparison between CAP and DMT can be quite involved and is the subject of much hot debate [2, 3]. However, both line codes have been adopted in practical xDSL systems around the world. For the rest of this thesis, we concentrate only on CAP and the performance of CAP receivers based on equalisation techniques. Information on DMT or general *multi-carrier modulation* (MCM) methods can be found in [4, 5].

With the Mbits/s data rates which xDSL technologies have brought to us, a new world of communication services becomes a close reality. Among them, we can have remote access to *local area network* (LAN), fast access to the Internet and multimedia databases, home shopping through the Internet, broadcast TV and video on demand. All these services can be made available to us through simple telephone wires. Indeed, these new technologies have the potential to significantly improve our access to information, hence our lives.

1.2 Overview of CAP Line Code

CAP has its origin from AT&T Bell Labs. In the mid-1970s, researchers and engineers there started to experiment with CAP transceiver systems. The word 'CAP' was coined by Falconer [6] in one of his internal memorandum at around the same time. CAP is generally known to be a bandwidth efficient 2–D passband line code and is closely related to QAM and PAM. It has been shown that, without coding, all the bandwidth efficient transmission schemes provide essentially the same theoretical performance in the presence of white Gaussian noise or (stationary) self-NEXT[2], provided their design parameters

[2]defined as the NEXT with the same spectrum as the data signal

are properly optimised [7]. However, similar theoretical performance does not necessarily translate into similar implementation complexity or similar performance in the presence of other types of noise. One of the key aspects in favour of CAP is that CAP systems are generally considered to have the best possible overall performance with the smallest amount of complexity for both coded and uncoded transceiver implementations.

Until the recent development of xDSL technologies, CAP was relatively unknown to the general engineering and research communities. A two-part tutorial on CAP is given in [8, 9]. In the first tutorial, general aspects of CAP such as theory of operation, its bandwidth efficiency, and the digital implementation of a CAP transmitter are explained. In the second tutorial, the author discusses some of the design parameters which influence the performance of CAP systems. The emphasis of the tutorials is on high-speed LAN applications using *unshielded twisted pair* (UTP) wiring. Other general information on CAP, such as receiver structures with decision feedback equalisers (DFE) can be found in [10].

The CAP line code has been proposed for various xDSL systems. The 16-CAP scheme was adopted by the Technical Committee of the *Asynchronous Transfer Mode* (ATM) LAN Forum for transmission of 51.48 Mb/s data rate over 100 m of UTP-3 copper wires [11]. Further discussions on this standard are given in [12]. In [13], the authors described in detail a technique called *NEXT equalisation* which uses a zero-forcing equaliser. However, the technique is only effective for data rates up to 100 Mb/s, for the given channel environment stated in the paper. For rates higher than 100 Mb/s, *NEXT cancellation* is generally required.

More recently, in [14], a *single carrier modulation* (SCM) technology which integrates both QAM and CAP line codes has been proposed for the upcoming VDSL systems. The authors gave an overview on VDSL technology and the main issues of VDSL system design. A dual mode CAP/QAM blind receiver, as well as a summary of the laboratory tests and field trials are also presented. Detailed discussions on the dual-mode receiver are given in [15] where several blind equalisation algorithms to start-up the receiver are compared.

The close relationship between CAP and QAM is discussed in [10] which showed that the CAP transceiver structure can be derived from the QAM structure. Despite this close relationship, the eye opening of CAP signals has been shown to be much smaller than that of the corresponding QAM signals. Hence, CAP is more sensitive to symbol timing errors [16]. The authors of [16] then re-examined some CAP receiver structures that have been proposed in the literature and showed that a modified QAM receiver can offer a significant advantage over the other receiver structures through its greater immunity to timing phase errors.

The discussions thus far pertains only to the 'standard' 2–D CAP line code, in which the impulse responses of the in-phase and quadrature transmit shaping filters form a Hilbert transform pair. It should be pointed out that this relationship is not necessary, and 2–D transceiver systems with other combinations of pulse shapes are also possible as shown in [8]. This leads to the concept of a generic CAP transceiver structure whose design imposes no constraints on the transmit pulse shaping filters. Further, if we expand the dimension of the generic 2–D CAP line code to 3 or higher, the question then arises – can

we find a new set of impulse responses suitable for the multi-dimensional system? This question is addressed in [17] and further refined in [18]. Basically, two approaches of expanding a 2–D CAP line code are shown. In the first approach, a 3–D system is designed so that the new overall transfer matrix maintains the *perfect reconstruction* (PR) of the transmitted information. The impulse responses of the shaping filters are found by solving a minimax optimisation problem using the *sequential quadratic programming* algorithm [19]. In the second approach which is referred to as *orthogonality division multiple access* (ODMA), the overall symbol rate for 2–D CAP is maintained in the multi-dimensional system and the same optimisation method is used to obtain dimensions higher than 3. This second approach, according to the author can be categorised as a sub-group of the well known *code division multiple access* (CDMA). The difference between the CDMA and ODMA is that CDMA code (words) are generated by a pseudo-random generator, while ODMA codes are generated by solving an optimisation problem. The second difference is that in CDMA, the cross correlation between different users is reciprocal to the number of users due to the characteristics of the wireless channel while ODMA can support only a small number of multiple-access users without sacrificing bandwidth efficiency.

1.3 Summary of Contributions

Our research work addresses the issues of performance bounds of CAP receivers using linear and DFE equalisers for data transmissions over unshielded copper wire pairs. More specifically, the contributions of this thesis are as follows

- The optimum linear CAP receiver and the corresponding MMSE in

the presence of either stationary or data-like cross-talks, and additive coloured Gaussian noise, have been derived.

- The optimum DFE CAP receiver and the corresponding MMSE in the presence of either stationary or data-like cross-talks and additive coloured Gaussian noise, have been derived .

- Finally, a novel adaptive linear CAP receiver was proposed and analysed. The new receiver leads to a modified least-mean square (LMS) algorithm which is shown to approximately doubles the performance of the standard LMS algorithm in terms of the initial convergence rate and misadjustment.

1.4 List of Publications

J. Gao, Y. H. Leung, "A New Adaptive Equaliser for Carrierless Amplitude and Phase (CAP) Receivers," in *Proc. 1999 IEEE International Symposium on Circuits and Systems*, vol. 3, pp. 90-93, Orlando, FL, May 1999.

J. Gao, Y. H. Leung and A. Cantoni, "Minimum Mean Square Error Receive Filters for Carrierless Amplitude and Phase Modulation," in *Proc. 2000 IEEE International Symposium on Circuits and Systems*, vol. 4, pp. 629-632, Geneva, Swizerland, May 2000.

J. Gao, Y. H. Leung, "Minimum Mean-Square Performance Analysis and Calculations for Carrierless AM/PM Receiver Using Decision Feedback Equalisers in Presence of Data-Like Cross-talk Signals," submitted to *IEEE Transactions on Communications.*

J. Gao, Y. H. Leung, "Minimum Mean-Square Performance Analysis and Calculations for Carrierless AM/PM Receiver Using Decision Feedback

Equalisers in Presence of Data-Like Cross-talk Signals," in *Proc. of International Conference on Communications*, vol. 1, pp. 69-73, New York City, NY, April-May 2002.

1.5 Thesis Outline

Chapter 2 gives an introduction to 2–D CAP line code and discusses its bandwidth efficiency in terms of multilevel encoding and spectral shaping. Using an ideal channel, we demonstrate how a CAP receiver separates the inphase and quadrature symbol streams. Receiver structures based on equalisation techniques are also introduced.

Chapter 3 covers channel models applicable to the cables commonly found in xDSL systems, the power spectra of the transmitted and received signals, and the power spectra of the received interference and noise. The SNR requirement is defined in relation to the system BER. For completeness, the matched filter bound (MFB) and channel capacity are also briefly discussed in this chapter.

Chapter 4 describes in detail the minimum mean-square error (MMSE) performance of optimum linear CAP receivers operating in the presence of either stationary or data-like cross-talks and background noise. First, we consider CAP systems in the presence of data-like cross-talks. We show that although it is possible to specialise the existing MMSE expression for a general multiple-input multiple-output (MIMO) system to the linear CAP receiver, the derived results appear to be rather cumbersome and do not give any insight. Next, in order to find an alternative expression, we reconsider the problem of minimising the MSE at the slicer. By exploiting the Hilbert transform pair relationship between the impulse responses of the inphase and quadrature transmit shaping filters, we obtain a new MMSE expression which offers better

understanding on the equalisation of data-like cross-talks.

Chapter 5 focuses on the MMSE performance of an ideal DFE receiver under the same channel environment. Instead of the standard 2–D line code, we start with a generic multi-dimensional CAP transceiver with data-like cross-talks. The optimum solution of the DFEs and the corresponding MMSE are next derived. These results are then applied to the standard 2–D CAP system. Again, the MMSE results for the case of stationary cross-talks are also included.

Chapter 6 provides three sets of numerical studies, based on the derived MMSE expressions for the optimum linear and DFE CAP receivers. In the first and second sets of the studies, we compare the MMSE performance of the linear and DFE CAP receivers operating in either stationary or data-like cross-talk, and Gaussian noise environment. In the last set of studies, using the DFE CAP receiver as an example, we further investigate the relationship between the MMSE performance and various system parameters in the presence of one data-like NEXT.

Chapter 7 deals with the implementation of an adaptive CAP receiver using fractionally-spaced equalisers (FSE). Based on an existing structure for linear CAP receivers, a novel CAP receiver is proposed. Further, we propose a modified LMS algorithm for the new receiver structure. Theoretical analysis on its convergence is then given. Finally, we compare the modified LMS algorithm against the standard LMS algorithm in terms of their initial convergence rates and misadjustments.

Chapter 8 summarises all the work presented in the thesis. Also included are discussions on issues which arise from this research work. From these discussions, we offer our suggestions for further research in the area of CAP

transceiver systems.

CHAPTER 2
2–D CAP TRANSCEIVER SYSTEM

In this chapter, we summarise the discussions on 2–D CAP line code given in [8]. We start with a review of the bandwidth efficiency of some well-known PAM line codes, and consider two common methods to improve bandwidth efficiency, i.e., through *multilevel encoding* and *spectral shaping*. We then discuss the CAP transceiver system and explain its principles of operation. Finally, we introduce two CAP receiver structures, one using linear equaliser and the other using DFE equaliser. The MMSE performance analysis of these receivers are the main topic of discussion of the later chapters.

2.1 Bandwidth Efficiency of PAM Lines Codes

The *bandwidth efficiency* of a line code [8] is defined as

$$\nu \triangleq \frac{\text{bit rate in bit/s (bps)}}{\text{bandwidth in Hz}}$$

We are interested in bandwidth efficiency for the simple reason that many systems are designed to transmit at high data rates within a relatively small bandwidth. For a given limited resource in terms of system bandwidth, bandwidth efficient line codes are selected to meet the ever increasing demand on system data rates. Two main factors that limit bandwidth efficiency are *inter-symbol interference* (ISI) and channel noise. It is well known, e.g., [20] that for ISI-free signalling, the maximum symbol rate of a line code is equal to twice the baseband channel bandwidth. This rate is called the *Nyquist rate* or *Nyquist signalling frequency*. For a voice band modem with a bandwidth of about 3.4

kHz, a binary line code which transmits one bit per symbol would mean a maximum data rate of 6.8 kbps. Clearly, this data rate is unsatisfactory for many applications to which we are accustomed nowadays. In the following, we demonstrate via examples methods of improving bandwidth efficiency which then lead to the bandwidth efficient CAP line code.

2.1.1 NRZ Line Code

At first, we consider the so-called *bipolar non-return-to-zero* (NRZ) line code. Conceptually, the transmitter of a NRZ line code can be considered to consist of a cascade of an encoder followed by a shaping filter[1] shown in Fig. 2.1. The encoder maps the incoming bits 0 and 1 into impulses or *symbols* equal to $+1$ and -1, respectively. This kind of encoder is called a *binary encoder*. The symbols generated by the encoder are fed to a shaping filter which has a rectangular-shaped impulse response with duration T, shown on the left of Fig. 2.2a. In the case considered here, the pulse width T equals the time interval between successive symbols. This time interval is called the *symbol period* and its inverse $1/T$ is called the *symbol rate*, expressed in bauds. For the NRZ line code, the symbol rate is also equal to the bit rate, i.e., $1/T = R$. An example of a NRZ signal waveform is shown in Fig. 2.3a.

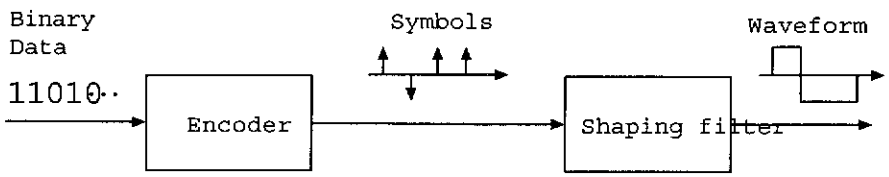

Figure 2.1: Transmitter model for the NRZ line code

[1]This concept also applies to the other line codes discussed here.

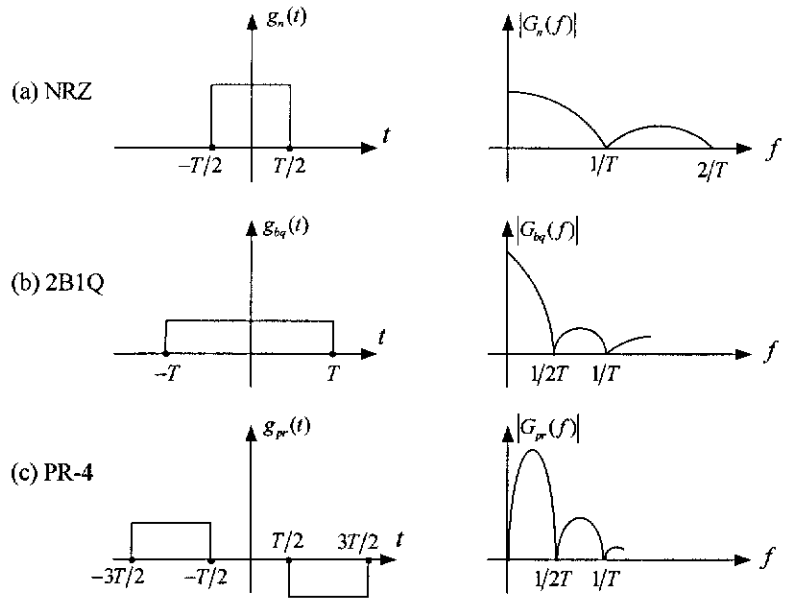

Figure 2.2: Shaping filters for (a) NRZ, (b) 2B1Q, (c) PR–4

Let $G_n(f)$ denote the transfer function of the shaping filter. The magnitude of $G_n(f)$ is also shown in Fig. 2.2a. If we assume that the bits to be transmitted are randomised, then the time-averaged power spectrum of the signal generated by a NRZ transmitter will also have the same shape as the square of the magnitude of $G_n(f)$. Note that this spectrum has nonzero frequency components around DC. For this reason, NRZ line code is called a baseband line code. The transfer function has its first null at $1/T$ Hz as shown. It is generally assumed that the frequency components above this first null can be neglected for this type of signalling pulse shape, so that the *effective bandwidth* denoted by W of the NRZ line code is $W = 1/T$. Since R bps are transmitted in the bandwidth of W Hz, we conclude that the bandwidth efficiency of the NRZ line code equals $R/W = 1$ bps/Hz.

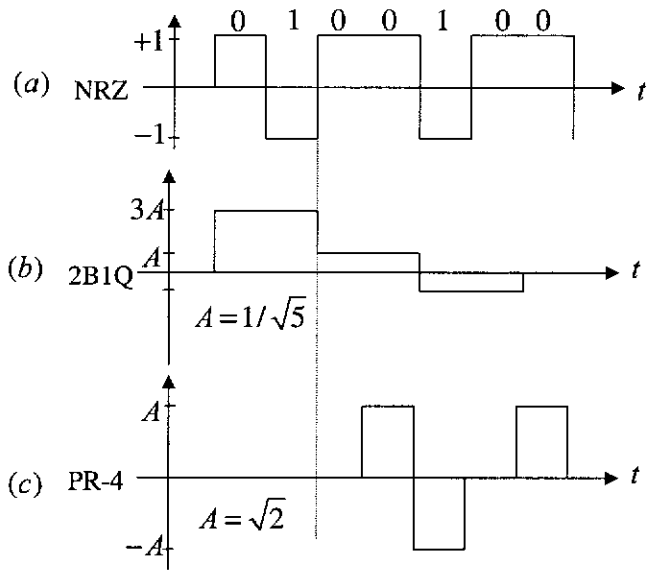

Figure 2.3: Example of signal waveform for (a) NRZ, (b) 2B1Q, (c) PR–4

2.1.2 2B1Q Line Code

We next consider another line code called *two-binary one-quaternary* (2B1Q). An example of a 2B1Q signal waveform is shown in Fig. 2.3b. In terms of the transmitter model of Fig. 2.1, a 2B1Q encoder encodes pairs of successive binary bits into one of four possible symbol values ± 1, ± 3. As a result, for the same input bit rate R, the 2B1Q line code has a symbol rate, denoted by $1/T_{bq}$, that is half the symbol rate used in the NRZ line code, i.e., $1/T_{bq} = R/2 = 1/2T$.

The shaping filter in the 2B1Q transmitter model has an impulse response and corresponding transfer function shown Fig. 2.2b. The impulse response has the same shape as the NRZ pulse, but twice the duration, due to the 50% reduction in symbol rate. As a result, in the frequency domain, the transfer function has its first null at $\frac{1}{2T}$ Hz which is the half of that used by the NRZ line code under the same data rate. Therefore, the bandwidth efficiency of

2B1Q line code is equal to 2 bps/Hz.

Thus, we see that by doubling the number of the symbol levels at the encoder, the 2B1Q line code achieves twice the bandwidth efficiency of the NRZ line code.

2.1.3 PR–4 Line Code

An alternative way of achieving better bandwidth efficiency than the NRZ line code is demonstrated by a line code called *partial response class–4* (PR–4). The block diagram of a binary PR–4 transmitter is shown in Fig. 2.4. The binary bits are first fed to a standard NRZ transmitter. The PR–4 signal is then obtained by subtracting a delayed version of the NRZ signal from the present NRZ signal. The duration of the introduced delay is equal to two symbol periods ($2T$). An example of a PR–4 signal waveform is shown in Fig. 2.3c.

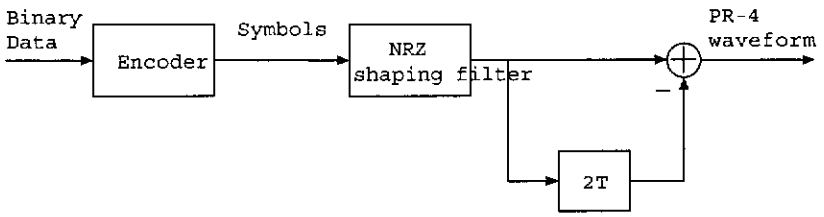

Figure 2.4: Transmitter model for PR–4 line code

The transmitter model in Fig. 2.1 can also be applied to this line code. In this case, the binary encoder is the same as that used for NRZ, where the symbol rate is equal to the bit rate, i.e., $1/T = R$. But, the shaping filter has a different impulse response and its transfer function shown in Fig. 2.2c, due to the additional delay path. The transfer function now has its first null at DC. Since there is no spectrum component at DC, we say that PR–4 line code

is a passband line code. The second null at $\frac{1}{2T}$ Hz gives an effective bandwidth of $\frac{1}{2T}$ Hz. Therefore, the bandwidth efficiency in this case is 2 bps/Hz which is the same as that of 2B1Q.

In this example, we see that instead of using a multiple level encoder to improve spectral efficiency, shaping filters with reduced effective bandwidth can also be used. Apart from reducing bandwidth, passband shaping filter has another highly attractive feature. It avoids the problem of DC coupling associated with line codes such as the NRZ [20].

2.1.4 Comparison of Bandwidth Efficiency

From the above examples, we have shown two independent techniques to improve the bandwidth efficiency of a line code, namely, by multilevel encoding and spectral shaping. Let I_{en} and I_{sh} denote the improvement factor due to multi-level encoding and spectral shaping, respectively[2]. Then the bandwidth efficiency ν of a line code may be expressed as

$$\nu \triangleq \frac{R}{W} = I_{en} \cdot I_{sh} \tag{2.1}$$

Table. 2.1 compares the bandwidth efficiencies for the 3 line codes discussed previously. We also include the 16-CAP scheme, which will be discussed in later sections.

2.2 The 2–D CAP Line Code

Fig. 2.5 shows a *generic* 2–D CAP transceiver system. A brief overview of the operation of CAP transceiver system is as follows. The incoming binary data are mapped into two multilevel pulses or symbol streams $\{a_k\}$ and $\{b_k\}$ by the encoder. Each of the two symbol streams then passes through a separate

[2] I_{en} and I_{sh} will be formally defined later in this chapter

Table 2.1: Comparison of bandwidth efficiency

Transceiver Characteristic			Improvement factor		
line code	data rate	bandwidth utilisation	multilevel encoding	spectral shaping	bandwidth efficiency
–	(Mb/s)	(MHz)	(I_{en})	(I_{sh})	($\frac{R}{W} = I_{en}I_{sh}$)
NRZ	100	100	1.0	1.0	1.0
2B1Q	100	50	2.0	1	2
PR-4	100	50	1.0	2.0	2
16-CAP	100	30	2	1.67	3.34

passband shaping (or transmit) filter. The shaping filters are chosen in such a way that their impulse responses are orthogonal to each other (more on the filters later). For this reason, the filters are called *inphase* (I) and *quadrature* (Q) filters, respectively. The corresponding output signals, which are now called the I and Q signals, are summed before being transmitted.

At the receiver side, the reverse process takes place. The received signal first passes through a pair of receive filters. Given an ideal AWGN channel, the optimum receive filters are the filters that are matched to the transmit filters, respectively. The baud rate samplers before the slicers separate I and Q signals. The estimated symbols $\{\hat{a}_k\}$ and $\{\hat{b}_k\}$ from the slicers are then decoded to recover the transmitted binary data.

In the following, we provide further details on the design of each of the main blocks shown in Fig. 2.5. The improvement factors due to multilevel encoding and spectral shaping are also included.

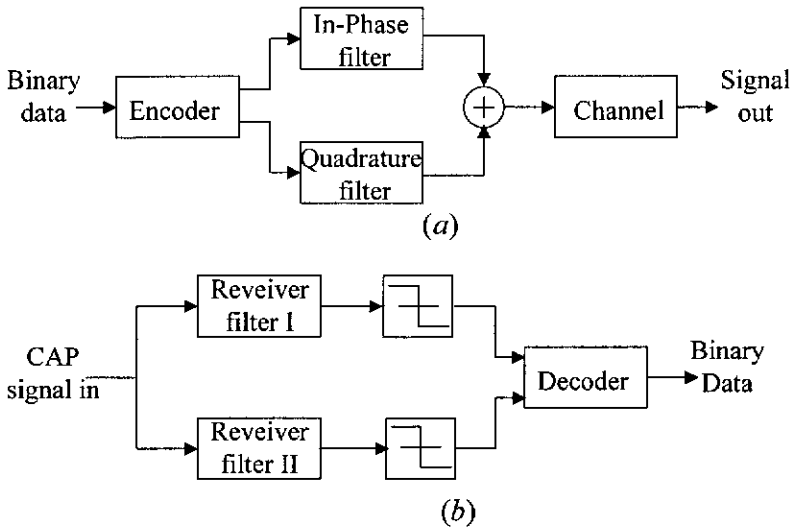

Figure 2.5: Generic 2–D CAP transceiver system (a) transmitter (b) receiver

2.2.1 Multilevel Encoding

One-dimensional mapping

An example of 1–D mapping is shown by the 2B1Q line code where two binary bits are mapped into one of four levels. In general, a block of b binary bits requires $p = 2^b$ different symbol levels. The line code generated is called p-PAM line code.

Analog and digital mapping

Thus far, no assumptions have been made on the nature of the output symbols provided by the mapping function of the encoder. For example, the numbers ± 1, ± 3 could represent voltage levels, in which case the mapping is *analog*. Alternatively, these numbers could be binary numbers in a digital signal processing environment, in which case the mapping is *digital*. Further, since most errors at the receiver are likely to occur between adjacent symbols, *Gray coding* can be also used in the mapping such that each symbol error will

usually translate into only one bit error.

Independent 2–D mapping

An example of independent 2–D mapping is the 16-CAP scheme shown in Fig. 2.6. In this case, blocks of four bits are encoded into two independent symbol streams. The first two bits in each block are mapped into the symbol a_k while the remaining two bits are mapped into the symbol b_k. Thus, the 2–D encoder generates symbol streams $\{a_k\}$ and $\{b_k\}$ each with four different levels ± 1, ± 3. Therefore, the total number of points in the signal constellation is 16. In general, m-CAP scheme has m number of constellation points, regardless of the mapping method used.

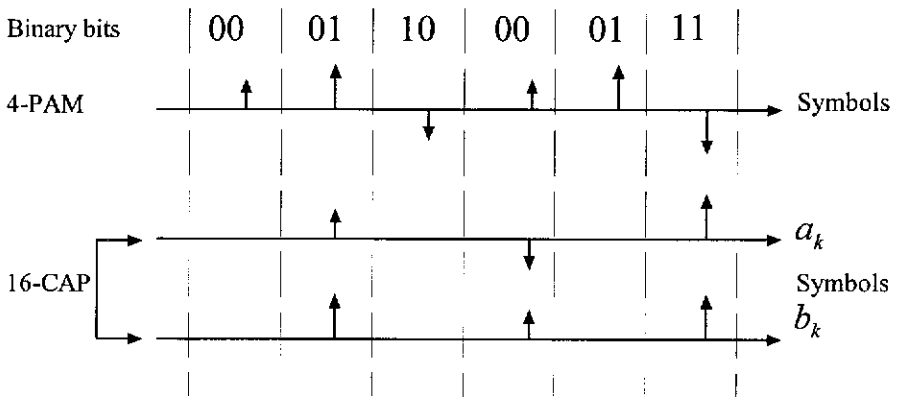

Figure 2.6: Independent 2–D mapping

True 2–D mapping

Fig. 2.7 shows an example of true 2–D mapping where a block of four bits are mapped into a 16-point signal constellation. In this case, the first two bits in the block are used to define the quadrant and the remaining two bits are used to define one of four possible points in each quadrant. The advantage of true

2–D mapping becomes apparent when it is used to map a block of odd number of bits into a pair of 2–D symbols. It can be easily verified for example, that independent mapping cannot be used to provide a straight forward mapping of a block of five bits in the case of the 32-CAP scheme.

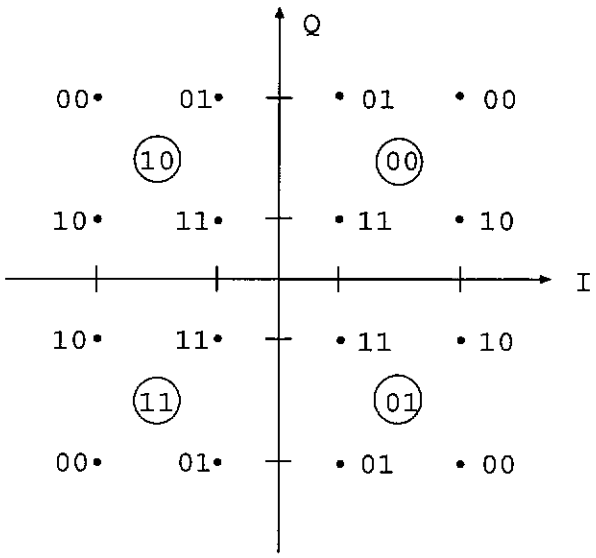

Figure 2.7: 16–CAP signal constellation with true 2–D mapping

Encoding improvement factor

The formal definition of the improvement factor I_{en} due to multilevel encoding is now given. The reference point for 1–D and 2–D line codes is 2–PAM and 4–CAP line codes, respectively. Both reference line codes transmit one bit in each symbol. Multilevel encoding reduces the bandwidth requirements with respect to these two line codes because of the reduction in symbol rate. The reduction is equal to the number of bits in each symbol. For instance, if a block of m_1 bits are mapped into a one-dimensional symbol for a PAM line code, then the symbol rate is reduced by a factor m_1 with respect to the 2–PAM line code. Likewise, if a block of m_2 bits is mapped into a pair of two-dimensional

symbols for a 2–D CAP line code, then the symbol rate is reduced by a factor of $m_2/2$ with respect to 4–CAP. Since m_1 and m_2 are also the ratios between the bit rate R and the symbol rates $1/T_1$ and $1/T_2$, the improvement factor (I_{en}) due to multilevel encoding may be defined by

$$I_{en} \triangleq m_1 = \frac{R}{1/T_1} \qquad \text{for 1–D line code} \tag{2.2a}$$

$$I_{en} \triangleq \frac{m_2}{2} = \frac{R}{2/T_2} \qquad \text{for 2–D line code} \tag{2.2b}$$

2.2.2 Spectral Shaping

Nyquist pulse

Apart from multilevel encoding, it is also possible to improve bandwidth efficiency by using better shaping filters. Typical impulse responses that are suitable for baseband and passband shaping filters are from the well-known *raised-cosine* (RC) family [20].

Fig. 2.8 shows the impulse responses of some baseband RC filters. The impulse responses of the filters have value one at the origin ($t = 0$) and zero at the time instants $t = \pm 1T,\ \pm 2T, \cdots$ where T is the symbol period of the input symbol sequence. Thus, when the symbol sequence is transmitted, there is no ISI at the epoch points $t = kT$ where k is an arbitrary integer. We call this type of pulse a *Nyquist pulse*.

Excess bandwidth

For a baseband PAM line code, assuming the same symbol sequence is being transmitted, the minimum theoretical bandwidth that a RC filter can assume is equal to half the symbol rate, i.e., $B_{min} = 1/2T$. Such a filter is in general difficult to implement and the system is sensitive to sampling jitter, due to the abrupt slope at $1/2T$ Hz. Consider now a baseband Nyquist

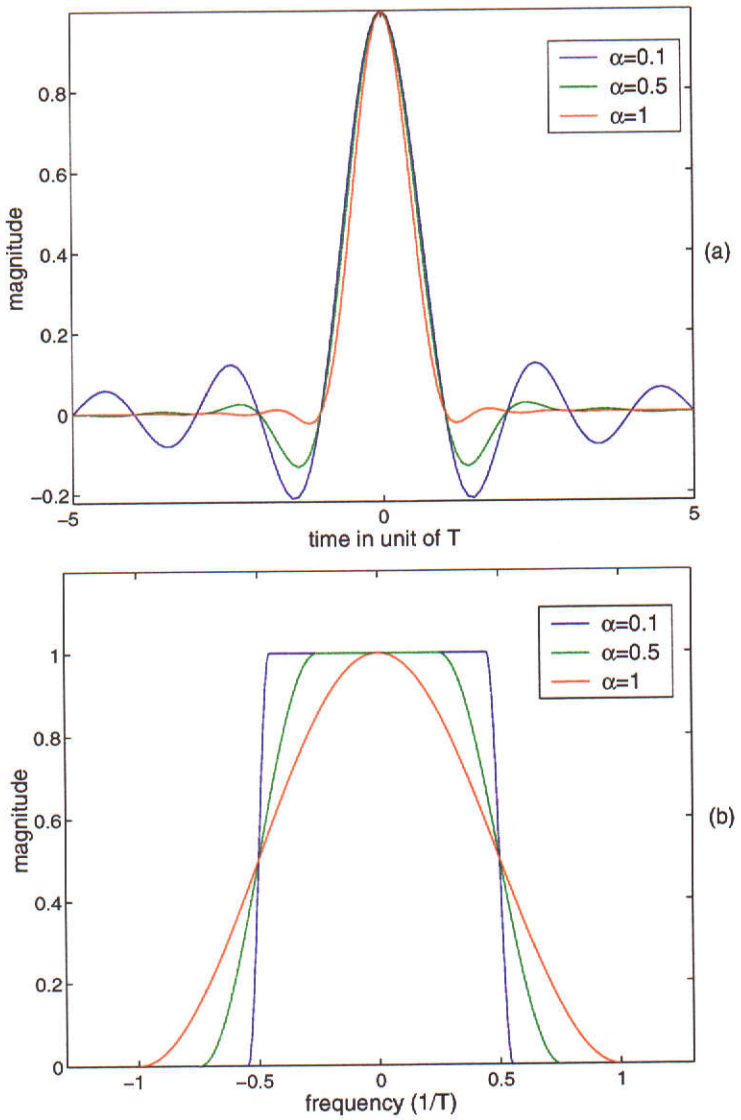

Figure 2.8: Baseband RC filters with roll-off factor $\alpha = 0.1, 0.5$, and 1, (a) impulse response, (b) transfer function

shaping filter with bandwidth $B \geq 1/2T$. The quantity $B - 1/2T$ is called the *excess bandwidth* and is usually expressed as a percentage (α) of the theoretical minimum $1/2T$. That is

$$B - \frac{1}{2T} = \alpha \cdot \frac{1}{2T} \quad \Rightarrow \quad \alpha = \frac{B - 1/2T}{1/2T} \tag{2.3}$$

for baseband shaping filter. The transfer functions of the RC filters in the previous example are also shown in Fig. 2.8.

The concept of excess bandwidth, defined in the baseband, can be extended to passband Nyquist pulses which have no DC component. Details on the design of a class of passband pulses is given in the next subsection. It can be shown that the minimum theoretical bandwidth of a passband pulse, is equal to the symbol rate $1/T$. Thus, for a passband shaping filter with bandwidth also denoted by $B \geq 1/T$, the excess bandwidth α is given by

$$B - \frac{1}{T} = \alpha \cdot \frac{1}{T} \quad \Rightarrow \quad \alpha = \frac{B - 1/T}{1/T}. \tag{2.4}$$

We now give the impulse response and transfer function of a RC filter. For $\alpha \leq 1$, the impulse response is given by

$$g_{rc}(t) \triangleq \frac{\sin(\pi t/T)}{\pi t/T} \frac{\cos \alpha \pi t/T}{1 - (2\alpha t/T)^2} \tag{2.5}$$

and its transfer function is defined by

$$G_{rc}(f) \triangleq \begin{cases} T, & \\ & 0 \leq |f| \leq \frac{1}{2T}(1-\alpha) \\ \frac{T}{2}\left[1 - \sin\left(\frac{\pi T}{\alpha}|f| - \frac{1}{2T}\right)\right], & \\ & \frac{1}{2T}(1-\alpha) \leq |f| \leq \frac{1}{2T}(1+\alpha) \end{cases} \tag{2.6}$$

It is also possible to have $\alpha \geq 1$. It is shown in later chapters that these RC filters are effective in suppressing data-like crosstalk. In this case ($\alpha \geq 1$), the transfer function is given by

$$G_{rc}(f) \triangleq \begin{cases} \frac{T}{2}\left[-\sin\left(\frac{\pi T}{\alpha}(f - \frac{1}{2T})\right) + \sin\left(\frac{\pi T}{\alpha}(f + \frac{1}{2T})\right)\right], & \\ & 0 \leq |f| \leq \frac{1}{2T}(\alpha - 1) \\ \frac{T}{2}\left[1 - \sin\left(\frac{\pi T}{\alpha}(|f| - \frac{1}{2T})\right)\right], & \\ & \frac{1}{2T}(\alpha-1) \leq |f| \leq \frac{1}{2T}(1+\alpha) \end{cases} \tag{2.7}$$

In communication systems, in order to suppress channel noise, the Nyquist pulse (RC pulse shape) used for signaling is split evenly between the transmit and receive shaping filters [21]. The resulting pulse shape is called *root-raised-cosine* (RRC) filter. Its transfer function is given by $G_{rrc}(f) = \sqrt{G_{rc}(f)}$ and impulse response is defined by

$$g_{rrc}(t) \triangleq \frac{\sin[\pi(1-\alpha)\,t'] + 4\alpha t' \cos[\pi(1+\alpha)\,t']}{\pi t'\,[1-(4\alpha t')^2]} \tag{2.8}$$

where $t' \triangleq t/T$.

Spectral shaping improvement factor

We now provide the formal definition of improvement factor due to spectral shaping I_{sh}. For both the baseband and passband cases, the point of reference is the shaping filter using 100% excess bandwidth. For the reference baseband filter, the filter bandwidth is equal to the symbol rate $1/T$. The improvement factor for a baseband line code using a bandwidth B is defined as $1/T \div B$. Similarly, for the reference passband filter, the filter bandwidth is equal to twice the symbol rate, i.e., $2/T$. The improvement factor for a passband line code using a bandwidth B is thus defined as $2/T \div B$. Using (2.3) and (2.4), the improvement factor (I_{sh}) due to shaping filters can be written as

$$I_{sh} \triangleq \frac{1/T}{B} = \frac{2}{1+\alpha}, \qquad \text{for baseband} \tag{2.9a}$$

$$I_{sh} \triangleq \frac{2/T}{B} = \frac{2}{1+\alpha}, \qquad \text{for passband} \tag{2.9b}$$

Notice that for both baseband and passband line codes, the improvement factors are identical and dependent only on α and they are upper bounded by 2 (at the smallest excess bandwidth $\alpha = 0$).

2.2.3 Inphase and Quadrature Shaping Filters

Design of shaping filters

We now show via an example how to design inphase and quadrature shaping filters, which have a passband characteristic. For this example, the symbol rate is $1/T = 25$ Mbauds, the excess bandwidth is 20% ($\alpha = 0.2$) and the maximum system frequency is 30 MHz. The first step is to design a pair of baseband RC filters using the same given parameters.

Let $g_0(t)$ be the impulse response of a baseband RRC. Its bandwidth, denoted by B_b is given by

$$B_b = \frac{(1+\alpha)}{2T} = 15 \quad \text{MHz} \tag{2.10}$$

Next, we choose a *centre frequency* $f_c \geq 15$ MHz such that the baseband filters are shifted into the desired passband, i.e., $f_a \leq f \leq 30$ MHz, where f_a is some positive frequency point. Suppose $f_c = 15$ MHz. The resulting passband shaping filters are then given by

$$g_t(t) \triangleq \sqrt{2}\, g_0(t) \cdot \cos(2\pi f_c t) \qquad \tilde{g}_t(t) \triangleq \sqrt{2}\, g_0(t) \cdot \sin(2\pi f_c t) \tag{2.11}$$

where $g_t(t)$ and $\tilde{g}_t(t)$ denote the impulse responses of the I and Q transmit shaping filters, respectively. The constant $\sqrt{2}$ is included such that the energies of the passband pulses are kept the same as those of the baseband pulses. Notice that $g_t(t)$ is an even function of f while $\tilde{g}_t(t)$ is an odd function of f.

Hilbert transform pair

For independent symbol streams a_k and b_k, optimal joint detection of $\{a_k, b_k\}$ become optimal detection of $\{a_k\}$ and $\{b_k\}$, provided the corresponding signal waveforms are orthogonal to each other at decision point. In the CAP system, the orthogonal is achieved by way of *Hilbert transform pair*.

Let $G_t(f)$ and $\tilde{G}_t(f)$ denote the transfer functions of the I and Q shaping filters, respectively. It can be shown that

$$\tilde{G}_t(f) = (-j)\,\mathrm{sgn}(f)G_t(f) \tag{2.12}$$

where $\mathrm{sgn}(\cdot)$ is the *signum* function [22]. Thus, $g_t(t)$ and $\tilde{g}_t(t)$ form a *Hilbert (transform) pair*. From (2.12), it can be shown that they are orthogonal to each other, i.e.,

$$\int_{-\infty}^{\infty} g_t(t) \cdot \tilde{g}_t(t)\,dt = 0 \tag{2.13}$$

Another interesting property of pulses that form a Hilbert pair is that the Hilbert-pair relationship still holds when the two pulses pass through the same linear channel. Let $h(t)$ be the impulse response of a transmission channel. Then, $g_t(t) \otimes h(t)$ and $\tilde{g}_t(t) \otimes h(t)$ where '$\otimes$' denotes convolution, are also Hilbert transform pair. This is easily shown in the frequency domain. From this property, we are assured that at the output of any linear channel the orthogonality of the signalling pulses is maintained.

2.2.4 Why CAP Line Code Works

To simplify the discussion, we assume the transmission channel is an ideal AWGN channel, i.e., $h(t) = \delta(t)$. The transmit shaping filters have impulse responses of $g_t(t)$ and $\tilde{g}_t(t)$, respectively.

Suppose the receive filter pair shown in Fig. 2.5b have impulse responses $g_r(t)$ and $\tilde{g}_r(t)$ and they are matched to the transmit filter pair. That is

$$g_r(t) = g_t(-t) \quad \text{and} \quad \tilde{g}_r(t) = \tilde{g}_t(-t) \tag{2.14}$$

Note that if $g_t(t)$ is strictly causal, then $g_t(-t)$ is strictly anti-causal. In a practical system, implementation of this type of filters requires appropriate

truncation and delay such that the resulting filter becomes strictly causal.

Let $w_{in}(t)$ denote the signal at the output of inphase receive filter. At the sampling time $t_s = kT$ where k is some integer, the sampled output is given by

$$w_{in}(kT) = \sum_l a_l p(kT - lT) + \sum_l b_l \tilde{p}(kT - lT) \tag{2.15}$$

where channel noise is ignored for the purpose of this discussion, the equivalent channels $p(t)$ and $\tilde{p}(t)$ are defined by

$$p(t) \triangleq g_t(t) \otimes g_t(-t) \quad \text{and} \quad \tilde{p}(t) \triangleq \tilde{g}_t(t) \otimes g_t(-t)$$

It can be shown that

$$p(t) = g_{rc}(t)\cos(2\pi f_c t) \quad \text{and} \quad \tilde{p}(t) = g_{rc}(t)\sin(2\pi f_c t) \tag{2.16}$$

where $g_{rc}(t)$ is a baseband RC filter whereupon it can be verified that $p(kT) = 0$ and $\tilde{p}(kT) = 0$ for any k, except when $k = 0$, $p(0T) = 1$. Therefore, we have

$$w_{in}(kT) = a_k \tag{2.17}$$

Similarly, it can be shown that without noise and at the sampling time $t_s = kT$, the sampled output of the quadrature receive filter is

$$w_{qd}(kT) = b_k. \tag{2.18}$$

From the above discussion, we see that due to the orthogonality relationship (2.13) between the signalling pulses $g_t(t)$ and $\tilde{g}_t(t)$, at $t_s = kT$ the sampled outputs of the matched filter pair have no interference from the other dimension. Hence, a 2–D CAP system may be thought as two passband PAM subsystems in parallel. The optimality of the receive filters for a CAP receiver can be deduced from that of a PAM subsystem. That is given that

the transmission channel is an ideal AWGN channel, the matched filter pair $g_t(-t)$ and $\tilde{g}_t(-t)$ are optimal, since they maximise the SNR at the slicer. The next question is then 'What are the optimal receive filters, given a non-ideal transmission channel ?' More importantly, we would like to know what is the achievable performance for the optimal receive filters. Answers to these questions are provided in the later chapters of this thesis.

2.3 CAP Receiver Structure

2.3.1 Optimum Receiver

Using the argument of equivalent parallel PAM subsystems, we showed that for an ideal AWGN channel, the optimum CAP receiver is a pair of filters matched to the transmit and receive filters. In the presence of channel ISI, it is well known, e.g., [5][20], that the *maximum-likelihood sequence detector* (MLSD) is the optimum receiver for detecting a sequence of data symbol. The front-end structure of a MLSD generally consists of a matched filter and a symbol rate sampler which is then followed by a whitening filter, provided such a filter exists. The combination of this structure, known as whitened matched filter (WMF), ensures a *canonical* equivalent channel which is monic, causal, and minimum-phase.

The computation load for such a detector is exponential in time (the length of the transmitted sequence). Although this problem can be dealt with by a dynamic programming algorithm known as the *Viterbi algorithm* (VA) [23], the resulting receiver is still quite complex. Suppose a M-QAM scheme is used and the canonical channel is modelled by a finite impulse response (FIR) filter of order ν, then an M^{ν}-state VA will be required. It can be seen that if M and/or ν is moderately large, then the VA is generally considered to be too

complex to implement.

2.3.2 Equalisation Based Receiver

In many cases, the performance of a suboptimal receiver based on the equalisation techniques with symbol-by-symbol detection is comparable to that of a sequence detector, but with a much reduced complexity. The two commonly known equalisation structures are the linear equaliser (LE) and the DFE. In contrast to the MLSD, they have much simpler complexity. Perhaps, more importantly, it has been shown [24, 25, 26] that it is not necessary to use the optimal MLSE structure to approach the channel capacity. In particular, [27] shows that the signal-to-noise ratio $\mathrm{SNR}_{\mathrm{MMSE\text{-}DFE}}$ of a MMSE-DFE with an unbiased decision rule is a *single* parameter that can be used to characterise an arbitrary linear Gaussian channel for coding purposes at any SNR, as long as the performance of an ideal (no error propagation e.g., Tomlinson-Harashima precoder) MMSE-DFE can be obtained. One of the key findings is that while the MLSE is in principle the optimum receiver technique, the MMSE-DFE in combination with powerful channel coding is also able to achieve near channel capacity. This result subsumes the previous result [24] where ZF-DFE is used on the assumption of sufficiently high SNR.

Linear CAP Receiver

Fig. 2.9a shows a CAP receiver structure which can be found in most of the open literature. The main feature of this receiver is the use of two parallel FSEs. Such a filter structure was first proposed for an all digital QAM receiver [28]. For non-ideal transmission channels, the FSE pair perform the combined function of matched filtering and channel equalisation. The transfer

function of the optimal FSEs and the corresponding MMSE are given in Chapter 4, in the presence of either stationary or data-like cross-talks. Further, we propose an alternative linear CAP receiver shown in Fig. 2.9b. It is shown in Chapter 7 that both receivers offer the same MMSE performance for ideal (infinite-length) FSEs. The important feature of the new structure is that the finite-length I and Q FSEs have the same MMSE solution. Because of this feature, it becomes possible to implement the standard LMS algorithm in a different way. The new algorithm is called the *modified LMS algorithm*. Analysis on its convergence shows that it approximately doubles the performance of the standard LMS algorithm [29].

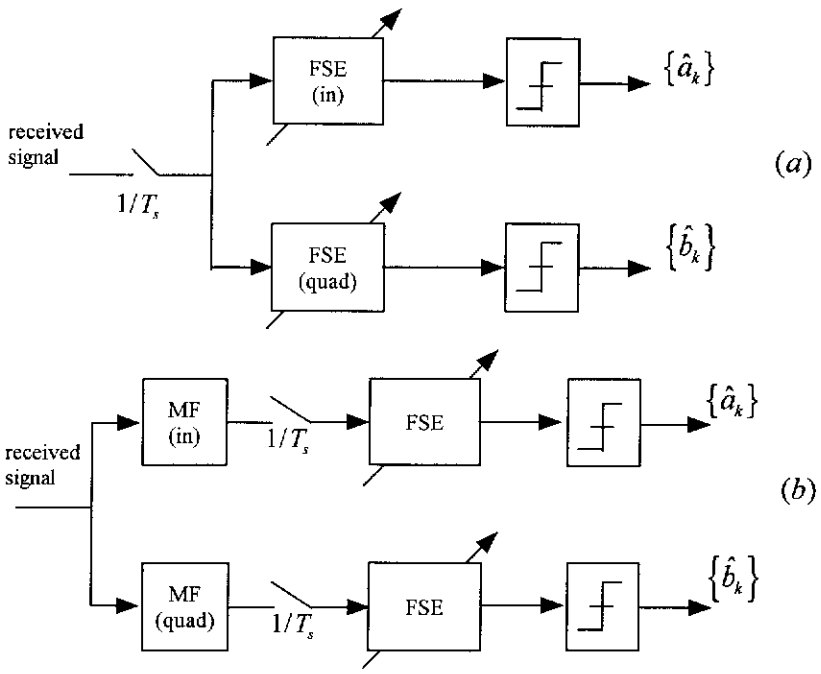

Figure 2.9: (a) Standard CAP receiver, (b) Proposed CAP receiver

DFE CAP Receiver

A number of CAP receivers with DFEs have been proposed in [10]. In this thesis, we focus on the performance of the receivers with the so-called *conventional DFE* structure [30]. This receiver structure is shown in Fig. 2.10, where the feedforward filter pair consists of two parallel FSEs, and the feedback filters consist of four cross-connected baud-rate equalisers.

The transfer functions of the optimal feedforward and feedback filters and the corresponding MMSE are derived in Chapter 5, under the same channel conditions as those considered in the analysis of the linear CAP receiver. Performance comparisons between the receivers in Fig. 2.9 and Fig. 2.10 are given in Chapter 6. Further, in the same chapter, we investigate the relationship between the performance of a DFE CAP receiver and system design parameters, such as CAP scheme, data rate, and excess bandwidth. Numerical results show that under certain situations, it is also viable to have a feedback structure with only two feedback filters, i.e., without the cross-connected feedback filters [31, 32].

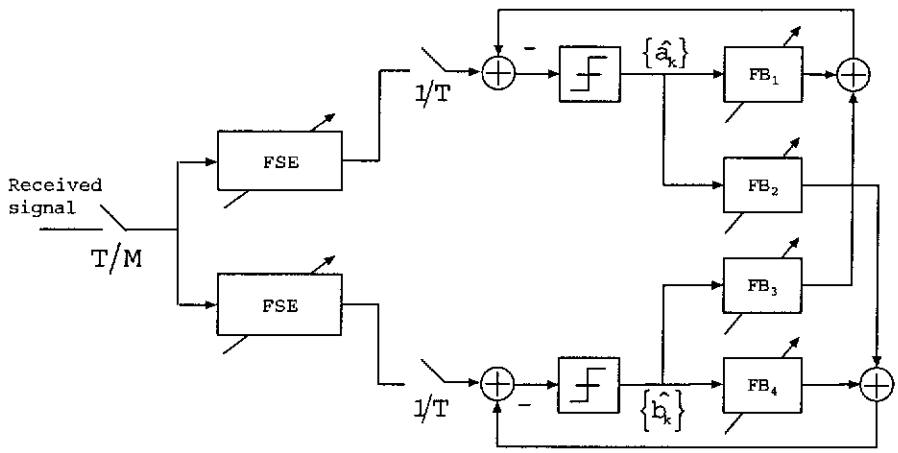

Figure 2.10: CAP receiver with conventional DFE structure

CHAPTER 3
CHANNEL ENVIRONMENT

3.1 Channel Modelling

Channel models for twisted-pair copper wires play an important role in the engineering of xDSL systems, and have been studied extensively in the open literature, e.g., [4, 33, 34]. In general, two types of channel models have been proposed, the *simplified* model and the *two-port network* model. In the following, we give a brief introduction to these two models. More information on the channel models for copper wire cables can be found in the references cited. The loss model for the cross-talk channel between adjacent wire pairs is also considered.

3.1.1 Simplified Channel Model

Simplified channel model is suitable for copper wire-pairs with a single wire gauge and perfect termination at both ends. According to [34], the transfer function for a copper wire-pair of length d is given by

$$H(d, f) = e^{-d\gamma(f)} = e^{-d\,\alpha(f)} e^{-j\,d\,\beta(f)} \tag{3.1}$$

where the *propagation constant* $\gamma(f)$ is defined by

$$\gamma(f) \triangleq \alpha(f) + j\,\beta(f)$$

and where $\alpha(f)$ and $\beta(f)$ are the real and imaginary parts of the propagation constant, respectively. From (3.1), the *channel attenuation* or *loss* in units of

dB may be written as

$$L_p(d,f) = -20\log|H(d,f)| = 8.686\, d\, \alpha(f) \tag{3.2}$$

For AWG#22, #24 and #26 wire pairs, which are found in most *public switched telephone network* (PSTN) systems, at frequencies $f \geq 250$ kHz[1], the transfer function of (3.1) may be approximated by

$$H(d,f) \approx e^{-d\,(k_1\sqrt{f}+k_2 f)} e^{-j\,(d\,k_3 f)} \tag{3.3}$$

where k_1, k_2 and k_3 are constants which are related to the type of copper wire pairs used, and are independent of cable length and frequency. Table 3.1 shows these constants for the wire pairs, assuming the cable length d is in units of mile and f in units of Hertz. Note the phase characteristic in (3.3) is linear.

Table 3.1: Constants for the simplified channel model

Gauge	k_1 (10^{-3})	k_2 (10^{-8})	k_3 (10^{-5})
AWG#22	3.0	0.035	4.865
AWG#24	3.8	-0.551	4.883
AWG#26	4.8	-1.709	4.907

By absorbing the constant 8.686 into $\alpha(f)$ in (3.2) and using the approximation in (3.3), the channel loss may also be written as

$$L_p(d,f) \approx d\,(a'\sqrt{f} + b' f) \tag{3.4}$$

For the wire pairs used in ATM LAN applications [12], the above approximation also holds. The corresponding constants a' and b' in (3.4) are specified

[1]This value is a conservative estimate and 150 kHz is quoted in [34]

by the TIA/EIA standard [11] and reproduced in Table 3.2.

Table 3.2: TIA/EIA-568 worst-case propagation loss at 20°C

Cable	L_p(dB/100m)	change/1°C	range(MHz)
UTP 3	$2.32\sqrt{f} + 0.238f + 0.00/\sqrt{f}$	1.2%	$0.772 \leq f \leq 16$
UTP 4	$2.05\sqrt{f} + 0.043f + 0.057/\sqrt{f}$	0.3%	$0.772 \leq f \leq 20$
UTP 5	$1.97\sqrt{f} + 0.023f + 0.05/\sqrt{f}$	0.3%	$0.772 \leq f \leq 100$

3.1.2 Two-port Network Model

As discussed, the channel transfer function of (3.1) applies only to channels constructed using a single wire gauge and with perfect terminations at both ends. A typical subscriber loop plant, however, will usually consist of many sections of different gauges and *bridge taps* which are un-used cables in shunt-connection with a subscriber loop, and is terminated with a resistive impedance. Consequently, the channel transfer function is not a simple product of the respective transfer functions given by (3.1). To accurately represent channels with mixed wire gauges and/or bridge taps, the concept of two-port network with $ABCD$ parameter representation are normally used.

Two-port network

A stand alone two-port network is shown in Fig. 3.1a. Let v_1 (i_1) and v_2 (i_2) denote the input and output voltages (currents), respectively. The input-and-output relationship of the network may be written as

$$\begin{bmatrix} v_1 \\ i_1 \end{bmatrix} = \begin{bmatrix} A & B \\ C & D \end{bmatrix} \begin{bmatrix} v_2 \\ i_2 \end{bmatrix} \tag{3.5}$$

where the network parameters $ABCD$ are defined by

$$A \triangleq \left.\frac{v_1}{v_2}\right|_{i_2=0} \qquad B \triangleq \left.\frac{v_1}{i_2}\right|_{v_2=0}$$

$$C \triangleq \left.\frac{i_1}{v_2}\right|_{i_2=0} \qquad D \triangleq \left.\frac{i_1}{i_2}\right|_{v_2=0}$$

The matrix which consists of these parameters is termed the *transfer matrix*. Some simple examples of transfer matrices are also shown in Fig. 3.1.

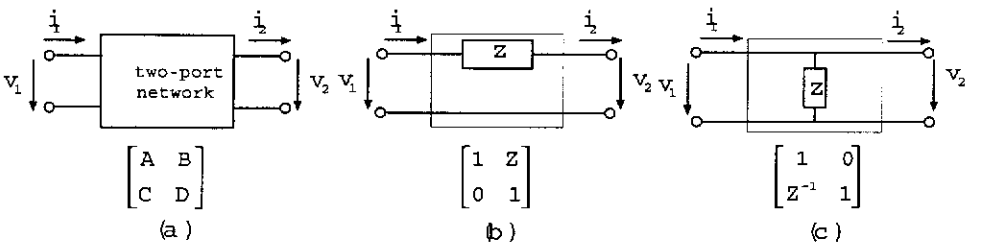

Figure 3.1: Two-port model (a) general form, (b) series impedance, (c) shunt impedance

In general, transfer matrices for two-port networks are complex and frequency dependent. Using (3.1), it can be shown [34] that the $ABCD$ parameters of a transfer matrix are given by

$$A(f) = D(f) = \cosh(d\,\gamma(f)) \tag{3.6a}$$

$$B(f) = Z_o(f)\sinh(d\,\gamma(f)) \tag{3.6b}$$

$$C(f) = \sinh(d\,\gamma(f))/Z_o(f) \tag{3.6c}$$

where $Z_o(f)$ is the *characteristic impedance* and is related to the transmission line distributed parameters $R(f)$, $L(f)$, $G(f)$ and $C(f)$ of the wire pair by

$$Z_o(f) \triangleq \sqrt{\frac{R + j2\pi fL}{C + j2\pi fC}}$$

Two-port networks in series and parallel

We now apply the theory of the stand-alone two-port networks developed so far to two networks connected in series or parallel. The aim is to find the $ABCD$ parameters of the equivalent network representing the two connected networks. For arbitrary number of such networks connected in series or parallel, the equivalent network parameters can be similarly derived. The importance of this development is that multi-gauge wire-pairs with/without bridge taps can be modelled as two or more two-port networks in series.

Fig. 3.2 shows some examples of two two-port networks in series and parallel. For the series connection, using (3.5), we may write input and output voltage and current relationship as

$$\begin{bmatrix} v_1 \\ i_1 \end{bmatrix} = \begin{bmatrix} A_1 & B_1 \\ C_1 & D_1 \end{bmatrix} \begin{bmatrix} A_2 & B_2 \\ C_2 & D_2 \end{bmatrix} \begin{bmatrix} v_3 \\ i_3 \end{bmatrix} \tag{3.7}$$

in which we simply substitute the output voltage and current of the first two-port network with the transfer matrix and output voltage and current of the second two-port network. The equivalent transfer matrix of the two series-connected two-port networks is then defined by

$$\begin{bmatrix} A_{eq} & B_{eq} \\ C_{eq} & D_{eq} \end{bmatrix} \triangleq \begin{bmatrix} A_1 & B_1 \\ C_1 & D_1 \end{bmatrix} \begin{bmatrix} A_2 & B_2 \\ C_2 & D_2 \end{bmatrix} \tag{3.8}$$

In contrast, the equivalent transfer matrix for two two-port networks connected in parallel is not as compact. Again, using (3.5), and the following equations

$$I_{eq,1} = I_1' + I_1'' \qquad \text{and} \qquad I_{eq,2} = I_2' + I_2'' \tag{3.9}$$

where $I_{eq,1}$ and $I_{eq,2}$ denote the input and output currents of the equivalent transfer matrix, respectively. It can be shown [33] that the equivalent transfer

matrix can be written as

$$\begin{bmatrix} A_{eq} & B_{eq} \\ C_{eq} & D_{eq} \end{bmatrix} \triangleq \frac{1}{B_1 + B_2} \begin{bmatrix} A_1B_2 + B_1A_2 & B_1B_2 \\ T_{21} & B_1D_2 + D_1B_2 \end{bmatrix} \tag{3.10}$$

where the term $T_{21} \triangleq (B_1 - B_1)(C_1 + C_2) - (A_1 - A_2)(D_1 - D_2)$

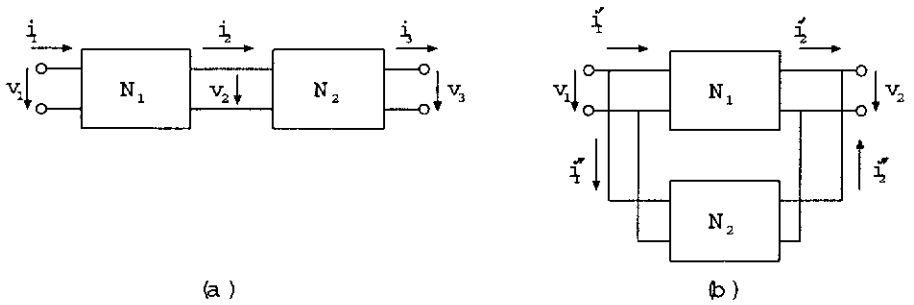

Figure 3.2: Two two-port networks (a) in series, (b) in parallel

3.1.3 Cross-Talk Models

One of the main characteristics of data transmission using unshielded copper wire pairs is the existence of cross-talks from adjacent pairs of copper wires. In many situations, they are the key limiting factors of the data throughput of the communication system. Depending on the relative location of the source of the disturbing signal with respect to the receiver, the cross-talk signals can be classified as being *near-end cross-talk* (NEXT) or *far-end cross-talk* (FEXT) as shown in Fig. 3.3a.

In system analysis, we model the total interference from cross-talks as being either a stationary Gaussian noise or a *data-like* signal. These two models represent two extreme situations that cross-talks may exhibit in a practical system. Which model to chose depends on the actual applications. In some applications such as HDSL systems [35], there is a large number of wire pairs in

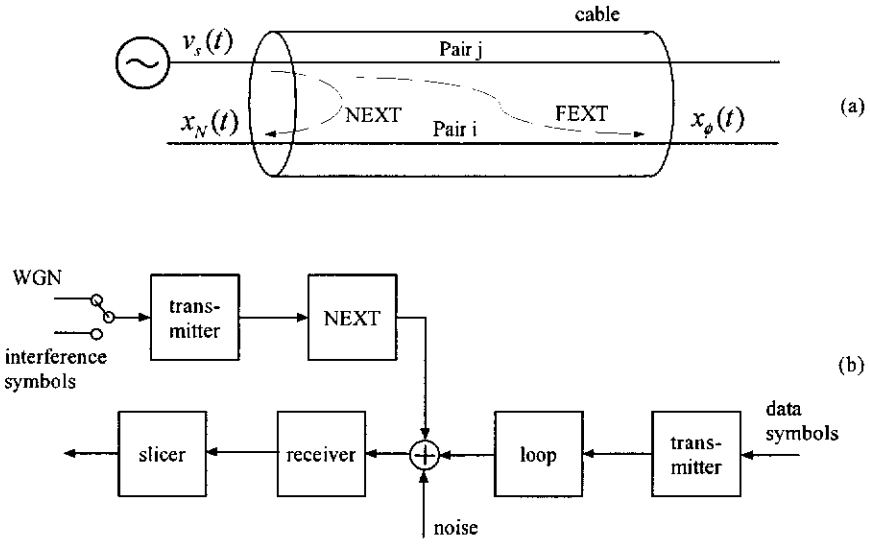

Figure 3.3: (a) NEXT and FEXT generation in a cable (b) simulation system model with NEXT

close proximity to the wire pair under consideration, and the total interference from these adjacent wire pairs may be best described by the stationary model through application of the *central limit* theorem.

In other applications such as ATM LAN using a UTP-3 wire pair [36], the number of adjacent wire pairs is much less and the total interference is generally dominated by the interference from one wire pair. In this case, the data-like model for the total interference is more appropriate.

Fig. 3.3b shows the simulation block diagram with NEXT. When the switch shown is connected to the noise source, the resulting cross-talk is stationary. On the other hand, when the switch is connected to the interference symbols, the resulting cross-talk is data-like.

Cross-talk channel losses are typically measured. From these measurements, the loss models of the cross-talk channels are generated. In ATM LAN applications, NEXT is in general far more damaging than FEXT [10]. For the

rest of this thesis, we deal only with NEXT channels.

Let $X(f)$ be the transfer function of a NEXT channel. Then, the worst-case pair-to-pair NEXT loss model can be approximated by

$$|X(f)|^2 = \chi f^{\frac{3}{2}} \quad \Leftrightarrow \quad L_x(f) \triangleq -10\log_{10}|X(f)|^2 = K_x - 15\log_{10} f \quad (3.11)$$

where for a given UTP cable, χ and K_x are some constants specified by the TIA/EIA standard [11], and are reproduced in Table 3.3.

Table 3.3: TIA/EIA-568 worst-case pair-to-pair NEXT loss

TIA/EIA Cable	Coupling coefficient χ	Pair-to-Pair NEXT loss L_x	Frequency range (MHz)
UTP 3	7.39×10^{-5}	$43 - 15\log f$	$0.772 \leq f \leq 16$
UTP 4	2.34×10^{-6}	$58 - 15\log f$	$0.772 \leq f \leq 20$
UTP 5	5.87×10^{-7}	$64 - 15\log f$	$0.772 \leq f \leq 100$

3.2 Signal-to-Noise/Interference Ratio

In Chapters 2, we showed that a CAP system may be thought as consisting of two passband PAM subsystems in parallel. In general, transmitted PAM signals are cyclostationary [37]. In other words, their autocorrelation functions are periodic in time, with period equalling the symbol duration. To avoid the complexity due to this periodicity, the received power (or spectrum) of a CAP signal is often averaged[2] over its symbol period T.

[2]With respect to the power spectrum of CAP signals, we always assume that the averaging process is implied

3.2.1 Signal Spectrum

The output power of a CAP transmitter is defined by

$$\bar{P}_t \triangleq \frac{1}{T}\int_0^T E[s_t^2(t)]\,\mathrm{d}t = \int_{-B}^{B} \frac{2\sigma^2}{T}|G_t(f)|^2\,df \tag{3.12}$$

where $s_t(t)$ is the transmitted CAP signal, B is the passband bandwidth[3] , and $G_t(f)$ is the transfer function of the inphase shaping filter. The integrand on the right of (3.12) may be thought as the *power spectrum* of the transmitted signal, i.e.,

$$\mathrm{PSD}_t(f) \triangleq \frac{2\sigma^2}{T}|G_t(f)|^2 \quad \rightarrow \quad \mathrm{PSD}_s(f) \triangleq \mathrm{PSD}_t(f)\cdot|H(f)|^2$$

where $H(f)$ is the transfer function of the transmission channel, and $\mathrm{PSD}_s(f)$ is the power spectrum of the received signal. The received signal power is given by

$$\bar{P}_s \triangleq \int_{-B}^{B} \mathrm{PSD}_s(f)\,df$$

3.2.2 Signal-to-Noise Ratio

The SNR at the input of a CAP receiver may be described by the received (average) SNR and the *spot* SNR which is SNR evaluated at a given frequency point. Let $S_n(f)$ denote the power spectrum of the channel noise. The spot SNR is the defined by

$$\mathrm{SNR}_n(f) \triangleq \frac{\mathrm{PSD}_s(f)}{S_n(f)} \tag{3.13}$$

and the received SNR is defined by

$$\overline{\mathrm{SNR}}_n \triangleq \frac{\bar{P}_s}{\bar{P}_n} = \frac{\int_{-B}^{B}\mathrm{PSD}_s(f)\,df}{\int_{-B}^{B}S_n(f)\,df} \tag{3.14}$$

[3]We assume that the lower band edge is at DC for convenience

Note, $\bar{P}_n$ is the total noise power within the system bandwidth only. In the case of white noise whose spectrum is a constant denoted by N_0, then the average SNR is given by

$$\overline{\mathrm{SNR}}_n = \frac{\bar{P}_s}{2BN_0} \tag{3.15}$$

3.2.3 Signal-to-Interference Ratio

When NEXT is present at the input of a CAP receiver, its power spectrum and received (average) power are defined by

$$\mathrm{PSD}_x(f) \triangleq \mathrm{PSD}_t(f) \cdot |X(f)|^2 \quad \rightarrow \quad \bar{P}_x \triangleq \int_{-B}^{B} \mathrm{PSD}_x(f)\, df$$

Analogous to channel noise, the spot signal-to-interference ratio is defined by

$$\mathrm{SIR}(f) \triangleq \frac{\mathrm{PSD}_s(f)}{\mathrm{PSD}_x(f)} = \frac{|H(f)|^2}{|X(f)|^2} \tag{3.16}$$

and the average signal-to-interference ratio is defined by

$$\overline{\mathrm{SIR}} \triangleq \frac{\bar{P}_s}{\bar{P}_x} = \frac{\int_{-B}^{B} \mathrm{PSD}_s(f)\, df}{\int_{-B}^{B} \mathrm{PSD}_x(f)\, df} \tag{3.17}$$

Note that $\mathrm{SIR}(f)$ is independent of the power spectrum of the transmitted signal $\mathrm{PSD}_t(f)$.

3.2.4 Matched Filter Bound

The concept of *matched filter bound* (MFB) is based on the idea that under certain assumptions on the channel [5], no receiver can have a lower error probability than the matched filter receiver for a one-term signal sequence.

Firstly, we consider a 1–D PAM system over an additive Gaussian noise channel. Suppose only one pulse is transmitted such that there is no ISI, and the design of the optimum receive filter is to maximise the SNR at the slicer.

This is called *isolated pulse* case. The resulting optimum filter is a *matched filter* and the maximum SNR is defined as the *matched filter bound* (MFB).

Consider next the standard 2–D CAP system. Under the same channel condition we design each receive filter as if it is a 1–D PAM system, i.e., the other dimension is ignored. Again, one pulse is transmitted in each dimension such that there is no ISI. Using the Hilbert transform pair relationship and assuming perfect symbol synchronisation, it can be easily shown that there is no *co-channel interference* (CCI) at the outputs of the matched filters and at the optimum sampling time. Let $p(t)$ and $\tilde{p}(t)$ denote the I and Q equivalent channels, respectively, and their Fourier transforms be given by $P(f) \triangleq \mathcal{F}[p(t)]$ and $\tilde{P}(f) \triangleq \mathcal{F}[\tilde{p}(t)]$. The optimum receive filters which maximise the SNR at the slicers, are then the matched filters given by

$$G_{mf}(f) = K_m \frac{P^*(f)}{S_n(f)} \quad \text{and} \quad \tilde{G}_{mf}(f) = K_m \frac{\tilde{P}^*(f)}{S_n(f)} \tag{3.18}$$

where $G_{mf}(f)$ and $\tilde{G}_{mf}(f)$ are the inphase and quadrature matched filters, respectively, and K_m is an arbitrary non-zero constant. The SNR at the optimum sampling instant is given by

$$\text{SNR}_{o,mf} = \sigma^2 \int_{-B}^{B} \frac{|P(f)|^2}{S_n(f)} df \tag{3.19}$$

In the case of white channel noise, i.e., $S_n(f) = N_0$ where N_0 is some positive constant, the matched filter pair may be written as

$$G_{mf}(f) = P^*(f) \quad \text{and} \quad \tilde{G}_{mf}(f) = \tilde{P}^*(f) \tag{3.20}$$

From (3.19), the SNR at the slicer is given by

$$\text{SNR}_{o,mf} = \frac{\sigma^2 \sigma_p^2}{N_0} \tag{3.21}$$

where σ_p^2 is defined by

$$\sigma_p^2 \triangleq \int_{-B}^{B} |P(f)|^2 \, df$$

3.3 System BER

Due to channel impairments, received signal samples before the slicer form a 'cloud' (of points) centered around certain points on a *Cartesian* plot. They are called *constellation* points. Assuming the sum of interference and background noise is white and Gaussian, a basic slicer first measures the *Euclidean* distance between the point which corresponds to the received signal sample and all the constellation points. It then determines the transmitted symbol from the constellation point which has the least distance to the point specified by the received signal sample. It can be shown, e.g., in [5], that the *minimum distance* receiver design is optimum in the *maximum likelihood* (ML) sense. Further, the BER can be estimated from the well-known *complementary distribution function*, denoted by $Q(x)$ which for a zero-mean Gaussian random variable X with variance $\sigma_x^2 = 1$,

$$Q(x) \triangleq \frac{1}{\sqrt{2\pi}} \int_x^{\infty} e^{-\alpha^2/2} \mathrm{d}\alpha$$

3.3.1 Signal Constellations

In Chapter 2, we gave a brief introduction on the constellation of the 16-CAP scheme. In general, for a m–CAP scheme, the number of bits-per-symbol is determined by $b = \log_2 m$. For example, for the 4–, 8–, 16–, and 32–CAP schemes, the number of bits-per-symbol is 2, 3, 4, and 5, respectively. The type of constellations used for even b is called the *QAM constellation*, and for

odd b, the *cross constellation.* Examples of a QAM and a cross constellation are shown in Fig. 3.4.

Let the constellation points used by CAP have levels $\pm 1d$, $\pm 3d$, $\cdots$, where d is some constant that normalises the symbol variance of the CAP scheme. It can be readily shown that the symbol variance σ^2 is given by

$$\sigma^2 = \frac{d^2(m-1)}{3} \qquad \text{for even } b \tag{3.22a}$$

$$\sigma^2 = \frac{d^2}{3}\left(\frac{31}{32}m - 1\right) \qquad \text{for odd } b \tag{3.22b}$$

Thus, by choosing d as shown in Fig. 3.4, the symbol variances of both constellations equals 1.

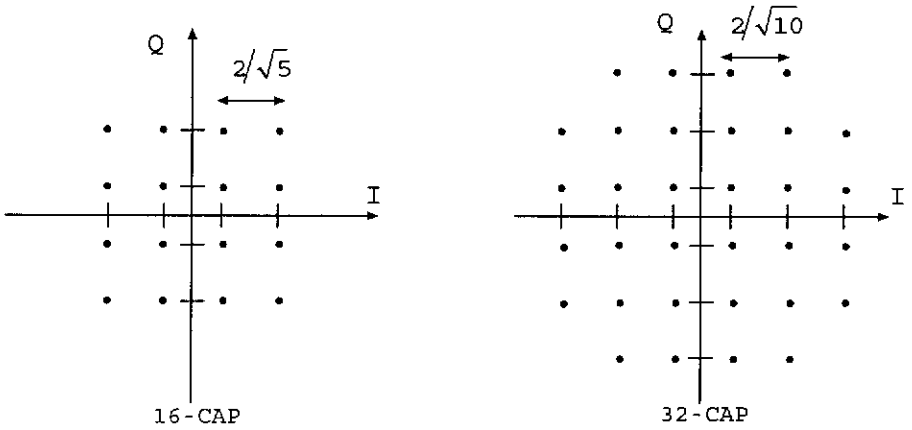

Figure 3.4: Normalised 2–D constellations for (a) 16–CAP, (b) 32–CAP

3.3.2 SNR Requirements

Assuming the total distortion at the slicer has a Gaussian amplitude distribution, then the *bit-error rate* (BER) of both the QAM and cross constellations are upper-bounded by[4] (e.g., [4]).

$$P_e \leq 4(1-\frac{1}{\sqrt{m}})Q\Big(\sqrt{\frac{3\cdot \mathrm{SNR}_{o,ref}}{m-1}}\Big), \quad \text{for even } b \tag{3.23a}$$

$$P_e \leq 4(1-\frac{1}{\sqrt{2m}})Q\Big(\sqrt{\frac{3\cdot \mathrm{SNR}_{o,ref}}{\frac{31}{32}m-1}}\Big), \quad \text{for odd } b \tag{3.23b}$$

Since $Q(x)$ is a decreasing function of x, $\mathrm{SNR}_{o,ref}$ may be thought of as being the minimum required SNR at the slicer. In ATM LAN applications [11], the specified BER is $P_e = 10^{-10}$. Using (3.23), the corresponding minimum required SNR for different CAP schemes are calculated and the results in units of dB are shown in Table. 3.4.

Table 3.4: Minimum required SNR (in dB) for a BER of $P_e = 10^{-10}$

m-CAP	4	8	16	32	64	128
b	2	3	4	5	6	7
$\mathrm{SNR}_{o,ref}$	16.21	19.82	23.29	26.33	29.55	34.47

3.4 Channel Capacity

Finally, for completeness, we briefly discuss the Shannon channel capacity and the maximum data rate for an uncoded CAP system given fixed BER.

[4]it appears that exact versions of these equations have recently been published [38].

3.4.1 Shannon Channel Capacity

The fundamental theorem governing the maximum capacity of a channel is given by the famous Shannon-Hartley law [39]. Without going into details, the theorem is based on the fact that as the number of signal levels increases at the same average signal power, the slicing levels get closer together until they become comparable with the AWGN fluctuations. For an ideal AWGN channel with bandwidth B, the maximum capacity (bps) of the channel is given by

$$C = B \log_2(1 + \text{SNR}) \tag{3.24}$$

where SNR is in units of Watt-to-Watt. Note (3.24) applies to both baseband and passband systems for the same transmitted power constraint, because that the baseband channel may be viewed as the passband channel for the specific carrier frequency $f_c = \frac{B}{2}$. The maximum attainable bandwidth efficiency is then given by

$$\nu_c = \log_2(1 + \text{SNR}) \tag{3.25}$$

3.4.2 Maximum Data Rate

The channel capacity in (3.24) serves as the ultimate bound on the rate of reliable information transmission over bandlimited AWGN channels. Often in practice, we would like to know the maximum data rate of an uncoded CAP system[5], for a given channel and required BER. The relationship was completely addressed in [27] as an optimisation problem where for some target BER, system bit rate is maximised over some class of transmission schemes

[5]the discussions shown here are equally applicable to passband PAM/QAM systems

which combine coding, shaping and equalisation. One of the key concepts proposed in the optimisation is the 'SNR gap', or SNR_{norm}, which was originally proposed by Price [24] for ZF-DFE. In the following, assuming ideal bandlimited AWGN channel, a simple, alternative expression for the maximum data rate of an uncoded system is derived.

For a given QAM or cross constellation, the BER of a CAP system may be expressed as [5]

$$P_e = K_c \cdot Q\left(\frac{D_{min}}{2\sigma_n}\right) \tag{3.26}$$

where K_c is the average number of the nearest neighbouring points in the constellation at the minimum distance D_{min} between pairs of constellation points, and σ_n^2 is the noise variance at the slicer.

Suppose symbol sequences take on the levels $\pm 1,\ \pm 3, \cdots$. As discussed previously, the SNR at the slicer is maximised by the matched filter $p(-t)$ where $p(t)$ is the impulse response of the transmit RRC filter. Then, it can be readily shown that $D_{min} = 2\sigma_p^2$ and $\sigma_n^2 = N_0\,\sigma_p^2$. Hence, the maximum SNR at the slicer is given by

$$\text{SNR}_o = \frac{\sigma^2 \cdot \sigma_p^2}{N_0 \cdot BT} \tag{3.27}$$

Now, since for a passband system, $BT = 1$ at the maximum symbol rate without ISI, (3.27) can be written as

$$\text{SNR}_o = \frac{\sigma^2 \cdot \sigma_p^2}{N_0} \tag{3.28}$$

Using (3.28), we can re-write (3.26) in the following form

$$P_e = K_c \cdot Q\left(\sqrt{\frac{\text{SNR}_o}{\sigma^2}}\right) \tag{3.29}$$

For m–CAP using a QAM constellation[6] and $d = 1$, (3.22) gives

$$\sigma^2 = \frac{m-1}{3} \tag{3.30}$$

For a given P_e, let Δ be the value such that $P_e = K_c \cdot Q(\Delta)$. Using (3.30) and (3.29), we have

$$\Delta \triangleq \sqrt{\frac{\mathrm{SNR}_o}{\sigma^2}} \quad \rightarrow \quad m = 1 + \frac{3}{\Delta^2} \cdot \mathrm{SNR}_o \tag{3.31}$$

Further, at the maximum date rate, the bandwidth efficiency of the CAP system can be written as

$$\nu_c = \frac{\log_2 m}{BT} = \log_2 m \tag{3.32}$$

Finally, using (3.31) and (3.32), the maximum data rate of the CAP system is given by

$$R_{max} = B \log_2(1 + \frac{3}{\Delta^2} \cdot \mathrm{SNR}_o) \tag{3.33}$$

Comparing (3.33) to the Shannon capacity in (3.24), we see that the minimum value of Δ is $\sqrt{3}$ and $R_{max} \leq C$. Under the constraint of BER, the maximum system data rate is reduced, due to the scaling factor $\frac{3}{\Delta^2} \leq 1$. Further, it appears that the Δ defined herein and the SNR_{norm} in [24, 27] have the following relationship

$$\mathrm{SNR}_{norm} = \frac{\Delta^2}{3} \tag{3.34}$$

The Δ can be evaluated as follows. For a given BER, e.g., $P_e = 10^{-7}$, ignoring the constant $K_c(=1)$[7], Δ can be estimated from solving

$$10^{-7} = \frac{1}{\sqrt{2\pi}} \int_{\Delta}^{\infty} e^{-\lambda^2/2} d\lambda \tag{3.35}$$

[6]The procedures shown for the QAM constellations also apply to the cross constellations

[7]In most practical situations, the contribution of K_c to the BER is relatively small, compared to the argument in the Q function.

Table. 3.5 shows Δ against different BERs

Table 3.5: Δ vs BER in the $Q(x)$ function

BER	10^{-2}	10^{-4}	10^{-6}	10^{-8}	10^{-10}
Δ	2.58	3.89	4.89	5.80	6.53

CHAPTER 4
MMSE PERFORMANCE – LINEAR CAP RECEIVER

4.1 Introduction

In Chapter 2, we introduced two CAP receiver structures based on the linear equaliser (LE) and DFE. Here we note that although symbol-by-symbol detection receivers are suboptimal, combining them with powerful coding techniques can, however, improve their performance to approach near channel capacity, in particular when the MMSE criterion is used [27, 46].

In this chapter, we first formulate the MMSE problem for a linear CAP receiver operating in the presence of data-like cross-talks and coloured Gaussian noise. Since the overall transceiver system including both data and interference symbol path may be viewed as a special case of the linear MIMO system considered in [40], we next summarise the existing MMSE results of the MIMO system.

Following the same procedures as in [40], we then reconsider the MMSE problem for CAP receiver, where in the derivation, we make explicit use of the Hilbert pair relationship of the transmit shaping filters. As will be shown below, compared to the existing results, the derived results appear to provide better insights into the performance of the optimum (MMSE) linear receiver in the presence of data-like cross-talk. Although we only consider the optimisation of the MIMO receiver, it is worth noting that the joint optimisation of the transmit and receive filters in linear MIMO systems was first considered in [41]. Yang and Roy [42] readdressed the problem but for a more general

class of MIMO systems where the system bandwidth is no longer limited to the Nyquist bandwidth, and arbitrary combinations of different numbers of input and output users and different numbers of channel inputs and outputs are possible.

Finally, we apply the derived MMSE results to the case of stationary cross-talk. Simulation results for both data-like and stationary cross-talk cases are also given.

4.2 System Model

Fig. 4.1 shows the system model of a 2–D CAP system subject to multiple data-like cross-talks and additive background Gaussian noise[1]. This model is also applicable to systems with stationary self-NEXT which is modelled as another Gaussian noise source as shown in Chapter 3. In this case, we simply set the cross-talk channels in the model to zero, and the spectrum of $n(t)$ equals the sum of the background noise and stationary cross-talk spectra. On the receiver side, only the inphase subsystem is shown, since the I and Q subsystems are independent of each other. The following treatment of the inphase receive filter is also applicable to the quadrature receive filter.

Let $\{a_k^{(1)}\}$ and $\{a_k^{(2)}\}$ denote the two desired data symbol sequences and $\{b_k^{(l)},\ 1 \leq l \leq L_b\}$ the interference symbol sequences. Stacking both the data and interference symbols at time k into a vector, we write

$$\mathbf{u}_k^T \triangleq [\mathbf{a}_k^T,\ \mathbf{b}_k^T]$$

where $\mathbf{a}_k^T \triangleq [a_k,\ b_k]$ and $\mathbf{b}_k^T \triangleq [b_1, \ldots, b_{L_b}]$.

The equivalent I and Q channels, denoted by $p(t)$ and $\tilde{p}(t)$, consist of

[1]Shaping filters and the actual transmission channels are not shown explicitly in the diagram

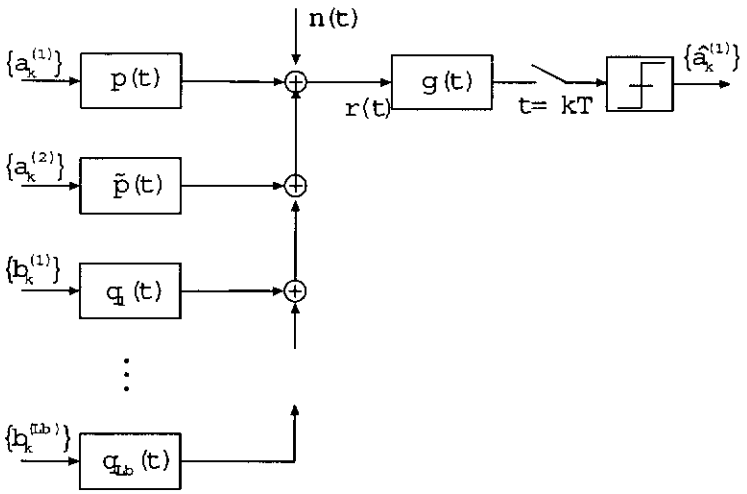

Figure 4.1: Linear transceiver system model for 2-D CAP in the presence of data-like cross-talk

the inphase and quadrature shaping filters, respectively, and the transmission channel. Similarly, the equivalent cross-talk channels, denoted by $q_l(t)$, $1 \leq l \leq L_b$ consist of the shaping filters and their respective transmission channels. Expressing all the equivalent channels in the form of a single vector, we write

$$\mathbf{g}_t^T(t) \triangleq [\mathbf{p}^T,\ \mathbf{q}^T](t)$$

where $\mathbf{p}^T = [p,\ \tilde{p}]$ and $\mathbf{q}^T \triangleq [q_1, \ldots, q_{L_b}]$. The received signal may be expressed as

$$r(t) \triangleq \sum_l \mathbf{g}_t^T(t - lT)\mathbf{u}_l + n(t)$$

where $n(t)$ is background WGN. Note that we assume that fixed timing offset for the interferers are aggregated into q_i for $1 \leq i \leq L_b$ and interferers transmit at the same symbol rate.

Let $g(t)$ be the inphase receive filter. At the sampling instant $t_s = kT$,

the sampled output of the received signal is given by

$$w(kT) \triangleq [r \otimes g](kT) = \sum_{l} [g \otimes \mathbf{g}_t^T](kT - lT)\mathbf{u}_l + [g \otimes n](kT)$$

where '$\otimes$' denotes convolution and

$$[g \otimes \mathbf{g}_t](t) \triangleq \int g(\tau)\mathbf{g}_t(t-\tau)\,d\tau \quad \text{and} \quad [g \otimes n](t) \triangleq \int g(\tau)n(t-\tau)\,d\tau$$

The error at the slicer is defined by $e(kT) \triangleq a_k - w(kT)$ and the MSE at the slicer is defined by $\varepsilon \triangleq E[e^2(kT)]$. The optimisation problem is to find the optimum receive filter, denoted by $g_o(t)$, such that ε is minimum. In mathematical terms, the optimum receive filter is given by

$$g_o(t) = \arg\Big\{\min_{g(t)} E\big[e^2(kT)\big]\Big\} \tag{4.1}$$

4.3 MMSE Results – Data-Like Cross-Talk

In the following derivations (and for the rest of this thesis), we assume the data and interference symbol sequences satisfy the following conditions.

$$\left.\begin{aligned} &E[a_m^{(l)}] = E[b_m^{(l)}] = 0 \\ &E[a_m^{(l)} b_n^{(j)}] = 0 \\ &E[a_m^{(l)} a_n^{(j)}] = E[b_m^{(l)} b_n^{(j)}] = \sigma^2 \delta_{mn}\delta_{lj} \end{aligned}\right\} \quad \forall m, n, l, j \in \mathbb{Z}. \tag{4.2}$$

i.e., all the symbol sequences consist of i.i.d zero-mean uniformly distributed symbols. Further, we assume that the slicers always make correct decisions.

4.3.1 Existing MIMO Results

According to [40], the structure of the optimum receive filter is shown in 4.2 where the total cross-talk sequences $\bar{\mathbf{a}}_k^T$ and its equivalent channel $\bar{\mathbf{P}}^T(f)$

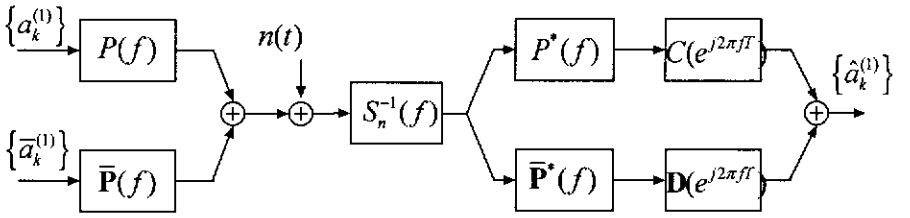

Figure 4.2: Structure of the optimum receive filter

are defined by

$$\bar{\mathbf{a}}_k^T \triangleq [a_k^{(2)}, b_k^{(1)}, \ldots, b_k^{(L_b)}]$$

$$\bar{\mathbf{P}}^T(f) \triangleq [\tilde{P}, Q_1, \ldots, Q_{L_b}](f)$$

Note the quadrature equivalent channel $\tilde{P}(f) = \mathcal{F}[\tilde{p}(t)]$ is treated as a part of total interference channel, as far as the detection of the data symbols transmitted over the inphase channel is concerned. The MMSE equaliser (receive filter) estimates all $L_b + 1$ interference symbols, in addition to the desired data symbol. Since the interfering symbols are superfluous, the MMSE equaliser consists of a total of $L_b + 2$ signal paths, each containing a matched filter followed by a tapped-delay-line filter, the outputs of which are summed to form the estimate of the current data symbol.

The total tapped-delay-line filter can be expressed as

$$\mathbf{Q}(z) \triangleq \begin{bmatrix} C(z) & \mathbf{D}(z) \\ E(z) & \mathbf{F}(z) \end{bmatrix}$$

where $z \triangleq e^{j2\pi fT}$, and $E(z)$ and $\mathbf{F}(z)$ are included to represent processing of the cross-talk data sequences. Note that $E(z)$ and $\mathbf{F}(z)$ are not shown in the Fig. 4.2 since the detection of the interference symbols sequence $\{\bar{\mathbf{a}}_k\}$ is not

required. The entries $C(z)$ and $\mathbf{D}(z)$ are given by

$$C(z) \triangleq \frac{[1+\sigma^2 S^{\bar{p}}]\sigma^2}{[1+\sigma^2 S^{p}][1+\sigma^2 S^{\bar{p}}] - \|\sigma^2 \mathbf{S}^{\bar{p}p}\|^2} \tag{4.3a}$$

$$\mathbf{D}(z) \triangleq \frac{\sigma^4 \mathbf{S}^{p\bar{p}}}{\|\sigma^2 \mathbf{S}^{\bar{p}p}\|^2 - (1+\sigma^2 S^{\bar{p}})(1+\sigma^2 S^{p})} \tag{4.3b}$$

where $\mathbf{S}^{p\bar{p}} = [\mathbf{S}^{\bar{p}p}]^H$, the notation $[\cdot]^H$ denotes Hermitian transpose, and on the unit circle, S^p, $S^{\bar{p}}$ and $\mathbf{S}^{\bar{p}p}$ are given by

$$S^{p}(e^{j2\pi fT}) \triangleq \frac{1}{T}\sum_k |P(f+\frac{k}{T})|^2 S_n^{-1}(f+\frac{k}{T})$$

$$S^{\bar{p}}(e^{j2\pi fT}) \triangleq \frac{1}{T}\sum_k |\bar{\mathbf{P}}(f+\frac{k}{T})|^2 S_n^{-1}(f+\frac{k}{T})$$

$$\mathbf{S}^{\bar{p}p}(e^{j2\pi fT}) \triangleq \frac{1}{T}\sum_k \bar{\mathbf{P}}(f+\frac{k}{T}) S_n^{-1}(f+\frac{k}{T}) P(f+\frac{k}{T})$$

Corresponding to the optimum receive filter, the system MMSE is given by

$$\text{MMSE} = T\int_{-\frac{1}{2T}}^{\frac{1}{2T}} C(e^{j2\pi fT})\, df \tag{4.4}$$

where $C(e^{j2\pi fT})$ is evaluated from (4.3).

Theoretically, it is possible to specialise the general result of (4.4) to the case of an optimum linear CAP receiver operating in the presence of data-like cross-talk. Such an approach was undertaken in [10, 43], but the derived results are complicated and do not offer any insight into the performance of the optimum CAP receiver. To the author's best knowledge, no simple meaningful MMSE expression is currently available.

Following the procedures in [40], but with the inclusion of the Hilbert pair property of the shaping filters in the derivation, we show next that an simple, elegant MMSE expression is possible.

4.3.2 Direct Derivation

Expanding the RHS of (4.1) and using the assumptions of (4.2), we have

$$\begin{aligned}\varepsilon = \sigma^2 &- 2\sigma^2 \int p(-\tau)g(\tau)\,d\tau \\ &+ \sigma^2 \iint \mathbf{g}_t^T(mT-\tau_1)\mathbf{g}_t(mT-\tau_2)g(\tau_1)g(\tau_2)\,d\tau_1\,d\tau_2 \\ &+ \iint R_n(\tau_1-\tau_2)g(\tau_1)g(\tau_2)\,d\tau_1\,d\tau_2 \end{aligned} \tag{4.5}$$

where $R_n(\tau_1 - \tau_2) = E[n(\tau_1)n(\tau_2)]$. Define $\varepsilon' \triangleq \varepsilon\sigma^{-2}$ and $R_{n'} \triangleq \sigma^{-2}R_n$. Further, we write

$$A(t,\tau) \triangleq \sum_m \mathbf{g}_t^T(mT-t)\mathbf{g}_t(mT-\tau) + R_{n'}(t-\tau)$$

and

$$[\mathcal{A}g](t) \triangleq \int A(t,\tau)g(\tau)\,d\tau$$

Using these definitions, the MSE of (4.5) may be expressed as

$$\varepsilon' = 1 - 2\int p(-\tau)g(\tau)\,d\tau + \int [\mathcal{A}g](\tau)g(\tau)\,d\tau \tag{4.6}$$

Using standard *calculus of variation* techniques, e.g., [44], it can be shown that the optimum receive filter satisfies

$$\int A(t,\tau)g(\tau)\,d\tau = p(-t) \tag{4.7}$$

Expanding the above equation, we write

$$\sum_m \mathbf{g}_t^T(mT-t)\mathbf{k}(mT) + \int R_{n'}(t-\tau)g(\tau)\,d\tau = p(-t) \tag{4.8}$$

where

$$[\mathbf{g}_t \otimes g](mT) \triangleq \mathbf{k}(mT)$$

Take Fourier transforms ($\mathcal{F}$) of both sides of (4.8)

$$\mathbf{G}_t^H(f)\mathbf{K}(e^{j2\pi fT}) + S_{n'}(f)G(f) = P^*(f) \tag{4.9}$$

where $\mathbf{G}_t(f) \triangleq \mathcal{F}[\mathbf{g}_t(t)]$, $\mathbf{K}(e^{j2\pi fT}) \triangleq \sum_m \mathbf{k}(mT)e^{-j2\pi fmT}$, $S_{n'}(f) \triangleq \mathcal{F}[R_{n'}(t)]$, $G(f) \triangleq \mathcal{F}[g(t)]$, and $P(f) \triangleq \mathcal{F}[p(t)]$.

Since $\mathbf{K}(e^{j2\pi fT})$ is periodic with period T, we write $\mathbf{K}_T(f) \triangleq \mathbf{K}(e^{j2\pi fT})$. Using the well known relationship

$$\mathbf{K}_T(f) = \frac{1}{T}\sum_l \mathbf{G}_t(f + \frac{l}{T})G(f + \frac{l}{T})$$

we can expand the first term in the LHS of (4.9) as follows

$$\begin{aligned}\mathbf{G}_t^H(f)\mathbf{K}_T(f) = {} & P^*(f)\frac{1}{T}\sum_l P(f + \frac{l}{T})G(f + \frac{l}{T}) \\ & + \tilde{P}^*(f)\frac{1}{T}\sum_l \tilde{P}(f + \frac{l}{T})G(f + \frac{l}{T}) + \mathbf{Q}^H(f)\bar{\mathbf{K}}_T(f)\end{aligned} \tag{4.10}$$

where $\mathbf{Q}(f) \triangleq [Q_1, \ldots, Q_{L_b}]^T(f)$ and $\bar{\mathbf{K}}_T(f)$ is defined by

$$\bar{\mathbf{K}}_T(f) \triangleq \frac{1}{T}\sum_l \mathbf{Q}(f + \frac{l}{T})G(f + \frac{l}{T})$$

Define $\bar{f} \in [-\frac{1}{2T}, \frac{1}{2T}]$ and for an arbitrary value of f, we may write $f = \bar{f} + \frac{k}{T}$ where k is some suitable integer (more on k later). Substituting $f = \bar{f} + \frac{k}{T}$ into (4.9) and using (4.10), after some re-arrangement, we have

$$\begin{aligned}& \frac{1}{T}\sum_l P^*(\bar{f} + \frac{k}{T})P(\bar{f} + \frac{l}{T})G(\bar{f} + \frac{l}{T}) \\ & \quad + \frac{1}{T}\sum_l \tilde{P}^*(\bar{f} + \frac{k}{T})\tilde{P}(\bar{f} + \frac{l}{T})G(\bar{f} + \frac{l}{T}) \\ & \quad + \sum_l W_{k,l}G(\bar{f} + \frac{l}{T}) = P^*(\bar{f} + \frac{k}{T})\end{aligned} \tag{4.11}$$

where $W_{k,l}$ is defined by

$$W_{k,l}(\bar{f}) \triangleq \frac{1}{T}\mathbf{Q}^H(\bar{f} + \frac{k}{T})\mathbf{Q}(\bar{f} + \frac{l}{T}) + S_{n'}(\bar{f} + \frac{l}{T})\delta_{lk}$$

For a given system bandwidth B_{sys} [2], (4.11) represents a set of equations for $|k| \leq K$ where the integer K is selected such that $B_{sys} \leq \frac{1}{2T} + \frac{K}{T}$. Combining all such equations, we have

$$\left[\mathbf{W} + \frac{1}{T}\mathbf{P}^*\mathbf{P}^T + \frac{1}{T}\tilde{\mathbf{P}}^*\tilde{\mathbf{P}}^T\right]\mathbf{G}_o = \mathbf{P}^* \tag{4.12}$$

where matrix $\mathbf{W} \triangleq [W_{k,l}]$ has its entries from $\{W_{k,l},\ -K \leq l,k \leq K\}$ with k and l corresponding to the row and column indices, respectively, and the vectors $\mathbf{G}_o$, $\mathbf{P}$ and $\tilde{\mathbf{P}}$ are defined by

$$\mathbf{G}_o(\bar{f}) \triangleq \begin{bmatrix} G(\bar{f} - \frac{K}{T}) \\ G(\bar{f} - \frac{K-1}{T}) \\ \vdots \\ G(\bar{f} + \frac{K}{T}) \end{bmatrix}, \quad \mathbf{P}(\bar{f}) \triangleq \begin{bmatrix} P(\bar{f} - \frac{K}{T}) \\ P(\bar{f} - \frac{K-1}{T}) \\ \vdots \\ P(\bar{f} + \frac{K}{T}) \end{bmatrix}, \quad \tilde{\mathbf{P}}(\bar{f}) \triangleq \begin{bmatrix} \tilde{P}(\bar{f} - \frac{K}{T}) \\ \tilde{P}(\bar{f} - \frac{K-1}{T}) \\ \vdots \\ \tilde{P}(\bar{f} + \frac{K}{T}) \end{bmatrix}$$

Assuming the optimum solution exists, from (4.12), we have, for the optimum linear CAP receiver

$$\mathbf{G}_o = \left[\mathbf{W} + \frac{1}{T}\mathbf{P}^*\mathbf{P}^T + \frac{1}{T}\tilde{\mathbf{P}}^*\tilde{\mathbf{P}}^T\right]^{-1}\mathbf{P}^* \tag{4.13}$$

where for ease of notations, we omit the variable $\bar{f}$ in $\mathbf{G}_o(\bar{f})$, $\mathbf{P}(\bar{f})$, and $\tilde{\mathbf{P}}(\bar{f})$. Note that by definition, $\mathbf{G}_o(\bar{f})$ completely specifies the desired optimum transfer function $G_o(f)$ within the frequency band of interest (B_{sys}).

Now, we find the MMSE of the optimum linear receiver, denoted by ε'_{min}. Substituting (4.7) into (4.6) and using *Parseval*'s theorem, it can be shown that

$$\begin{aligned} \varepsilon'_{min} &= 1 - \int p(-\tau)g(\tau)\,d\tau = 1 - \int P(f)G(f)\,df \\ &= 1 - \int_{-\frac{1}{2T}}^{\frac{1}{2T}} \mathbf{P}^T\mathbf{G}_o\,df \end{aligned} \tag{4.14}$$

[2]For convenience, we assume the lower band edge is at DC

and substituting (4.13) into (4.14), we get

$$\varepsilon'_{min} = 1 - \int_{-\frac{1}{2T}}^{\frac{1}{2T}} \mathbf{P}^T \left[\mathbf{W}_E + \frac{1}{T}\tilde{\mathbf{P}}^*\tilde{\mathbf{P}}^T \right]^{-1} \mathbf{P}^* \, df \tag{4.15}$$

where $\mathbf{W}_E$ is defined as

$$\mathbf{W}_E \triangleq \mathbf{W} + \frac{1}{T}\mathbf{P}^*\mathbf{P}^T$$

Using the *matrix inversion lemma*, we can write

$$\left[\mathbf{W}_E + \frac{1}{T}\tilde{\mathbf{P}}^*\tilde{\mathbf{P}}^T \right]^{-1} = \mathbf{W}_E^{-1} - \frac{\frac{1}{T}\mathbf{W}_E^{-1}\tilde{\mathbf{P}}^*\tilde{\mathbf{P}}^T\mathbf{W}_E^{-1}}{1 + \frac{1}{T}\tilde{\mathbf{P}}^T\mathbf{W}_E^{-1}\tilde{\mathbf{P}}^*} \tag{4.16}$$

Further, we express

$$\mathbf{W}_E^{-1} = (R\mathbf{W}^{-1} - \frac{1}{T}\mathbf{W}^{-1}\mathbf{P}^*\mathbf{P}^T\mathbf{W}^{-1})R^{-1} \tag{4.17}$$

where $R(\bar{f}) \triangleq 1 + \frac{1}{T}\mathbf{P^T}\mathbf{W}^{-1}\mathbf{P}^*$.

Substituting (4.16) and (4.17) into the integrand of (4.15), it can be shown that the integrand contains the following terms

$$\mathbf{P}^T\mathbf{W}_E^{-1}\mathbf{P}^* = T - TR^{-1} \tag{4.18a}$$

$$\mathbf{P}^T\mathbf{W}_E^{-1}\tilde{\mathbf{P}}^* = R^{-1}\mathbf{P}^T\mathbf{W}^{-1}\tilde{\mathbf{P}}^* \tag{4.18b}$$

$$\tilde{\mathbf{P}}^T\mathbf{W}_E^{-1}\mathbf{P}^* = R^{-1}\tilde{\mathbf{P}}^T\mathbf{W}^{-1}\mathbf{P}^* \tag{4.18c}$$

$$1 + \frac{1}{T}\tilde{\mathbf{P}}^T\mathbf{W}_E^{-1}\tilde{\mathbf{P}}^* = R - R^{-1}\frac{1}{T^2}\tilde{\mathbf{P}}^T\mathbf{W}^{-1}\mathbf{P}^* \cdot \mathbf{P}^T\mathbf{W}^{-1}\tilde{\mathbf{P}}^* \tag{4.18d}$$

We now prove that the real part of $\tilde{\mathbf{P}}^T\mathbf{W}_E^{-1}\mathbf{P}^*$ is zero. Firstly, define the unitary matrix

$$\mathbf{\Lambda}(f) \triangleq \mathrm{diag}[\underbrace{j, \cdots, j}_{K}, (-j)\,\mathrm{sgn}(f), \underbrace{-j, \cdots -j}_{K}]$$

Then, we have

$$\tilde{\mathbf{P}}(f) = \mathbf{\Lambda}(f)\mathbf{P}(f) \tag{4.19}$$

It is shown in Appendix A that when cross-talks have the same 2–D CAP line

code,

$$\mathbf{\Lambda}^H\mathbf{W}^{-1}\mathbf{\Lambda} = \mathbf{W}^{-1} \qquad \text{or} \qquad \mathbf{\Lambda}^H\mathbf{W}^{-1} = \mathbf{W}^{-1}\mathbf{\Lambda}^H. \tag{4.20}$$

Let $\mathbf{P}^T\mathbf{W}^{-1}\tilde{\mathbf{P}}^* \triangleq a' + jb'$ where a' and b' are some real-value functions of $\bar{f}$. Using (4.19), (4.20) we have

$$2a' = \mathbf{P}^T\mathbf{W}^{-1}\tilde{\mathbf{P}}^* + \mathbf{P}^H\mathbf{W}^{-1}\tilde{\mathbf{P}} = \mathbf{P}^H\mathbf{W}^{-1}(\mathbf{\Lambda} + \mathbf{\Lambda}^H)\mathbf{P} = 0$$

Since $\mathbf{P}^H\mathbf{W}^{-1}\tilde{\mathbf{P}} = \tilde{\mathbf{P}}^T\mathbf{W}^{-1}\mathbf{P}^*$, then $\tilde{\mathbf{P}}^T\mathbf{W}^{-1}\mathbf{P}^*$ is the complex conjugate of $\mathbf{P}^T\mathbf{W}^{-1}\tilde{\mathbf{P}}^*$. Therefore, using (4.18), we have

$$\frac{1}{T}\mathbf{P}^T\mathbf{W}_E^{-1}\tilde{\mathbf{P}}^* \cdot \tilde{\mathbf{P}}^T\mathbf{W}_E^{-1}\mathbf{P}^* = Tb^2R^{-2} \tag{4.21}$$

where $b(\bar{f}) \triangleq \frac{1}{T}\mathrm{Im}\{\mathbf{P}^T\mathbf{W}^{-1}\tilde{\mathbf{P}}^*\}$. Substituting (4.21) into (4.18), the MMSE in (4.15) now becomes

$$\varepsilon'_{min} = 1 - \int_{-\frac{1}{2T}}^{\frac{1}{2T}} \left[T - \frac{T}{R} - \frac{Tb^2}{R(R^2-b^2)}\right] df = T\int_{-\frac{1}{2T}}^{\frac{1}{2T}} \frac{R}{R^2-b^2}\, df$$

We note that $R(f)$ is even whereas $b(f)$ is odd. Hence,

$$\int_{-\frac{1}{2T}}^{\frac{1}{2T}} \frac{1}{R+b}\, df = \int_{-\frac{1}{2T}}^{\frac{1}{2T}} \frac{1}{R-b}\, df$$

and the final MMSE expression can be written as

$$\varepsilon'_{min} = T\int_{-\frac{1}{2T}}^{\frac{1}{2T}} \frac{1}{R(f)+b(f)}\, df \tag{4.22}$$

where $R(f)$ and $b(f)$ are given by

$$R(\bar{f}) = 1 + \frac{1}{T}\mathbf{P}^{\mathrm{T}}\mathbf{W}^{-1}\mathbf{P}^* \quad \text{and} \quad b(\bar{f}) = \frac{1}{T}\mathrm{Im}\{\mathbf{P}^T\mathbf{W}^{-1}\tilde{\mathbf{P}}^*\}$$

4.3.3 Discussion

First, for the simplest case when the roll-off factor $\alpha = 0$, we have $k = -1, 0, \text{and } 1$. It can be seen that $\mathbf{W}$ is then diagonal, due to the zero excess bandwidth. This is equivalent to the case when cross-talk is modelled as stationary noise. Indeed, this is the expected result, because it is only under this condition ($\alpha = 0$) that the baud-rate sampled sequence of a PAM signal is stationary, rather than cyclostationary [37].

Next, for non-zero excess bandwidth, the non-diagonal terms in $\mathbf{W}$ have the potential to reduce the contribution of interference to the MMSE shown in (4.22). This reduction depends on the relative phase between the signal and cross-talk channels, as indicated by $\mathbf{P^T W^{-1} P^*}$ and $\mathbf{P}^T\mathbf{W}^{-1}\tilde{\mathbf{P}}^*$ in $R(f)$ and $b(f)$, respectively. Numerical results which support these observations are given in Chapter 5 where DFE CAP receivers are analysed in the same channel environment. In contrast, the general MMSE expression in (4.4) does not appear to offer similar insights.

4.4 MMSE Results – Stationary Cross-Talk

For stationary cross-talks which are modelled as another stationary additive Gaussian noise, we can incorporate it into the channel background noise. In Fig. 4.1, we set the cross-talk channels $Q_l(f) = 0$ for $1 \leq l \leq L_b$ and the new channel noise now has the combined spectrum of the background and cross-talk spectra. In this case, $W_{k,l}(\bar{f})$ reduces to $S_n(\bar{f} + \frac{k}{T})\delta_{kl}$.

Define

$$\hat{\mathbf{S}}_{n'}(\bar{f}) \triangleq \text{diag}\left[S_{n'}(\bar{f} - \frac{K}{T}), S_{n'}(\bar{f} - \frac{K-1}{T}), \ldots, S_{n'}(\bar{f} + \frac{K}{T})\right]$$

then

$$\mathbf{W} = \hat{\mathbf{S}}_{n'} \quad \text{and} \quad \mathbf{W}^{-1} = \hat{\mathbf{S}}_{n'}^{-1} \tag{4.23}$$

Assuming $S_{n'}(f) \neq 0$ for $|f| \leq B_{sys}$ (and for the rest of this thesis), we define $\Gamma(f) \triangleq |P(f)|^2/S_{n'}(f)$. Expanding $R(\bar{f})$ and $b(\bar{f})$, it can be shown that the sum $S_{rb}(\bar{f}) \triangleq R(\bar{f}) + b(\bar{f})$ is given by

$$S_{rb}(\bar{f}) = \frac{1}{T}\Big[2\sum_{k=1}^{K}\Gamma(\bar{f}+\frac{k}{T}) + (1+\mathrm{sgn}(\bar{f}))\Gamma(\bar{f})\Big] + 1 \tag{4.24}$$

To simplify the expression further, define a new variable $\bar{f}^{+} \in [0,\ \frac{1}{T}]$. Firstly, for $0 \leq \bar{f} < \frac{1}{2T}$, we substitute $\bar{f}$ with $\bar{f}^{+}$ into (4.24)

$$S_{rb}(\bar{f}^{+}) = \frac{2}{T}\sum_{k=0}^{K}\Gamma\big(\bar{f}^{+}+\frac{k}{T}\big) + 1, \qquad 0 \leq \bar{f}^{+} \leq \frac{1}{2T} \tag{4.25}$$

Secondly, for $-\frac{1}{2T} \leq \bar{f} < 0$, we substitute $\bar{f}$ with $\bar{f}^{+} - \frac{1}{T}$ into (4.24)

$$S_{rb}(\bar{f}^{+}) = \frac{2}{T}\sum_{k=0}^{K-1}\Gamma\big(\bar{f}^{+}+\frac{k}{T}\big) + 1, \qquad \frac{1}{2T} \leq \bar{f}^{+} < \frac{1}{T} \tag{4.26}$$

Now, assuming $\Gamma(f) = 0$ for $f \geq B_{sys}$, we can combine (4.25) and (4.26) into a single equation

$$S_{rb}(\bar{f}^{+}) = \frac{2}{T}\sum_{k=0}^{K}\Gamma\big(\bar{f}^{+}+\frac{k}{T}\big) + 1, \qquad 0 \leq \bar{f}^{+} \leq \frac{1}{T} \tag{4.27}$$

In summary, for stationary cross-talk, the MMSE of (4.22) may be written as

$$\varepsilon'_{min} = T\int_{0}^{\frac{1}{T}} \frac{1}{\frac{2}{T}\sum_{k=0}^{K}\Gamma\big(f+\frac{k}{T}\big)+1}\,df \tag{4.28}$$

Recognising that we can also express the quantity

$$\frac{1}{T}\Gamma(f) = \frac{\sigma^2}{T}\frac{|P(f)|^2}{S_n(f)} = \mathrm{SNR}_n(f) \tag{4.29}$$

where $\mathrm{SNR}_n(f)$ is the spot SNR at the input of the receiver defined by (3.13)

in Chapter 3, we may also write (4.28) in the following form [45]

$$\varepsilon'_{min} = T \int_0^{\frac{1}{T}} \frac{1}{2\sum_{k=0}^{K} \mathrm{SNR}_n\left(f + \frac{k}{T}\right) + 1}\, df \tag{4.30}$$

The transfer function of the optimum linear CAP receiver can be found as follows. Since $Q_l(f) = 0$ for $1 \le l \le L_b$, then from (4.9), we write

$$S_{n'}(f)G(f) = P^*(f)\left[1 - K_T(f) - j\,\mathrm{sgn}(f)\tilde{K}_T(f)\right] \tag{4.31}$$

where $K_T(f)$ and $\tilde{K}_T(f)$ are defined by

$$K_T(f) \triangleq \frac{1}{T}\sum_m P(f + \frac{m}{T})G(f + \frac{m}{T})$$
$$\tilde{K}_T(f) \triangleq \frac{1}{T}\sum_m \tilde{P}(f + \frac{m}{T})G(f + \frac{m}{T})$$

$K_T(f)$ and $\tilde{K}_T(f)$ may be viewed as the *folded spectrum* of $K(f)$ and $\tilde{K}(f)$ which are defined by

$$K(f) \triangleq P(f)\,G(f) \qquad \text{and} \qquad \tilde{K}(f) \triangleq \tilde{P}(f)\,G(f)$$

Define $X(f) \triangleq 1 - K_T(f) - j\,\mathrm{sgn}(f)\tilde{K}_T(f)$. Then, from (4.31), we get

$$G(f) = \frac{P^*(f)}{S_{n'}(f)}X(f) \tag{4.32}$$

and from (4.29), we get

$$K(f) = \Gamma(f)X(f) \tag{4.33a}$$

$$\tilde{K}(f) = (-j)\,\mathrm{sgn}(f)\Gamma(f)X(f) \tag{4.33b}$$

It is shown in Appendix B that $X(f)$ is given by

$$X(f) = \left[\frac{2}{T}\sum_{k=0}^{K}\Gamma(\bar{f}^+ + \frac{k}{T}) + 1\right]^{-1} \tag{4.34}$$

where $\bar{f}^+ = |f| - \frac{m^+}{T}$ for some positive suitable integer m^+. Equation (4.34)

may be interpreted as follows – for an arbitrary frequency point f, the value $X(f)$ is given by the function of f^+ shown in the RHS of (4.34), and f^+ is related to f by some suitable integer m^+ such that the quantity $0 \leq |f| - \frac{m^+}{T} = \bar{f}^+ \leq \frac{1}{T}$. This relationship is shown in Fig. 4.3.

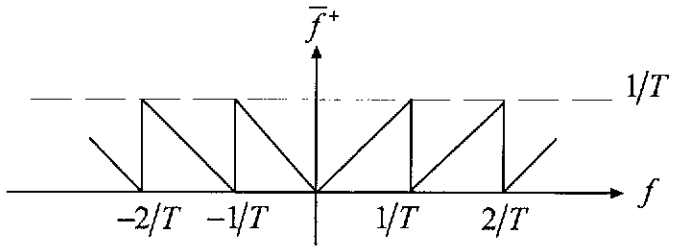

Figure 4.3: Relationship between f and $\bar{f}^+$

Substituting (4.34) into (4.32), the transfer function of the optimum inphase receive filter is given by

$$G_{io}(f) \triangleq G_o(f) = \frac{S_{n'}^{-1}(f)P^*(f)}{\frac{2}{T}\sum_{k=0}^{K}\Gamma(\bar{f}^+ + \frac{k}{T}) + 1} \tag{4.35}$$

Similarly, it can be shown that the transfer function of the optimum quadrature receiver filter is given by

$$G_{qo}(f) = \frac{S_{n'}^{-1}(f)\tilde{P}^*(f)}{\frac{2}{T}\sum_{k=0}^{K}\Gamma(\bar{f}^+ + \frac{k}{T}) + 1} \tag{4.36}$$

In the case where channel noise is just white, i.e., $S_{n'}(f) = \sigma^{-2}N_0$, (4.35) and (4.36) may be written as

$$G_{io}(f) = \frac{\sigma^2 P^*(f)}{\frac{2\sigma^2}{T}\sum_{k=0}^{K}|P(\bar{f}^+ + \frac{k}{T})|^2 + N_0} \tag{4.37}$$

$$G_{qo}(f) = \frac{\sigma^2 \tilde{P}^*(f)}{\frac{2\sigma^2}{T}\sum_{k=0}^{K}|P(\bar{f}^+ + \frac{k}{T})|^2 + N_0} \tag{4.38}$$

Moreover, if the transmission channel is ideal, i.e., $P(f) = G_t(f)$, then (4.37)

and (4.38) reduce to the simple matched filter pair

$$G_{io}(f) = \frac{\sigma^2}{\sigma^2 + N_0} P^*(f) \tag{4.39}$$

$$G_{qo}(f) = \frac{\sigma^2}{\sigma^2 + N_0} \tilde{P}^*(f) \tag{4.40}$$

From (4.28), the corresponding MMSE for an ideal transmission channel is given by

$$\frac{\varepsilon}{\sigma^2} = \frac{1}{\frac{\sigma^2}{N_0} + 1} \tag{4.41}$$

Define the SNR at the slicer $\text{SNR}_{o,mmse} \triangleq \frac{\sigma^2}{\varepsilon}$ and recognising that $\text{SNR}_{o,mf} = \frac{\sigma^2}{N_0}$ from (3.21) in Chapter 3, we have the following well-known relationship [46]

$$\text{SNR}_{o,mmse} = \text{SNR}_{o,mf} + 1 \tag{4.42}$$

4.5 Simulation

4.5.1 System Setup

The simulation model for the linear CAP transceiver system is shown in Fig. 4.4. On the transmitter side, the passband inphase and quadrature transmit filters are given by $g_t(t) \triangleq g_o(t)\cos(2\pi f_c t)$ and $\tilde{g}_t(t) \triangleq g_o(t)\sin(2\pi f_c t)$, where $g_o(t)$ is the impulse response of a RRC filter with roll-off factor $\alpha = 1.2$ whose transfer function is given by (2.7). For convenience, we select $f_c = \frac{(1+\alpha)}{2T}$ such that the starting frequency of the system bandwidth is at DC. One data-like self-NEXT is generated using an inphase and a quadrature shaping filter identical to $g_t(t)$ and $\tilde{g}_t(t)$, respectively. The 16–CAP scheme is used to transmit data at a rate of 51.48 Mb/s, and its constellation is normalised so that the total transmitted power is 1 Watt. The channel noise power spectrum is fixed and computed assuming that the transmitted signal has a 30 MHz bandwidth

and a $\overline{\text{SNR}}_n = 30$ dB at the receiver.

The transmission channel is 100 m of UTP–3 copper wire pair. It is modelled by the simplified channel model given by (3.4). The NEXT channel model is given by (3.11). The parameters for both channel models are given in Table 3.2 and Table 3.3 in Chapter 3. Note that for convenience, we extend the frequency range of the models to include frequencies from near DC to over 30 MHz. We assume the transfer functions of the data and cross-talk channels have only amplitude distortion, i.e., they have linear phase. Further, we also assume the relative phase between the transfer functions, denoted by ϕ, is zero at all frequencies. The phase effects on the performance of the linear receiver are left to Chapter 6 where the linear and DFE CAP receivers are compared.

On the receiver side, the optimum receive (analog) filters are simulated by the two FSEs shown in Fig. 4.4. In order to reduce aliasing due to the finite length of the FSEs, 8 time oversampling is used for the FSEs, each of which has 320 taps, covering 40 symbol periods. The standard LMS algorithm [47] is used for the adaptive FSEs. The optimum transfer function for the inphase FSE is estimated from its average weights at convergence. System performance is evaluated by the SNR at the slicer.

4.5.2 Numerical Results

The simulated and theoretical curves for the optimum transfer functions are shown in Fig. 4.5. From the figure, it can be seen that the transfer functions follow each other closely. Further, we compare these curves with those shown in [13], since both use almost identical set of simulation parameters, except for the FSE length, number of simulation runs and averaging method in obtaining the optimum filter weights. We note that both simulation curves

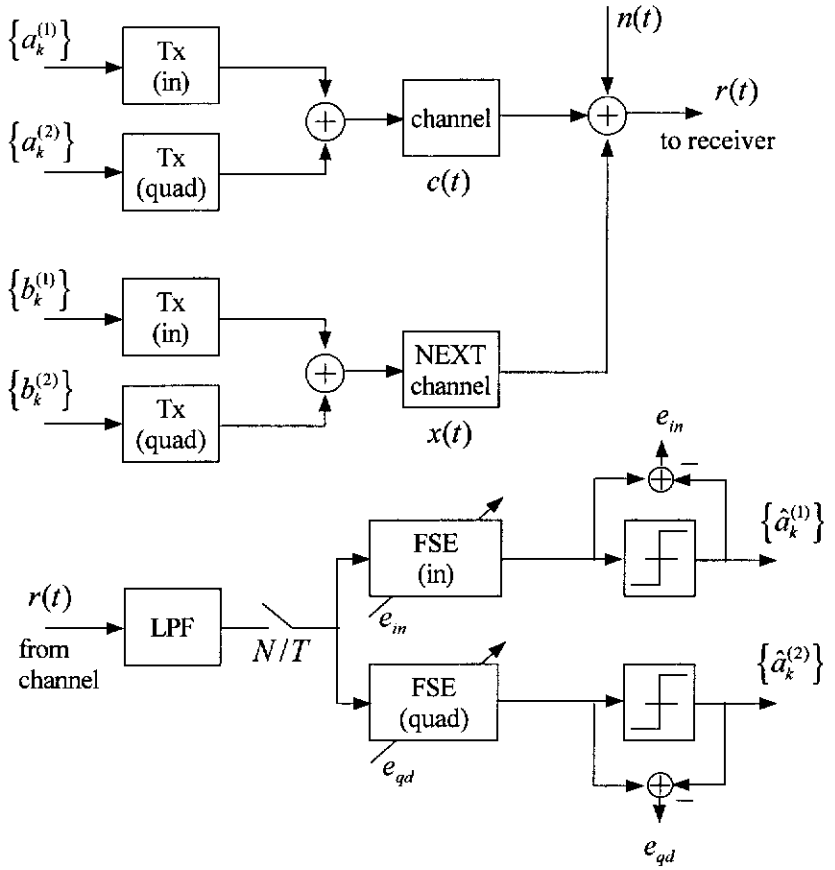

Figure 4.4: Simulation model of a linear CAP transceiver system, one NEXT

are remarkably similar. The theoretical curves in [13] differ from the simulated curves, since the theoretical curves are derived under the zero-forcing condition.

Our simulation also shows that if data-like self-NEXT is present, the LMS convergence speed is relatively slow, compared to the case without. The same result has been observed in [13], where the authors further suggest that the slowness of the convergence may be due to the fact that the adaptive FSE tries to jointly equalise the channel and suppress the self-NEXT. Fig. 4.5 clearly shows this dual function of the equaliser. However, due to time limitation, this issue is not investigated further in this thesis.

We also include the simulation curves for AWGN only which are shown in Fig. 4.6. Comparing this optimum transfer function with that shown in Fig. 4.5, we see that there is significant change in shape. Also, in the absence of the self-NEXT, the LMS algorithm converges after 500 symbols, in contrast to the 20,000 symbols required when the self-NEXT is present.

The MMSE performance results are given in Table 4.1. In the table, we include the average signal-to-background-noise ($\overline{\text{SNR}}_n$) and the average signal-to-interference ratios ($\overline{\text{SIR}}$) at the input of the CAP receiver. The quantity $\text{SNR}_{o,x}$ and $\text{SNR}_{o,n}$ are the SNR at the slicer with and without the presence of the self-NEXT, respectively. The results show that although $\overline{\text{SIR}}$ is relatively high at the input, it can be effectively suppressed by the linear receiver, due to the extra degree of freedom introduced in the signal bandwidth by the large roll-off factor. This technique is called *NEXT equalisation* in [13].

Table 4.1: MMSE performance of the optimum linear CAP receiver over a 100 m UTP-3 cable, 51.84 Mb/sec, roll off factor $\alpha = 1.2$, one data-like self-NEXT, relative phase $\phi = 0$

	$\overline{\text{SNR}}_n$	$\overline{\text{SIR}}$	$\text{SNR}_{o,x}$	$\text{SNR}_{o,n}$
Computed	28.25	12.75	25.2	31.6
Simulated	28.5	13	25.0	31.5

4.6 Summary

In this chapter, we studied the MMSE performance of a linear CAP receiver operating in the presence of additive background noise, and either stationary or data-like cross-talks. We started with a general model with multiple data-like cross-talks. This model can be viewed as a special case of a

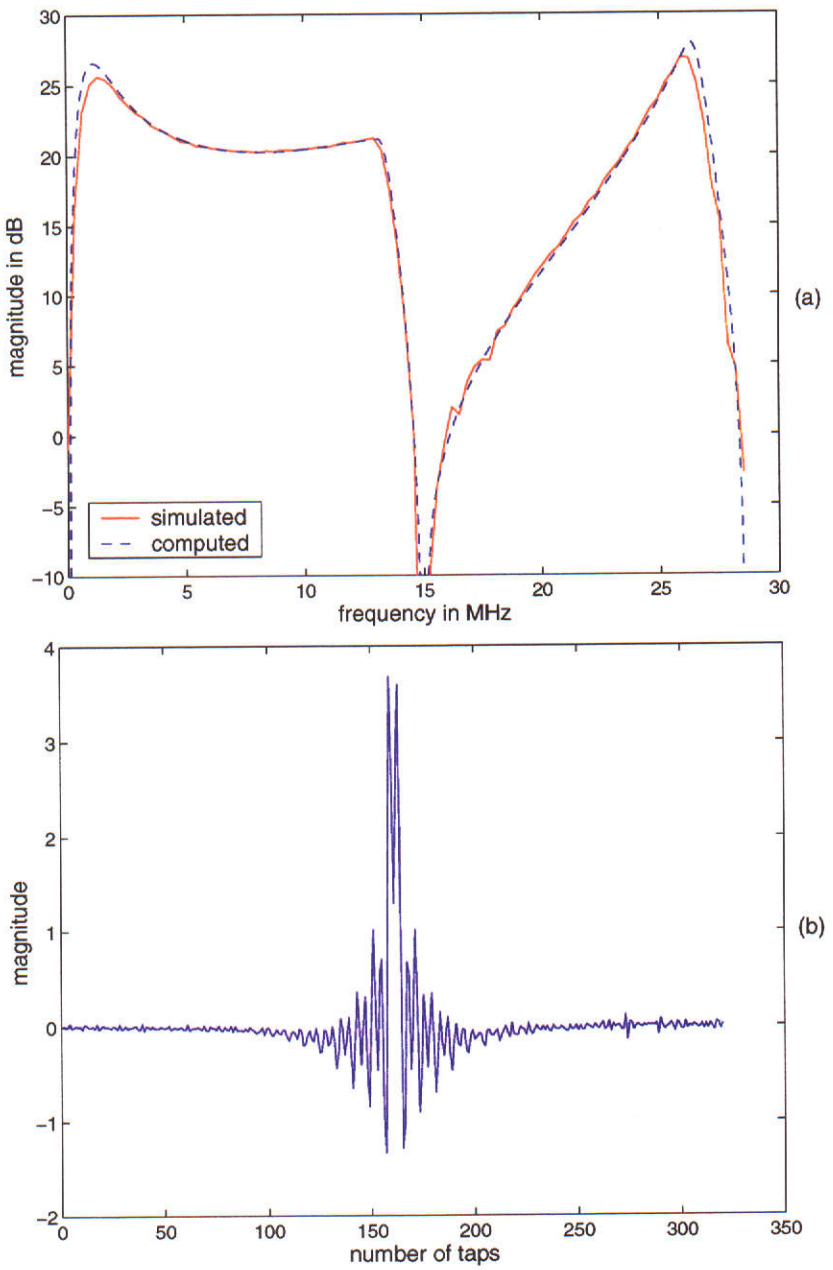

Figure 4.5: Linear CAP transceiver operating at 51.84 Mb/sec over 100 m of UTP-3 cable, 16–CAP scheme, $\alpha = 1.2$, one data-like self-NEXT, relative phase $\phi = 0$, and AWGN (a) magnitude of the optimum transfer function, (b) weights of the optimum FSE

MIMO system. Although the MMSE solution for the MIMO system exists, it is relatively complex and does not offer any insights into the operation of

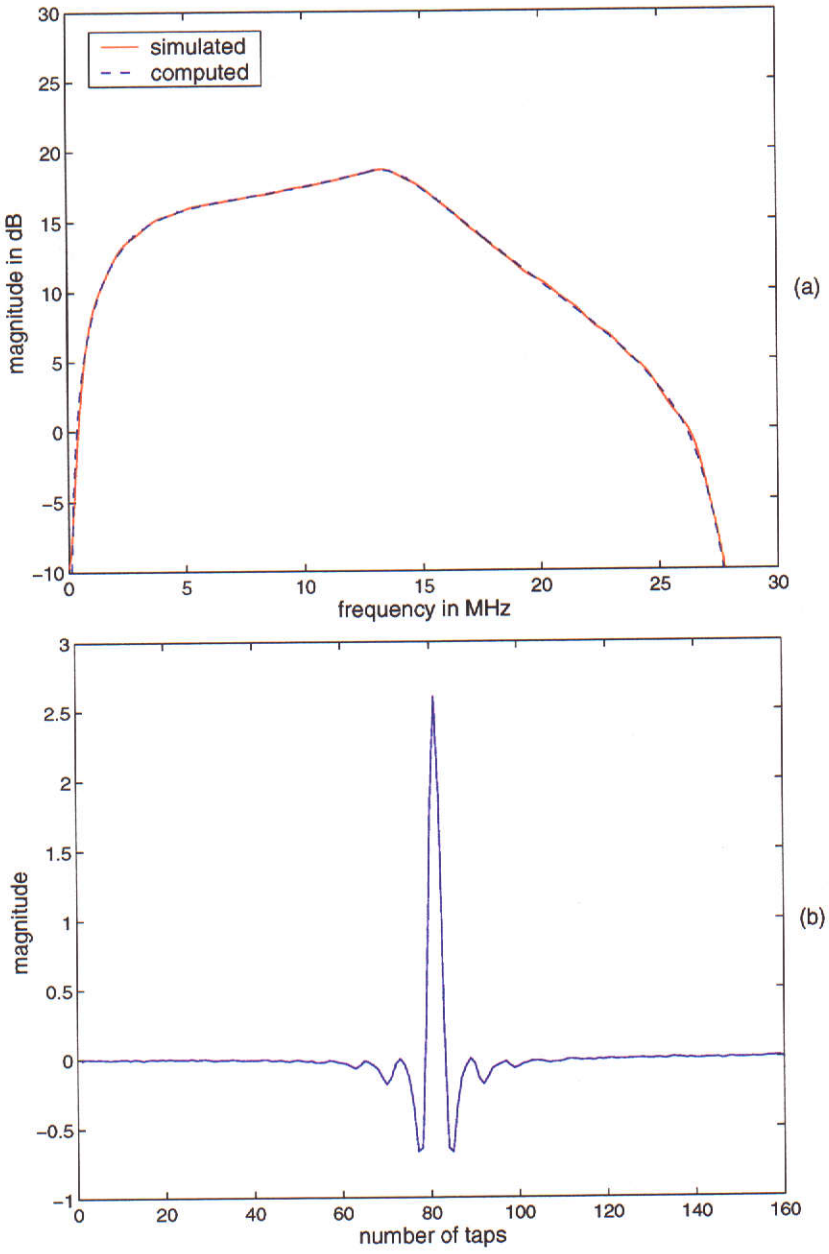

Figure 4.6: Linear CAP transceiver operating at 51.84 Mb/sec over 100 m of UTP-3 cable, 16–CAP scheme, $\alpha = 1.2$, and AWGN only, (a) magnitude of the optimum transfer function, (b) weights of the optimum FSE

the CAP receiver. We then gave a direct derivation. Using the Hilbert pair relationship in the derivation, we arrived at an elegant and more meaningful

MMSE expression, as well as the corresponding transfer functions of the optimum I and Q receiver filters. The new MMSE results were then specialised to the case where only stationary cross-talk is present. Simulation results were also given to support our theoretical analysis.

CHAPTER 5
MMSE PERFORMANCE – DFE CAP RECEIVER

5.1 Introduction

In Chapter 4, we analysed the MMSE performance of a linear CAP receiver operating in the presence of either stationary or data-like cross-talks, and background noise. In this chapter, we investigate the MMSE performance of another popular receiver structure. This structure employs a *non-linear* equaliser called the decision feedback equaliser (DFE) operating under the same channel conditions. The nonlinearity of the DFE stems from the feedback of the estimated symbols by a slicer which is non-linear in nature.

The type of issues that are addressed here belongs to the category of MMSE analysis of a MIMO system with a DFE which was studied by a number of authors. Among them, Duel-Hallen [48] studied the performance of a MIMO DFE for an asynchronous CDMA channel; Yang et al [49] presented results on the joint transmitter and receiver optimisation of a MIMO system with a DFE by minimising the *geometric mean-square* of the error at the slicer (defined as the determinant of the error covariance matrix); Tidestav et al [50] considered a MIMO DFE system with emphasis on the realizability of the feedforward filter in a IIR channel environment; and the performance of a finite-length MMSE-DFE in a MIMO environment was investigated in [51].

With respect to the approach used in the previous chapter, a different approach is used in the derivation of the optimum DFE in this chapter. Firstly, we study the MMSE performance of a *generic* multi-dimensional (multi–D)

CAP transceiver system using an ideal DFE in the receiver, in the presence of multiple data-like interferers. The results from the study is then applied to the *standard* 2–D CAP transceiver system with which we are familiar from the discussions in the previous chapters. In doing so, we gain additional understanding of the standard 2–D CAP transceiver system in relation to a multi-D CAP system.

The DFE receiver for a generic multi–D CAP transceiver system consists of a bank of receive filters, the number of which equals the dimension of the CAP line code, and a full cross-connected feedback *matrix filter*. Using *spectral matrix* factorisation, the optimum DFE and the corresponding MMSE at the slicer can be found. However, both results are in general difficult to compute, since they require the factorisation of the channel spectral matrix. In specialising the results to the standard 2–D CAP line codes, we exploit the Hilbert transform pair property of its transmit shaping filters to obtain an explicit expression of the MMSE. Here, we would like to stress that our aim is to find the MMSE performance of the DFE receiver for the 2–D CAP line code. The additional results on the multi–D CAP line code should be viewed in light of our objective in finding the results for the 2–D CAP transceiver system.

This chapter is organised as follows. First, we describe the model of a generic multi–D CAP system and formulate the problem of finding the transfer function of the optimum DFE and corresponding MMSE. Next, we show the derivations of the optimum DFE and the MMSE. Finally, we specialise the MMSE results to the standard 2–D CAP system.

5.2 System Model

The system model for a generic multi–D CAP transceiver system with data-like cross-talks is shown in Fig. 5.1, in which all quantities are assumed

to be real. Similar to the linear system model, this model also applies to the situation when cross-talk is modelled as anther Gaussian source. In this case, we set the cross-talk channels to zero, and spectrum of the channel noise in the figure now equals the combined spectra of both the background noise and the stationary cross-talk.

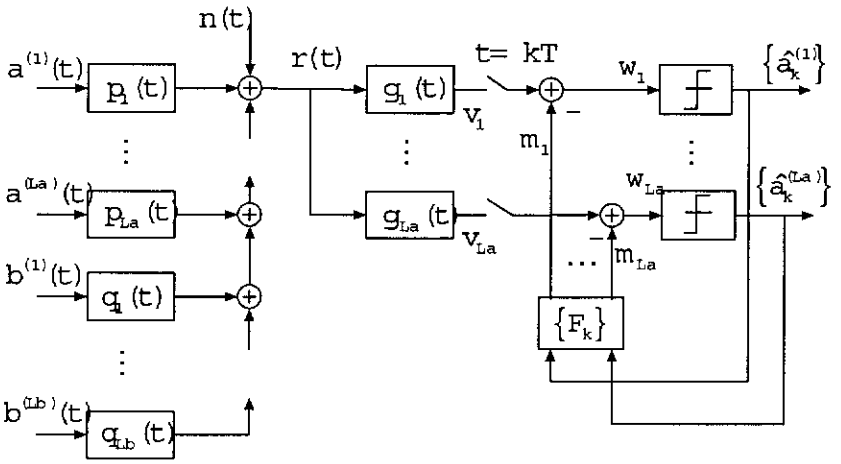

Figure 5.1: System model for a multi-dimensional CAP with data-like cross-talks

We define firstly the input data signal $\mathbf{a}(t)$ and cross-talk signal $\mathbf{b}(t)$ as follows

$$\mathbf{a}^T(t) \triangleq [a^{(1)}, \ldots, a^{(L_a)}](t) \quad \text{and} \quad \mathbf{b}^T(t) \triangleq [b^{(1)}, \ldots, b^{(L_b)}](t)$$

where L_a is the dimension of the CAP line code, L_b is the number of cross-talks

$$a^{(l)}(t) \triangleq \sum_n a_n^{(l)} \delta(t - nT) \quad \text{and} \quad b^{(l)}(t) \triangleq \sum_n b_n^{(l)} \delta(t - nT)$$

and where $a_n^{(l)}$ and $b_n^{(l)}$ denote the nth symbol in the lth input data symbol and interferer symbol sequence, respectively. The total input signal $\mathbf{u}(t)$ can

then be expressed as

$$\mathbf{u}^T(t) \triangleq [\mathbf{a}^T, \mathbf{b}^T](t).$$

Let $\mathbf{p}^T(t) \triangleq [p_1, \ldots, p_{L_a}](t)$ be the impulse responses of the equivalent data channels which consist of the shaping filters and transmission channel, $\mathbf{q}^T \triangleq [q_1, \ldots, q_{L_b}](t)$ be the impulse responses of the equivalent interference channels which consist of the shaping filters and cross-talk channels. Note that for the generic multi-D CAP system, the shaping filters can assume any pulse shapes. In other words, this structure is the most general among all the CAP-like structures. Combining all the impulse responses of the equivalent channel, we define

$$\mathbf{g}_t^T(t) \triangleq [p_1, \ldots, p_{L_a}, q_1, \ldots, q_{L_b}](t) = [\mathbf{p}^T, \mathbf{q}^T](t).$$

The received signal $r(t)$ is then given by

$$\begin{aligned} r(t) &\triangleq [\mathbf{g}_t^T \otimes \mathbf{u}](t) + n(t) \\ &= \sum_{l=-\infty}^{\infty} \mathbf{g}_t^T(t - lT)\mathbf{u}_l + n(t) \end{aligned}$$

where $\mathbf{u}_l \triangleq \mathbf{u}(lT)$, and $n(t)$ is the channel noise.

Let $\mathbf{g}_r^T(t) \triangleq [g_1, \ldots, g_{L_a}](t)$ denote the bank of receive filters. The output of $\mathbf{g}_r(t)$ is given by

$$\mathbf{v}^T(t) \triangleq [v_1, \ldots, v_{L_a}](t) = \mathbf{g}_r^T \otimes r(t).$$

At the sampling instant $t_s = kT$ where k is an arbitrary integer, the sampled signal before the slicer is given by

$$\mathbf{w}^T(kT) \triangleq [w_1, \ldots, w_{L_a}](kT) = \mathbf{v}^T(kT) - \mathbf{m}^T(kT)$$

where the feedback signal $\mathbf{m}(kT)$ is given by

$$\mathbf{m}(kT) \triangleq \sum_{n=1}^{\infty} \mathbf{F}_n \hat{\mathbf{a}}(kT - nT)$$

in which $\hat{\mathbf{a}}^T(nT) \triangleq [\hat{a}_n^{(1)}, \ldots, \hat{a}_n^{(L_a)}]$ denotes the estimated symbol vector at $t = nT$ and the matrix sequence $\{\mathbf{F}_n\}$ is the impulse response of the cross-connected feedback matrix filter $\mathbf{F}$. We denote the (i,j)th elements of $\mathbf{F}_n$ by f_n^{ij}, $1 \leq i,j \leq L_a$.

The error $\mathbf{e}(kT)$ at the input to the slicers is defined by

$$\mathbf{e}^T(kT) \triangleq [e_1, \ldots, e_{L_a}](kT) = \mathbf{w}^T(kT) - \mathbf{a}^T(kT)$$

and the MSE at the slicer is defined by

$$\varepsilon \triangleq E\left[\|\mathbf{e}(kT)\|_2^2\right]$$

where $\|\cdot\|_2$ denotes the mathematical 2-norm. The optimisation problem we addressed is the derivation of the optimum $\mathbf{g}_r(t)$ and $\mathbf{F}$ that minimise ε. Let $\mathbf{g}_o(t)$ and $\mathbf{F}_o$ denote the optimum receive and feedback filter respectively. Mathematically, they are the solutions to the following problem

$$[\mathbf{g}_o(t), \mathbf{F}_o] = \arg\left\{\min_{[\mathbf{g}_r(t),\mathbf{F}]} E\left[\|\mathbf{e}(kT)\|_2^2\right]\right\}. \tag{5.1}$$

5.3 MMSE Results – Data-Like Cross-Talks

5.3.1 MMSE – Multi-Dimensional CAP

Since all signals shown in Fig. 5.1 are real, we write the MSE as follows

$$\varepsilon = E\left[\mathbf{e}^T(kT)\mathbf{e}(kT)\right] = \mathrm{tr}\, E\left[\mathbf{e}(kT)\mathbf{e}^T(kT)\right] \tag{5.2}$$

where 'tr' denotes trace. Expanding $\mathbf{e}(kT)\mathbf{e}^T(kT)$ and using the assumptions (4.2), it is shown in Appendix C that

$$\mathbf{E}_e(\mathbf{g}_r, \mathbf{F}) = \mathbf{E}_f(\mathbf{g}_r, \mathbf{F}) + \mathbf{E}_g(\mathbf{g}_r) \tag{5.3}$$

where the matrices $\mathbf{E}_e$, $\mathbf{E}_f$ and $\mathbf{E}_g$ are defined by

$$\mathbf{E}_e \triangleq E[\mathbf{e}(kT)\mathbf{e}^T(kT)]\,\sigma^{-2}$$

$$\mathbf{E}_f \triangleq \sum_{l=1}^{\infty}\Big(\int \mathbf{g}_r(\tau)\mathbf{p}^T(-\tau+lT)\,\mathrm{d}\tau - \mathbf{F}_l\Big)\Big(\int \mathbf{g}_r(\tau)\mathbf{p}^T(-\tau+lT)\,\mathrm{d}\tau - \mathbf{F}_l\Big)^T \tag{5.4}$$

and

$$\begin{aligned}\mathbf{E}_g \triangleq &\iint A(\tau_1,\tau_2)\mathbf{g}_r(\tau_1)\mathbf{g}_r^T(\tau_2)\,\mathrm{d}\tau_1\,\mathrm{d}\tau_2 \\ &- \int \mathbf{g}_r(\tau)\mathbf{p}^T(-\tau)\,\mathrm{d}\tau - \int \mathbf{p}(-\tau)\mathbf{g}_r^T(\tau)\,\mathrm{d}\tau + \mathbf{I}.\end{aligned}$$

The scalar $A(\tau_1, \tau_2)$ is defined by

$$\begin{aligned}A(\tau_1,\tau_2) \triangleq &\sum_{m=-\infty}^{\infty} \mathbf{q}^T(-\tau_1 - mT)\mathbf{q}(-\tau_2 - mT) \\ &+ \sum_{m=-\infty}^{0} \mathbf{p}^T(-\tau_1 - mT)\mathbf{p}(-\tau_2 - mT) + \sigma^{-2}r_n(\tau_1 - \tau_2)\end{aligned}$$

where $r_n(\tau) \triangleq E[n(t+\tau)n(t)]$.

From (5.3), the MMSE is found in two steps as follows. Firstly, we fix the receive filter $\mathbf{g}_r(t)$ and optimise with respect to the feedback matrix filter $\mathbf{F}$. Given the optimum $\mathbf{F}_o$, the receive filter $\mathbf{g}_r(t)$ is then optimised. The trace of $\mathbf{E}_e$ in (5.3) is minimised when the trace of $\mathbf{E}_f$ is minimised, since $\mathbf{E}_g$ does not depend on $\mathbf{F}$. It is clear from (5.4) that the optimum filter $\mathbf{F}_o$ is selected when $\mathbf{E}_f = \mathbf{0}$. That is, the lth coefficient of the optimum filter $\mathbf{F}_o$ must satisfy

$$\mathbf{F}_{o,l} = \int \mathbf{g}_r(\tau)\mathbf{p}^T(lT-\tau)\,\mathrm{d}\tau \qquad \text{for} \quad l \geq 1. \tag{5.5}$$

This equation shows that, due to the full cross-connected structure, the optimum feedback filter $\mathbf{F}_o$ completely cancels out the postcursor ISI due to the equivalent data channel. It, however, has no effect on the cross-talk signal.

We next solve for the optimum receive filter. Let $\mathcal{A}$ be an integral operator with kernel $A(\tau_1, \tau_2)$ and we write

$$[\mathcal{A}\mathbf{g}_r](t) \triangleq \int A(t,\tau)\mathbf{g}_r(\tau)\,\mathrm{d}\tau.$$

Then

$$\begin{aligned}\mathbf{E}_g = &\int [\mathcal{A}\mathbf{g}_r](t)\mathbf{g}_r^T(t)\,\mathrm{d}t - \int \mathbf{g}_r(t)\mathbf{p}^T(-t)\,\mathrm{d}t \\ &- \int \mathbf{p}(-t)\mathbf{g}_r^T(t)\,\mathrm{d}t + \mathbf{I}. \end{aligned} \tag{5.6}$$

Define matrix $\mathbf{J}$ as follows

$$\mathbf{J}(t, \mathbf{g}_r(t)) \triangleq [\mathcal{A}\mathbf{g}_r](t)\mathbf{g}_r^T(t) - \mathbf{g}_r(t)\mathbf{p}^T(-t) - \mathbf{p}(-t)\mathbf{g}_r^T(t) + \delta(t)\mathbf{I}.$$

Then

$$tr\mathbf{E}_g = \int \mathrm{tr}\,\mathbf{J}(t, \mathbf{g}_r(t))\,\mathrm{d}t. \tag{5.7}$$

Thus, the optimisation problem becomes a one-dimensional variational problem [44]. A brief derivation of the optimum function $\mathbf{g}_o(t)$ is described below.

Consider the family of functions which contains the extremal $\mathbf{g}_o(t)$

$$\mathbf{g}(t) \triangleq \mathbf{g}_o(t) + \mu\mathbf{o}(t)$$

where the vector $\mathbf{o}(t)$ is some suitable point function and μ is a scalar constant. Note that in doing so, we restrict $\mathbf{g}(t)$ to a subset of the set of admissible functions. However, it is clear that this subset of functions must contain the

extremal when $\mu = 0$. For a fixed $\mathbf{o}(t)$, from (5.7), we write

$$\operatorname{tr} \mathbf{E}_g(\mu) = \operatorname{tr} \int \mathbf{J}[t, \mathbf{g}_o(t) + \mu \mathbf{o}(t)] \, \mathrm{d}t. \tag{5.8}$$

The stationary function can be found by taking the derivative with respect to μ at $\mu = 0$ and setting the result to zero. Using *Leibniz's rule* for differentiation under the integral sign, we have

$$\frac{d}{d\mu}[\operatorname{tr} \mathbf{E}_g(\mu)] = \int \frac{\partial}{\partial \mu} \operatorname{tr} \mathbf{J}[t, \mathbf{g}_o(t) + \mu \mathbf{o}(t)] \, \mathrm{d}t = 0. \tag{5.9}$$

Since $A(t, \tau)$ is symmetric, after some algebra, (5.9) simplifies to

$$\begin{aligned} &\frac{d}{d\mu}[\operatorname{tr} \mathbf{E}_g(\mu)]\Big|_{\mu=0} = \\ &2 \int \mathbf{o}^T(\tau) \Big\{ \int A(t, \tau) \mathbf{g}_o(t) \, \mathrm{d}t - \mathbf{p}(-\tau) \Big\} \, \mathrm{d}\tau = 0. \end{aligned} \tag{5.10}$$

By the *fundamental lemma* of the calculus of variations [44], the stationary function, and hence the extremal $\mathbf{g}_o(t)$ in (5.10), must satisfy the following condition

$$\int A(t, \tau) \mathbf{g}_o(t) \, \mathrm{d}t = \mathbf{p}(-\tau). \tag{5.11}$$

Substituting (5.11) into (5.6), we find that the minimum $\operatorname{tr} \mathbf{E}_g$ is given by

$$\operatorname{tr}[\mathbf{E}_g]_{\min} = L_a - \int \mathbf{p}^T(-t) \mathbf{g}_o(t) \, \mathrm{d}t. \tag{5.12}$$

Before solving for the optimum receive filters $\mathbf{g}_o(t)$, we first investigate its structure. Expanding the LHS of (5.11) and after some simplification, we get

$$\mathbf{p}(-t) = \sum_{l=-\infty}^{\infty} \bar{\mathbf{K}}_l \mathbf{q}(lT - t) + \sum_{l=-\infty}^{0} \mathbf{K}_l \mathbf{p}(lT - t) + \int r_{n'}(t - \tau) \mathbf{g}_o(\tau) \, \mathrm{d}\tau \tag{5.13}$$

where $r_{n'} \triangleq \sigma^{-2} r_n$ and

$$\bar{\mathbf{K}}_l \triangleq \bar{\mathbf{K}}(lT) \triangleq [\mathbf{g}_o \otimes \mathbf{q}^T](lT) \quad \text{and} \quad \mathbf{K}_l \triangleq \mathbf{K}(lT) \triangleq [\mathbf{g}_o \otimes \mathbf{p}^T](lT).$$

Re-writing (5.13) in the following form

$$\begin{aligned} &\int r_{n'}(t-\tau)\mathbf{g}_o(\tau)\,\mathrm{d}\tau \\ &= \sum_{l=-\infty}^{0} (\mathbf{I}\delta_{l0} - \mathbf{K}_l)\,\mathbf{p}(lT-t) + \sum_{l=-\infty}^{\infty} \left(-\bar{\mathbf{K}}_l\right)\mathbf{q}(lT-t). \end{aligned} \tag{5.14}$$

Equation (5.14) reveals the structure of the optimum receive filters. On the RHS, the first summation corresponds to the cascade of the matched filters $\mathbf{p}(-t)$ and *anti-causal tapped-delay-line* filters with coefficients $\{\mathbf{I}\delta_{l0} - \mathbf{K}_l\}$ for $l \leq 0$. The second summation is interpreted as a cascade of the matched filters $\mathbf{q}(-t)$ and tapped-delay-line filters with coefficients $\{-\bar{\mathbf{K}}_l\}$ for $-\infty < l < \infty$. The LHS of the equation is the convolution of the auto-correlation function of the channel noise and the optimum receive filters. A block diagram description of the optimum receive filters $\mathbf{g}_o(t)$ is shown in Fig. 5.2, where the matched filters are normalised by the scaled spectrum of the channel noise and the tapped-delay-line filters are implemented in digital form.

Next, we derive the explicit formula for the optimum receive filter $\mathbf{g}_o(t)$ and an expression for the MMSE at the slicer. Let $\mathbf{P}(f) \triangleq \mathcal{F}[\mathbf{p}(t)]$ and $\mathbf{Q}(f) \triangleq \mathcal{F}[\mathbf{q}(t)]$

$$\mathbf{K}_-(e^{j\theta}) \triangleq \sum_{l=-\infty}^{0} \mathbf{K}_l e^{-jl\theta} \quad \text{and} \quad \bar{\mathbf{K}}(e^{j\theta}) \triangleq \sum_{l=-\infty}^{\infty} \bar{\mathbf{K}}_l e^{-jl\theta}$$

where $\theta \triangleq 2\pi f T$. We use $(\cdot)_-$ to denote the transformation of a sequence with subscripts from $-\infty$ to 0. A related operator $(\cdot)_{++}$ denotes the transformation of a sequence with subscripts from 1 to ∞, e.g., $\mathbf{K}_{++}(e^{j\theta}) \triangleq \sum_{l=1}^{\infty} \mathbf{K}_l e^{-jl\theta}$.

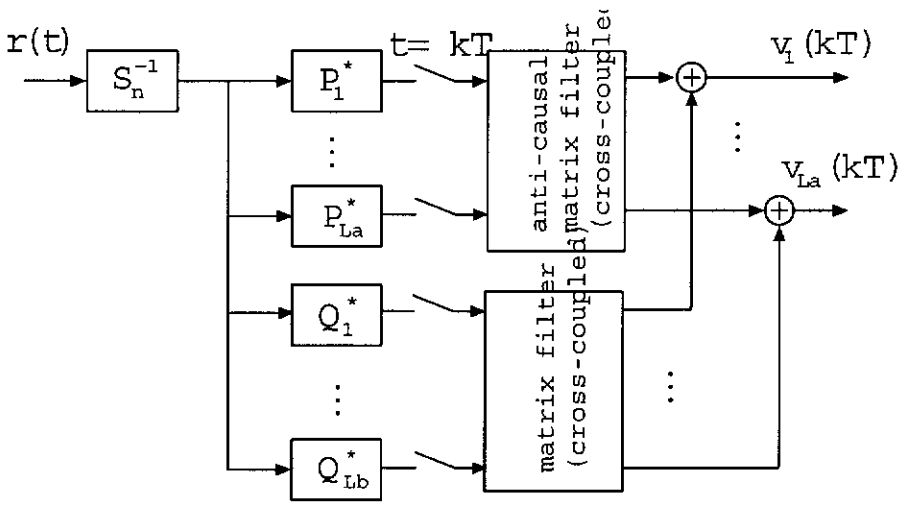

Figure 5.2: Equivalent structure for the optimum feedforward filters of a DFE

Taking Fourier transforms of both sides of (5.13), we get

$$\mathbf{P}^*(f) = \bar{\mathbf{K}}(e^{j\theta})\mathbf{Q}^*(f) + \mathbf{K}_-(e^{j\theta})\mathbf{P}^*(f) + S_{n'}(f)\mathbf{G}_o(f) \tag{5.15}$$

where $S_{n'}(f) \triangleq \mathcal{F}[r_{n'}(t)]$ and $\mathbf{G}_o(f) \triangleq \mathcal{F}[\mathbf{g}_o(t)]$.

Now, let $\bar{f}$ denote frequency within the *Nyquist interval* $[-\frac{1}{2T}, \frac{1}{2T}]$. Then, any frequency point f can be written as $f = \bar{f} + k/T$ where k is some integer (more on k later). Replacing f with $\bar{f} + k/T$ in (5.15), we obtain, after some simplification

$$\begin{aligned}\mathbf{P}^*(\bar{f} + \frac{k}{T}) = \frac{1}{T}\sum_{l=-\infty}^{\infty} \mathbf{G}_o(\bar{f} + \frac{l}{T})\mathbf{Q}^T(\bar{f} + \frac{l}{T})\mathbf{Q}^*(\bar{f} + \frac{k}{T}) \\ + \mathbf{K}_-(e^{j\theta})\mathbf{P}^*(\bar{f} + \frac{k}{T}) + S_{n'}(\bar{f} + \frac{k}{T})\mathbf{G}_o(\bar{f} + \frac{k}{T})\end{aligned} \tag{5.16}$$

where we made use of the fact that $\mathbf{K}_-(e^{j\theta})$ is periodic in θ with a period of 2π, or equivalently periodic in f with a period of $1/T$, and $\bar{\mathbf{K}}(e^{j\theta})$ was replaced by the RHS of

$$\bar{\mathbf{K}}(e^{j\theta}) = \frac{1}{T}\sum_{l=-\infty}^{\infty} \mathbf{G}_o(\bar{f} + \frac{l}{T})\mathbf{Q}^T(\bar{f} + \frac{l}{T}). \tag{5.17}$$

Recall now the definition given in Chapter 4

$$W_{k,l}(\bar{f}) \triangleq \frac{1}{T}\mathbf{Q}^H(\bar{f}+\frac{k}{T})\mathbf{Q}(\bar{f}+\frac{l}{T}) + S_{n'}(\bar{f}+\frac{k}{T})\delta_{kl}$$

From (5.16), we obtain for integer k

$$\mathbf{P}^*(\bar{f}+\frac{k}{T}) = \sum_{l=-\infty}^{\infty} W^*_{k,l}(\bar{f})\mathbf{G}_o(\bar{f}+\frac{l}{T}) + \mathbf{K}_-(e^{j\theta})\mathbf{P}^*(\bar{f}+\frac{k}{T}). \tag{5.18}$$

Note that since $|\bar{f}| \leq \frac{1}{2T}$, the frequency support of this equation is determined by the integer k. Combining all such equations for values of $|k| \leqslant K$ where K is selected such that the system bandwidth $B_{sys} \leq \frac{1}{2T} + K/T$, and define

$$\check{\mathbf{P}}(\bar{f}) \triangleq \begin{bmatrix} \mathbf{P}^T(\bar{f}-\frac{K}{T}) \\ \mathbf{P}^T(\bar{f}-\frac{K-1}{T}) \\ \vdots \\ \mathbf{P}^T(\bar{f}+\frac{K}{T}) \end{bmatrix} \quad \text{and} \quad \check{\mathbf{G}}_o(\bar{f}) \triangleq \begin{bmatrix} \mathbf{G}^T(\bar{f}-\frac{K}{T}) \\ \mathbf{G}^T(\bar{f}-\frac{K-1}{T}) \\ \vdots \\ \mathbf{G}^T(\bar{f}+\frac{K}{T}) \end{bmatrix}$$

then,

$$\check{\mathbf{P}}^*(\bar{f}) = \check{\mathbf{P}}^*(\bar{f})\mathbf{K}_-^T(e^{j\theta}) + \mathbf{W}^*\check{\mathbf{G}}_o(\bar{f}) \tag{5.19}$$

where the matrix $\mathbf{W} \triangleq [W_{k,l}](\bar{f})$ for $-K \leq l,k \leq K$. It is easily shown that $\mathbf{W}$ is Hermitian and positive definite assuming $S_n(f) > 0$ (or equals zero but only at isolated frequency points) for $|f| \leq B_{sys}$. Hence,

$$\check{\mathbf{G}}_o(\bar{f}) = \mathbf{W}^{*-1}(\bar{f})\check{\mathbf{P}}^*(\bar{f})[\mathbf{I} - \mathbf{K}_-^T(e^{j\theta})]. \tag{5.20}$$

The anti-causal coefficients of the function $\mathbf{K}_-(e^{j\theta})$ can be solved using spectral matrix factorisation as follows.

From (5.20), pre-multiplying both side by $\frac{1}{T}\check{\mathbf{P}}^T(\bar{f})$ and defining $\mathbf{M} \triangleq$

$\frac{1}{T}\check{\mathbf{P}}^H(\bar{f})\mathbf{W}^{-1}\check{\mathbf{P}}(\bar{f})$[1], and using the fact that $\mathbf{K}(e^{j\theta}) = \frac{1}{T}\check{\mathbf{G}}_o^T(\bar{f})\check{\mathbf{P}}(\bar{f})$, we have

$$\mathbf{K}(e^{j\theta}) = [\mathbf{I} - \mathbf{K}_-(e^{j\theta})]\mathbf{M}. \tag{5.21}$$

From this equation, it is clear that $\mathbf{M}$ may be thought as a function of $e^{j\theta}$ and in the following, we write $\mathbf{M}(e^{j\theta})$ instead. Express $\mathbf{K}(e^{j\theta})$ as $\mathbf{K} = \mathbf{K}_-(e^{j\theta}) + \mathbf{K}_{++}(e^{j\theta})$. Then

$$\mathbf{K}_-(e^{j\theta})\left[\mathbf{I} + \mathbf{M}(e^{j\theta})\right] + \mathbf{K}_{++}(e^{j\theta}) = \mathbf{M}(e^{j\theta}).$$

In the z domain, we express $\mathbf{M}(e^{j\theta})$, $\mathbf{K}_-(e^{j\theta})$ and $\mathbf{K}_{++}(e^{j\theta})$ as $\mathbf{M}(z)$, $\mathbf{K}_-(z)$ and $\mathbf{K}_{++}(z)$ respectively. Let $\mathbf{\Phi}(z) \triangleq \mathbf{I} + \mathbf{M}(z)$, then

$$\mathbf{K}_{++}(z) + \mathbf{K}_-(z)\mathbf{\Phi}(z) = \mathbf{M}(z). \tag{5.22}$$

Note that $\mathbf{\Phi}(z)$ may be viewed as a matrix polynomial in z and its matrix coefficients are real, since the underlying system model contains only real signals. From spectral matrix factorisation, we may write

$$\mathbf{\Phi}(z) = \mathbf{H}(z^{-1})\mathbf{H}^T(z) \tag{5.23}$$

where $\mathbf{H}(z) \triangleq \sum_{l=0}^{\infty} \mathbf{\Gamma}_l z^{-l}$ for some matrix coefficients $\mathbf{\Gamma}_l$ which are determined by the actual factorisation algorithms. Note that $\mathbf{H}(z)$ is causal and all the poles and zeros of its determinant are inside the unit circle, and hence its inverse $\mathbf{H}^{-1}(z)$ is also causal and stable. Also, $\mathbf{H}(z)$ is unique up to an unitary matrix post-multiplication [52, 53].

Substituting (5.23) into (5.22), we get

$$\mathbf{K}_{++}(z)\mathbf{H}^T(z)^{-1} + \mathbf{K}_-(z)\mathbf{H}(z^{-1}) = \mathbf{H}(z^{-1}) - \mathbf{H}^T(z)^{-1}. \tag{5.24}$$

[1]Thus $\mathbf{M}$ is also positive definite

Equating coefficients with the like powers of z on both sides of (5.24), we get

$$\mathbf{K}_{-}(z) = \mathbf{I} - [\mathbf{\Gamma}_0^T]^{-1}\mathbf{H}(z^{-1})^{-1}. \tag{5.25}$$

Finally, substituting (5.25) into (5.21), we obtain in z notation

$$\begin{aligned}\mathbf{K}(z) =& [\mathbf{\Gamma}_0^T]^{-1}\mathbf{H}(z^{-1})^{-1}\mathbf{M}(z) \\ =& [\mathbf{\Gamma}_0^T]^{-1}\mathbf{H}(z^{-1})^{-1}[\mathbf{H}(z^{-1})\mathbf{H}^T(z) - \mathbf{I}] \\ =& [\mathbf{\Gamma}_0^T]^{-1}[\mathbf{H}^T(z) - \mathbf{H}(z^{-1})^{-1}].\end{aligned} \tag{5.26}$$

From our previous discussions, we see that, given the optimum solutions $\mathbf{F}_o$ and $\mathbf{g}_o$, the MMSE is given by

$$\begin{aligned}\varepsilon'_{\min} &= \operatorname{tr}\mathbf{E}_e(\mathbf{g}_o, \mathbf{F}_o) \\ &= \operatorname{tr}\mathbf{E}_f(\mathbf{g}_o, \mathbf{F}_o) + \operatorname{tr}\mathbf{E}_g(\mathbf{g}_o) = \operatorname{tr}\mathbf{E}_g(\mathbf{g}_o)\end{aligned} \tag{5.27}$$

where $\varepsilon'_{min} \triangleq \varepsilon_{min}/\sigma^2$. Substituting (5.12) into (5.27), we have

$$\varepsilon'_{\min} = L_a - \int \mathbf{p}^T(-t)\mathbf{g}_o(t)\,\mathrm{d}t = L_a - \operatorname{tr}\mathbf{K}_0 \tag{5.28}$$

Further, from (5.26)

$$\mathbf{K}_0 = [\mathbf{\Gamma}_0^T]^{-1}[\mathbf{\Gamma}_0^T - \mathbf{\Gamma}_0^{-1}] = \mathbf{I} - [\mathbf{\Gamma}_0\mathbf{\Gamma}_0^T]^{-1}. \tag{5.29}$$

thus,

$$\varepsilon'_{\min} = \operatorname{tr}[\mathbf{\Gamma}_0\mathbf{\Gamma}_0^T]^{-1}. \tag{5.30}$$

In summary, we have completely solved the optimisation problem for a generic multi-dimensional CAP transceiver system, operating in the presence of data-like cross-talks. The optimum receive filter $\mathbf{g}_o(t)$ and ideal feedback filter $\mathbf{F}_o$ are given by (5.5), (5.20) and (5.25), and the corresponding MMSE is given by (5.30). From these equations, it is clear that both the optimum DFE and the

MMSE depend on the factorisation of the spectral matrix $\mathbf{\Phi}(z)$. Algorithms for such factorisation exist, as shown in [52] [53] for spectral matrices in the form of a rational function of z.

5.3.2 MMSE for Standard 2–D CAP

In the case of the standard 2–D CAP schemes, the two transmit filters form a Hilbert transform pair [8]. In this section, we show that it is possible to exploit this condition to derive an explicit expression for the MMSE without actually performing the spectral matrix factorisation.

In his treatment on the most general form of a QAM system, Falconer [54] showed that for a passband QAM system, explicit factorisation of the spectral matrix may be avoided in the MMSE expression. We show that the same is also true for standard 2–D CAP, in the presence of data-like cross-talks.

Define the matrix $\mathbf{E}_\gamma \triangleq \left[\mathbf{\Gamma}_0\mathbf{\Gamma}_0^T\right]^{-1}$. Note that for standard 2–D CAP, $\mathbf{E}_\gamma$ is a (2×2) symmetric matrix. Under this situation, it can be shown that

$$\mathrm{tr}[\mathbf{E}_\gamma] \geq 2\sqrt{\det(\mathbf{E}_\gamma)} \tag{5.31}$$

which holds with equality if and only if $\mathbf{E}_\gamma$ is a scalar multiples of the identity matrix $\mathbf{I}$, or so-called *scalar matrix* [54]. From (5.23), it follows that

$$\det[\mathbf{\Phi}(e^{j\theta})] = \det[\mathbf{H}(e^{-j\theta})]\det[\mathbf{H}^T(e^{j\theta})]. \tag{5.32}$$

Hence, from one-dimensional factorisation

$$\det[\mathbf{E}_\gamma] = \exp\left\{-\frac{1}{2\pi}\int_{-\pi}^{\pi} \ln\left[\det\mathbf{\Phi}(e^{j\theta})\right] d\theta\right\}. \tag{5.33}$$

We now prove that $\mathbf{E}_\gamma$ is a scalar matrix. For the standard 2–D CAP scheme, the inphase and quadrature shaping filters form a Hilbert transform pair. Denote the impulse responses of the equivalent I and Q data channels by

$p(t) \triangleq p_1(t)$ and $\tilde{p}(t) \triangleq p_2(t)$ respectively. Their Fourier transforms, denoted by $P(f) \triangleq \mathcal{F}[p(t)]$ and $\tilde{P}(f) \triangleq \mathcal{F}[\tilde{p}(t)]$, have the following relationship

$$\tilde{P}(f) = (-j)\,\mathrm{sgn}(f)P(f) \quad \text{for} \quad -\infty < f < \infty \tag{5.34}$$

Define two new vectors

$$\mathbf{P}(\bar{f}) \triangleq \begin{bmatrix} P(\bar{f} - \frac{K}{T}) \\ P(\bar{f} - \frac{K-1}{T}) \\ \vdots \\ P(\bar{f} + \frac{K}{T}) \end{bmatrix} \quad \text{and} \quad \tilde{\mathbf{P}}(\bar{f}) \triangleq \begin{bmatrix} \tilde{P}(\bar{f} - \frac{K}{T}) \\ \tilde{P}(\bar{f} - \frac{K-1}{T}) \\ \vdots \\ \tilde{P}(\bar{f} + \frac{K}{T}) \end{bmatrix}.$$

In terms of $\mathbf{P}(\bar{f})$ and $\tilde{\mathbf{P}}(\bar{f})$, the matrix $\check{\mathbf{P}}(\bar{f})$ and $\mathbf{M}$ may be re-written as

$$\check{\mathbf{P}} = \left[\mathbf{P}, \tilde{\mathbf{P}}\right] \quad \text{and} \quad \mathbf{M} = \frac{1}{T}\begin{bmatrix} \mathbf{P}^H\mathbf{W}^{-1}\mathbf{P} & \mathbf{P}^H\mathbf{W}^{-1}\tilde{\mathbf{P}} \\ \tilde{\mathbf{P}}^H\mathbf{W}^{-1}\mathbf{P} & \tilde{\mathbf{P}}^H\mathbf{W}^{-1}\tilde{\mathbf{P}} \end{bmatrix}. \tag{5.35}$$

Again, as in Chapter 4, we make use of the Hilbert pair relationship of the standard 2–D CAP receiver. Using (4.19) and (4.20), we have the diagonal terms of $\mathbf{M}$ satisfy

$$\tilde{\mathbf{P}}^H\mathbf{W}^{-1}\tilde{\mathbf{P}} = \mathbf{P}^H\Lambda^H\mathbf{W}^{-1}\Lambda\mathbf{P} = \mathbf{P}^H\mathbf{W}^{-1}\mathbf{P}. \tag{5.36}$$

Next, assume the non-diagonal term $\mathbf{P}^H\mathbf{W}^{-1}\tilde{\mathbf{P}}$ on the RHS of $\mathbf{M}$ in (5.35) equals $a' + jb'$ where a' and b' are some real numbers. The sum of the non-diagonal terms of the Hermitian matrix $\mathbf{M}$ is given by

$$\begin{aligned} &\mathbf{P}^H\mathbf{W}^{-1}\tilde{\mathbf{P}} + \tilde{\mathbf{P}}^H\mathbf{W}^{-1}\mathbf{P} = 2a' \\ &= \mathbf{P}^H\mathbf{W}^{-1}\Lambda\mathbf{P} + \mathbf{P}^H\Lambda^H\mathbf{W}^{-1}\mathbf{P} \\ &= \mathbf{P}^H\mathbf{W}^{-1}(\Lambda^H + \Lambda)\mathbf{P} = 0. \end{aligned} \tag{5.37}$$

The matrix $\mathbf{\Phi}(e^{j\theta})$ thus has the form

$$\mathbf{\Phi} = \mathbf{I} + \mathbf{M} = \begin{bmatrix} R & jb \\ -jb & R \end{bmatrix} \tag{5.38}$$

where

$$R(\bar{f}) \triangleq \frac{1}{T}\mathbf{P}^H\mathbf{W}^{-1}\mathbf{P} + 1 \quad \text{and} \quad b(\bar{f}) \triangleq \frac{1}{T}\,\mathrm{Im}\left\{\mathbf{P}^H\mathbf{W}^{-1}\tilde{\mathbf{P}}\right\}$$

Note that since $\mathbf{W}$ is positive definite, $R(\bar{f}) > 0$. Also, it is easily shown that $R(\bar{f})$ is even and $b(\bar{f})$ is odd. Therefore, using arguments similar to those in [54], we conclude that $\mathbf{E}_\gamma$ is indeed a scalar matrix and

$$\mathrm{tr}[\mathbf{E}_\gamma] = 2\sqrt{\det(\mathbf{E}_\gamma)}. \tag{5.39}$$

For convenience, the derivation of (5.39) is given in Appendix D.

From (5.38), we recognise that

$$\det(\mathbf{\Phi}) = (R+b)(R-b) > 0. \tag{5.40}$$

Since $R(\bar{f}) > 0$ from definition, both $(R+b)$ and $(R-b)$ are positive. Re-write (5.40) as follows

$$\begin{aligned} &\ln\left[\det\left(\mathbf{\Phi}(e^{j\theta})\right)\right] \\ &= \ln\left[R(\bar{f}) + b(\bar{f})\right] + \ln\left[R(\bar{f}) - b(\bar{f})\right]. \end{aligned} \tag{5.41}$$

Observe that since $R(\bar{f})$ is even and $b(\bar{f})$ is odd, hence

$$\int_{-\pi}^{\pi} \ln\left[R(\bar{f}) - b(\bar{f})\right] d\theta = \int_{-\pi}^{\pi} \ln\left[R(\bar{f}) + b(\bar{f})\right] d\theta. \tag{5.42}$$

Therefore, from (5.33)

$$\det(\mathbf{E}_\gamma) = \exp\left\{-2T\int_{-\frac{1}{2T}}^{\frac{1}{2T}} \ln\left[R(f) + b(f)\right] df\right\}. \tag{5.43}$$

Finally, from (5.30), (5.39) and the above equation, the MMSE of a standard 2–D CAP receiver is given by

$$\varepsilon'_{\min} = 2\exp\left\{-T\int_{-\frac{1}{2T}}^{\frac{1}{2T}} \ln\left[R(f)+b(f)\right]df\right\}. \tag{5.44}$$

Define the SNR at the slicer as

$$\mathrm{SNR}_o \triangleq \frac{2}{\varepsilon'_{\min}}.$$

Then from (5.44), we have

$$\mathrm{SNR}_o = \exp\left\{T\int_{-\frac{1}{2T}}^{\frac{1}{2T}} \ln\left[R(f)+b(f)\right]df\right\}. \tag{5.45}$$

5.4 MMSE Results – Stationary Cross-Talk

As in Section 4.4, if the total interference of all cross-talks is modelled by a stationary Gaussian noise, then we simply combine it with the background noise and set the cross-talk channels zero, i.e., $Q_l(f) = 0$ for $1 \le l \le L_b$. Accordingly, the elements of $\mathbf{W}$ become

$$W_{k,l} = S_{n'}(\bar{f}+\frac{k}{T})\delta_{kl}, \qquad -K \le l,k \le K \tag{5.46}$$

and it follows that

$$\mathbf{P}^H\mathbf{W}^{-1}\mathbf{P} = \sum_{k=-K}^{K} S_{n'}^{-1}(\bar{f}+\frac{k}{T})|P(\bar{f}+\frac{k}{T})|^2 \tag{5.47a}$$

$$\begin{aligned}\mathbf{P}^H\mathbf{W}^{-1}\tilde{\mathbf{P}} &= \mathbf{P}^H\mathbf{W}^{-1}\mathbf{\Lambda}\mathbf{P}\\ &= (-j)\sum_{k=-K}^{K} \mathrm{sgn}(\bar{f}+\frac{k}{T})S_{n'}(\bar{f}+\frac{k}{T})|P(\bar{f}+\frac{k}{T})|^2\end{aligned} \tag{5.47b}$$

Therefore, using (5.47), we have

$$R(\bar{f}) - b(\bar{f}) = \frac{1}{T}\left[2\sum_{k=0}^{K}\Gamma(\bar{f}+\frac{k}{T}) + [1+\mathrm{sgn}(\bar{f})]\Gamma(\bar{f})\right] + 1 \tag{5.48}$$

where $\Gamma(f) = |P(f)|^2 S_{n'}^{-1}(f)$ same as that defined in Chapter 4. Using the same argument as from (4.24) to (4.27), we conclude that the MMSE expression for the stationary noise only environment is given by

$$\varepsilon' = \exp\left\{-T \int_0^{\frac{1}{T}} \ln\left[\frac{2}{T}\sum_{k=0}^{K} \Gamma(f + \frac{k}{T}) + 1\right] df\right\} \tag{5.49}$$

Similar to the MMSE of the linear CAP receiver, we can re-write the MMSE expression of (5.49) in terms of the input $\mathrm{SNR}_n(f)$ which now has the same spectral shape as the sum of the spectra of the stationary cross-talk signals and background noise, i.e.,

$$\varepsilon' = \exp\left\{-T \int_0^{\frac{1}{T}} \ln\left[\sum_{k=0}^{K} \mathrm{SNR}_n(f + \frac{k}{T}) + 1\right] df\right\} \tag{5.50}$$

In the case where the noise spectrum is white, i.e., $S_n(f) = N_0$, (5.50) simplifies to

$$\varepsilon' = \exp\left\{T \int_0^{\frac{1}{T}} \ln\left[\frac{N_0}{\frac{2\sigma^2}{T}\sum_{k=0}^{K}|P(f + \frac{k}{T})|^2 + N_0}\right] df\right\} \tag{5.51}$$

5.5 Simulation

5.5.1 System Setup

The simulation model for a 2–D CAP transceiver system with a DFE is shown in Fig. 5.3. The CAP transmitter, and transmission and cross-talk channels are identical to those used in Chapter 4, except that we simulate the system performance for 4 different roll-off factors (α). As before, the relative phase between the received signal and interference is also fixed to $\phi = 0$ and the effect of different ϕ on the MMSE performance is left to the following chapter.

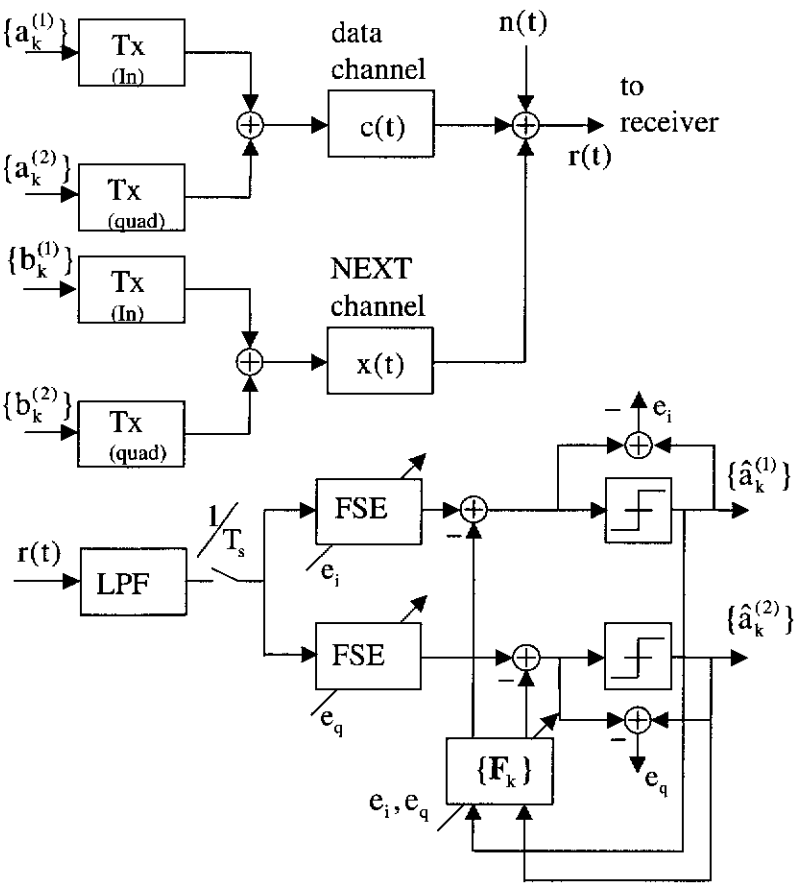

Figure 5.3: Simulation model of a DFE CAP transceiver system, one data-like NEXT

On the receiver side, the optimum analog feedforward (FF) filters are simulated by two adaptive FSEs, and the ideal feedback (FB) matrix filter is simulated by four cross-connected, baud-spaced, adaptive, finite-length equalisers. Both the FF and FB filters have the same length of $25T$. As before, the sampling rate of the FSEs is selected such that there is no aliasing in the input signal samples. The standard LMS algorithm is used for the adaptive DFEs. System performance is evaluated in terms of the SNR at the slicer.

Table 5.1: SNR_o (dB) at slicer for 100 m of UTP–3 cable in the presence of one self-NEXT and AWGN

$R = 51.48$ Mb/s, $\mathrm{SNR}_m = 30$ dB, $\phi = 0$				
	$\alpha = 0.2$	$\alpha = 0.7$	$\alpha = 1$	$\alpha = 1.5$
Computed	22.65	23.92	25.37	26.16
Simulated	21.65	23.21	24.79	26.06

5.5.2 Results

Table 5.1 shows both the computed and simulated values of SNR_o for 4 different roll-off factors. We notice that as the excess bandwidth increases the performance also improves. From $\alpha = 0.2$ to 1.5, the improvement is about 4.5 dB which is quite significant for many applications. However, the tradeoff of this improvement is that the required bandwidth for $\alpha = 1.5$ is more than double that for $\alpha = 0.2$. Clearly, further investigation is required in selecting various system parameters to achieve best performance. This issue is the main topic of the next chapter.

The theoretical transfer function of the optimum DFE requires the computation of $\check{\mathbf{G}}_o$ in (5.20) which in turn requires the spectral matrix $\mathbf{\Phi}(z)$ to be factorised. For the given transmission and NEXT channels (given in a continuous or analog form), this is non-trivial since one is required to explicitly write $\mathbf{\Phi}(z)$ in the desired form(s) as specified by the factorisation algorithms [52, 53]. Notwithstanding, we plot the transfer functions of the simulated optimum FF filters in Fig 5.4 and compare them to the corresponding optimum linear receivers.

As in the linear case, the equalisation of NEXT can be seen from the

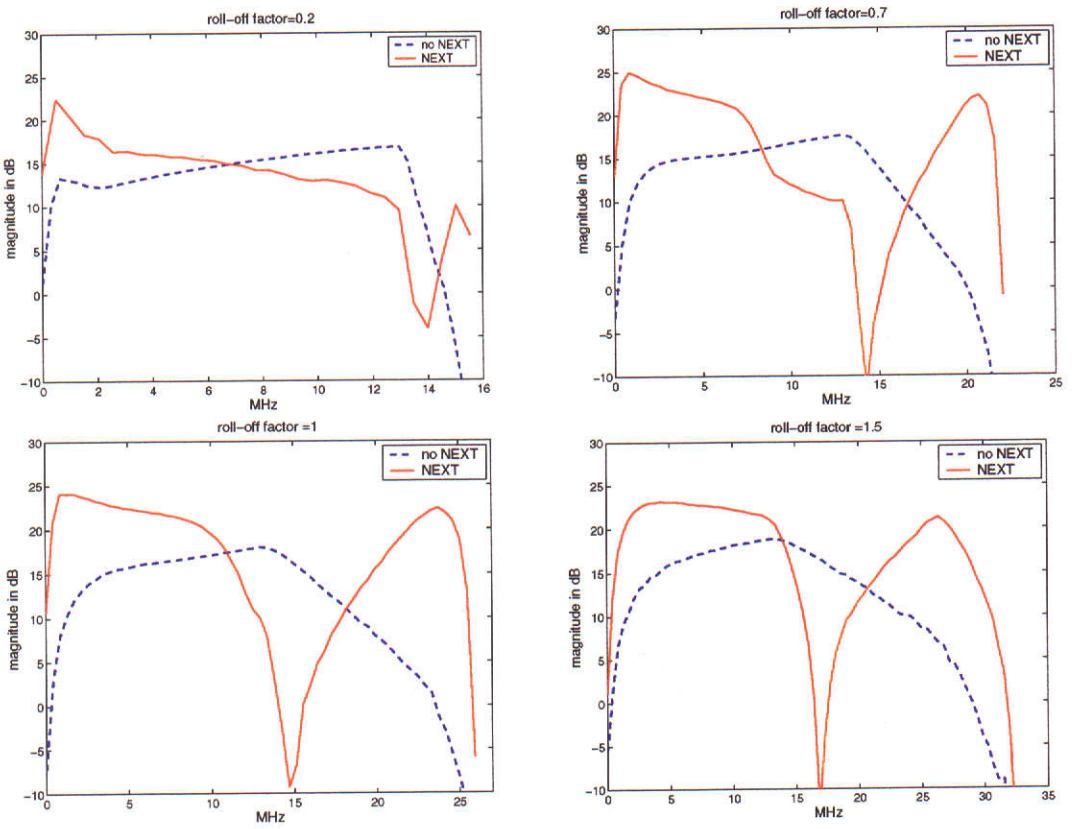

Figure 5.4: Optimum transfer functions with α=0.2, 0.7, 1 and 1.5, data rate $R = 51.84$ Mb/s and $\text{SNR}_{in} = 30$ dB with respect to a system bandwidth of 30 MHz and $\phi = 0$

estimated transfer functions of the optimum FF filters shown as solid curves in Fig 5.4. In all these curves, we first notice that there are two regions in frequency where the gain is significant, albeit in the case of $\alpha = 0.2$, the area of upper frequency region is rather small compared to the lower frequency region. The same feature can also be found in the transfer function of the optimum linear receiver shown in Chapter 4. Next, for approximately the same value of α, we also notice that compared to the optimum linear receiver, the magnitude of the transfer function of the optimum FF filters is flatter in the lower frequency region. We give our explanations as follows.

From the derivations in the previous and this chapters, we see that when operating in the presence of data-like cross-talks, both the linear and DFE receivers try to jointly equalise the ISI and cross-talk channels within the system bandwidth. Note that the FB filters play no role in suppressing data-like interference. Thus, the optimum FF filters utilise the extra bandwidth in very much the same way as the receive filters in the linear receiver in the equalisation of data-like cross-talks. For the ISI channels, it is well known [5] that because of the FB filters, the FF filters are required to only partially equalise the channels and the resulting channels are causal. This gives the FF filters extra degrees of freedom in manipulating the signal spectra. As a result, the noise variance at the slicer given by the transfer functions of the optimum FF filters is no greater than that by the optimum linear receivers

5.6 Summary

In this chapter, we analysed the MMSE performance of a 2–D CAP receiver with ideal DFEs operating in the presence of channel background noise, and either stationary or data-like cross-talks. First, we considered the system model for a multi-D CAP system. It was shown that the optimum solution and the MMSE required the factorisation of a discrete channel spectral matrix. Although there exist algorithms that will perform the factorisation, to the author's best knowledge, they are limited in the sense that they require the channel spectral matrix to satisfy certain conditions. Next, we applied the derived results to a standard 2–D CAP system. By exploiting the Hilbert transform pair property of the shaping filters in the standard 2–D CAP system, we were able to circumvent the need to factorise the channel spectral matrix and derive a more meaningful MMSE result. Also, by using the 2–D MMSE result, we gave the MMSE expression for the case when cross-talks were

modelled as another additive Gaussian noise source. Finally, we simulated the FF and FB filters of the optimum DFE by adaptive FSEs and a finite-length baud-rate, matrix equaliser. The CAP system considered was operating in the presence of a single data-like self-NEXT. The predicted MMSE results are closely matched by the simulated results.

CHAPTER 6
PERFORMANCE EVALUATIONS

In Chapters 4 and 5, we derived the optimum linear and DFE CAP receivers and their corresponding MMSE. The derivations took into account both stationary and data-like cross-talks. In this chapter, based on the previously derived results, we conduct a number of numerical studies on the performance of linear and DFE 2–D CAP receivers.

First, we investigate the performance of the optimum linear and DFE CAP receivers in a stationary cross-talk environment. Three transmission channels selected from the test channels for xDSL systems [33] are used. We consider two interference scenarios, both of which are often found in xDSL applications. In the first scenario, the spectrum of the interference source has the same spectrum as the transmitted CAP signal. The corresponding NEXT is called (stationary) *self-NEXT*. In the second scenario, there are four different interference sources, namely, DSL, HDSL, T1, and another CAP. The total effect of these NEXT sources is called (stationary) *mixed-NEXT*.

Next, we compare the performance of the optimum linear and DFE receivers over 100 m of UTP–3 cable in a single data-like cross-talk and AWGN only environment. We show two sets of numerical results computed with the same set of parameters, except for different background noise levels.

Finally, using the DFE CAP receiver as an example, we study the relationship between data-like NEXT suppression and system parameters which include excess bandwidth, data rate, CAP scheme, and relative phase between

the received signal and the NEXT signal.

6.1 MMSE Results – Stationary Cross-Talk

The MMSE results of the linear and DFE CAP receivers are examined for a single-loop HDSL (SHDSL) system operating at a data rate of $R_b = 1.6$ Mbits/s over the three selected test channels. For a transmitted power fixed at 13.5 dBm and background noise spectrum of -140 dBm/Hz, the system performance is evaluated in terms of the *performance margin* which will be defined shortly. A block diagram description of the system in the presence of stationary NEXT is shown in Fig. 6.1

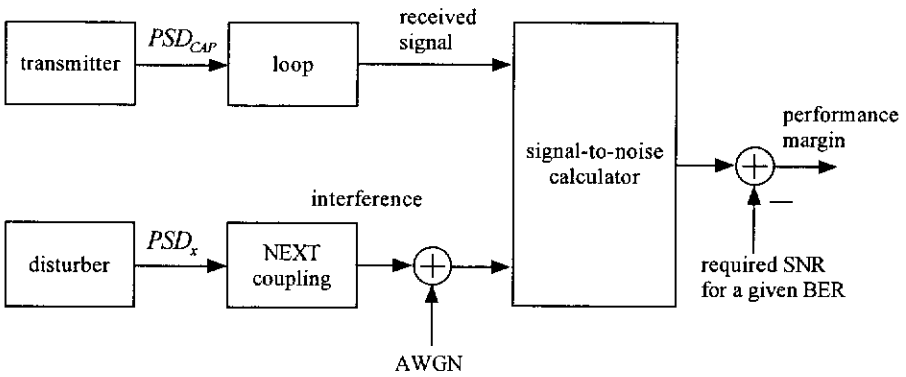

Figure 6.1: Block diagram for performance evaluation in the presence of stationary NEXT

6.1.1 Test Channels and NEXT Channel

Denote the test channels by test channel A, B, and C. The first two test channels are single AWG#24 and AWG#26 wire pairs of variable lengths. The third channel consists of 7.7 kilo feet (kft) of AWG#26 wire pair, with a bridge tap of length 0.6 kft at 1.8 kft from one terminal. Fig. 6.2 shows the configurations of these test channels.

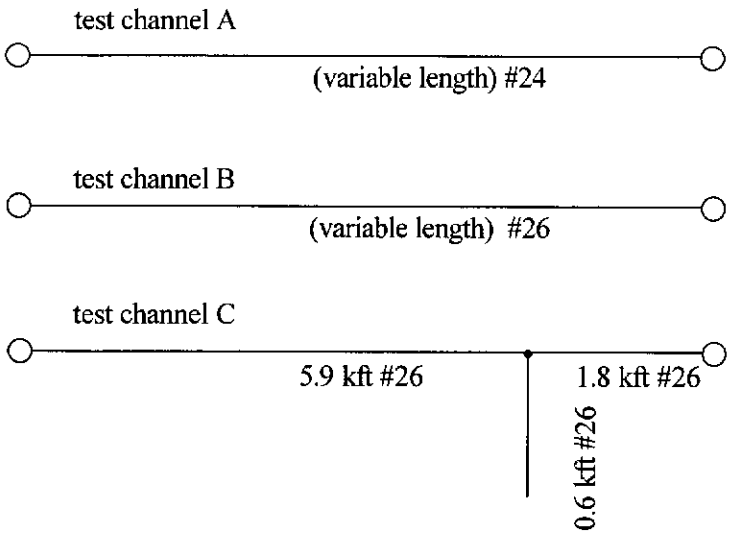

Figure 6.2: Test channels for stationary cross-talk

The test channels are described by their *insertion loss* which is defined by

$$H_{in}(f) \triangleq \frac{Z_t + Z_s}{Z_s(CZ_t + D) + AZ_t + B}$$

where Z_s and Z_t are the source and terminal impedances, respectively, and $ABCD$ are the 2-port parameters of the channel discussed in Chapter 3. For a zero-length transmission cable, we have $A = D = 1$ and $C = D = 0$ which translates to $H_{in}(f) = 1$. For a non-zero length cable, the reduction of the received signal power (in dB) is equal to $20\log|H_{in}(f)|$. The insertion losses and the corresponding impulse responses of the selected test channels, terminated by 100 Ω impedances are computed from the data given in [33]. The results are shown in Fig. 6.3.

The transfer function of the NEXT channel, denoted by $X_N(f)$, is the 15 dB/decade model defined in Appendix B of the ADSL specification [1]. It

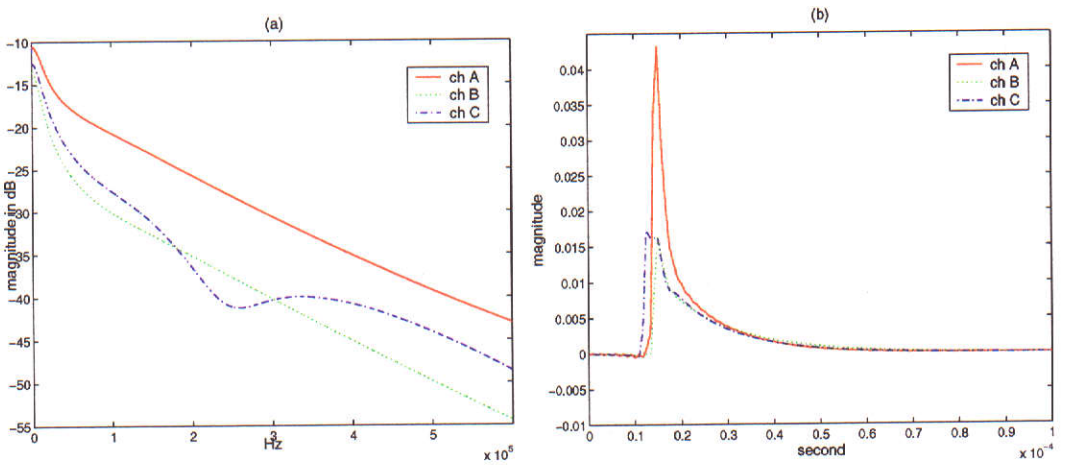

Figure 6.3: (a) Transfer functions, (b) impulse responses of test channels A (9 kft), B (9 kft), and C

is given by

$$|X_N(f)|^2 \triangleq 0.882 \times 10^{-14}\, N^{0.6}\, f^{1.5}$$

where $N = 49$ is the number of NEXT disturbers. Note that for a given CAP input signal, the output of $X_N(f)$ models the sum of 49 self-NEXT signals.

6.1.2 Transmitted Spectra

The transmitter block in Fig. 6.1 generates the PSD of the CAP signal of the interest. The CAP spectrum has the shape of a passband RC filter, with a lower band edge at DC. For a given roll-off factor α, the centre frequency f_c of the CAP spectrum is given by

$$f_c = \frac{1+\alpha}{2T}$$

where T is the symbol period of the 2–D CAP line code. The CAP spectrum is modelled by

$$\mathrm{PSD}_{\mathrm{CAP}}(f) = \begin{cases} K_o, & f_n \le 1-\alpha \\ K_o \frac{1}{2}\left[\cos\pi\left(\frac{f_n-1}{2\alpha}+\frac{1}{2}\right)+1\right], & 1-\alpha \le f_n \le 1+\alpha \\ -200 \text{ dBm/Hz}, & f_n \ge 1+\alpha \end{cases} \qquad (6.1)$$

where K_o is some constant such that the output power of the CAP transmitter is at 13.5 dBm, the stop band spectrum is simulated by the -200 dBm/Hz term, and f_n is the normalised frequency given by

$$f_n \triangleq 2T\,|f - f_c|$$

The disturber block in Fig. 6.1 generates the stationary interference spectrum $\mathrm{PSD}_x(f)$. We consider two interference scenarios. In the first scenario, the transmitted interference spectrum is the same as that of a transmitted CAP signal

$$\mathrm{PSD}_x(f) = \mathrm{PSD}_{\mathrm{CAP}}(f) \tag{6.2}$$

In the second scenario, the transmitted interference spectrum consists of the sum of the spectra of a DSL, HDSL, T1, and another CAP signal, i.e.,

$$\mathrm{PSD}_x(f) = \mathrm{PSD}_{\mathrm{DSL}}(f) + \mathrm{PSD}_{\mathrm{HDSL}}(f) + \mathrm{PSD}_{\mathrm{T1}}(f) + \mathrm{PSD}_{\mathrm{CAP}}(f) \tag{6.3}$$

where, according to Appendix B of the ADSL specification [1], the spectra of these interfering signals, all with the same transmitted power of 13.6 dBm, are given by

$$\mathrm{PSD}_{\mathrm{DSL}}(f) \triangleq \frac{0.0514}{80\times10^3}\,\mathrm{sinc}^2\Big(\frac{f}{80\times10^3}\Big)\frac{1}{1+\big(\frac{f}{80\times10^3}\big)^4},$$

$$\mathrm{PSD}_{\mathrm{HDSL}}(f) \triangleq \frac{0.06}{392\times10^3}\,\mathrm{sinc}^2\Big(\frac{f}{392\times10^3}\Big)\frac{1}{1+\big(\frac{f}{196\times10^3}\big)^8},$$

$$\mathrm{PSD}_{\mathrm{T1}}(f) \triangleq \frac{0.2592}{1.544\times10^6}\,\mathrm{sinc}^2\Big(\frac{f}{1.544\times10^6}\Big)\sin^2\Big(\frac{\pi f}{2\times1.544\times10^6}\Big)\cdot \frac{1}{1+\big(\frac{f}{3\times10^6}\big)^6}\,\frac{1}{1+\big(\frac{40\times10^3}{f}\big)^2},$$

6.1.3 Received Spectra

From the transmitted signal and interference spectra, the received signal and NEXT spectra are computed as follows. The received signal spectrum is computed from

$$\mathrm{PSD}_r(f) = |H_{in}(f)|^2 \cdot \mathrm{PSD}_{\mathrm{CAP}}(f) \tag{6.4}$$

and the received NEXT spectrum from

$$\mathrm{PSD}_N(f) = |X_N(f)|^2 \cdot \mathrm{PSD}_x(f) \tag{6.5}$$

Fig. 6.4a shows the spectra of the transmitted and received signals and mixed-NEXT for test channel A. The cable length is 9 kft and $\alpha = 0.15$. The transfer functions of the test and NEXT channels are also shown in the figure. The corresponding results for test channel C are shown in Fig. 6.4b, except that we now have stationary self-NEXT. We have not included the spectra for test channel B, since it is similar to test channel A, except the latter has much less channel loss than the former.

6.1.4 Performance Margin

In the presence of stationary cross-talk and background noise, the theoretical MMSE and normalised SNRs at the slicer for the linear and DFE CAP receivers are given in Chapters 4 and 5. For convenience, we repeat below the normalised SNRs which are given by (4.28) and (5.49). For the linear CAP receiver

$$\mathrm{SNR}_o = \left\{ T \int_0^{\frac{1}{T}} \Big[\sum_{k=0}^{K} \mathrm{SINR}(f + \frac{k}{T}) + 1 \Big]^{-1} df \right\}^{-1} \tag{6.6}$$

and for the DFE CAP receiver

$$\mathrm{SNR}_o = \exp\left\{ T \int_0^{\frac{1}{T}} \ln\Big[\sum_{k=0}^{K} \mathrm{SINR}(f + \frac{k}{T}) + 1 \Big] df \right\} \tag{6.7}$$

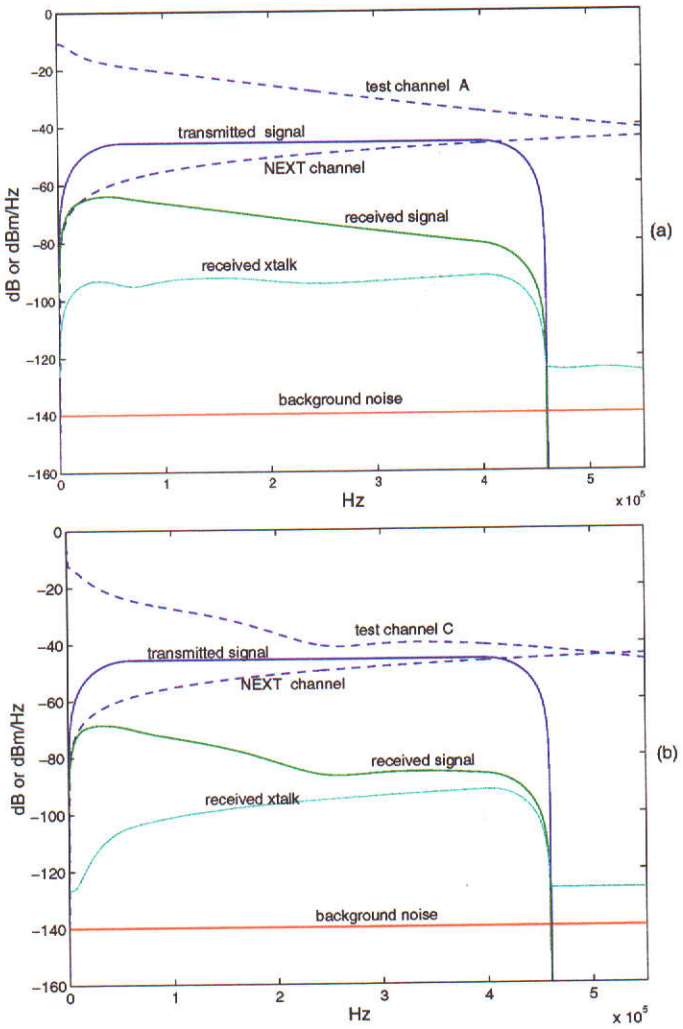

Figure 6.4: Spectra at the input of CAP receiver for roll-off factor $\alpha = 0.15$, (a) test channel A (9 kft) with mixed-NEXT, (b) test channel C with self-NEXT

where $\mathrm{SINR}(f)$ is the frequency-dependent signal-to-interference-plus-noise ratio (SINR) at the input of the receiver and it is defined by

$$\mathrm{SINR}(f) \triangleq \frac{\mathrm{PSD}_r(f)}{\mathrm{PSD}_x(f) + S_n(f)}.$$

For a given BER, assuming the sum of residual ISI, filtered total interference and noise has a Gaussian amplitude distribution, the required SNR denoted by $\mathrm{SNR}_{\mathrm{o,ref}}$ is given by (3.23). $\mathrm{SNR}_{\mathrm{o,ref}}$ for various QAM and cross

Table 6.1: Required SNR (in dB) for QAM and cross constellations

	$P_e = 10^{-7}$ (xDSL)	$P_e = 10^{-10}$ (ATM-LAN)
16–CAP	21.64	23.29
32–CAP	24.69	26.33
64–CAP	27.91	29.55
128–CAP	30.84	32.47
256–CAP	34.00	35.63

constellations are shown in Table 6.1

The system performance is evaluated by the *performance margin* which is defined by

$$\Delta_m \triangleq \mathrm{SNR}_o(\text{in dB}) - \mathrm{SNR}_{o,\mathtt{ref}}(\text{in dB}) \tag{6.8}$$

where positive margins are generally required. In order to accommodate for hardware implementation losses, Δ_m is often required to be at least 6 dB. Another useful practical performance criterion is the *maximum reach* of a cable. The maximum reach is defined as the cable length beyond which the performance margin drops below a desired performance margin. The advantage of the maximum reach criterion is that it enables comparisons between different CAP schemes as shown in the numerical results below.

6.1.5 Numerical Results

Fig 6.5 shows the system performance margins for test channel A with respect to a required BER $P_e = 10^{-7}$. This test channel includes mixed-NEXT and background noise. As can be seen, the system performance depends on

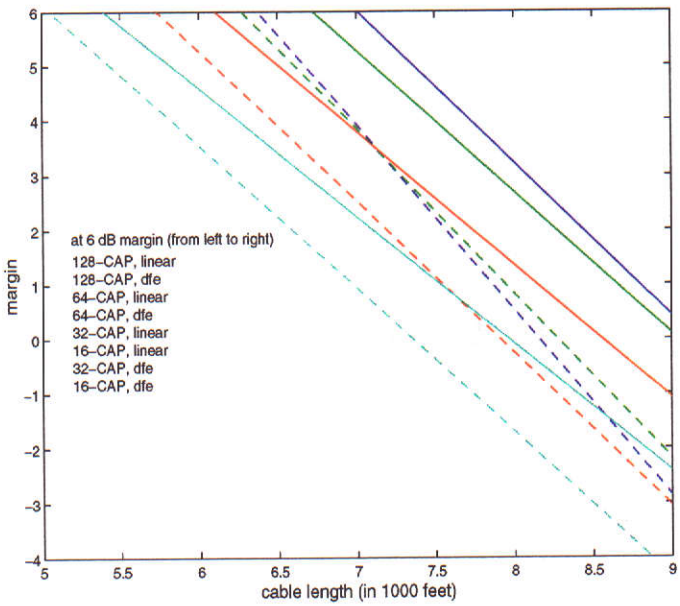

Figure 6.5: Performance margins for linear and DFE CAP receivers, test channel A, $P_e = 10^{-7}$, $\alpha = 0.15$, mixed-NEXT, background noise level of -140 dBm/Hz, roll-off factor $\alpha = 0.15$

the CAP scheme. Suppose the desired performance margin is 6 dB. For the linear receiver, the maximum reach of the cable length with respect to the desired P_e is 6.4 kft while for the DFE receiver, the maximum reach is 7 kft. In both cases, the applicable CAP scheme is the 16–CAP.

Fig. 6.6 shows the system performance margin for test channel B, with respect to the same P_e. This test channel has only stationary self-NEXT and background noise. At the 6 dB margin points, the maximum reach is 5.2 kft for the linear receiver using the 32–CAP scheme and it is 6.5 kft for the DFE receiver using the 16–CAP scheme.

We note that, despite under the much worse interference condition, test channel A (AWG#24) has a longer reach than test channel B (AWG#26) for both the linear and DFE receiver structures. The reason is that the AWG#24 cable has much less attenuation than the AWG#26 cable. For $\alpha = 0.15$, the

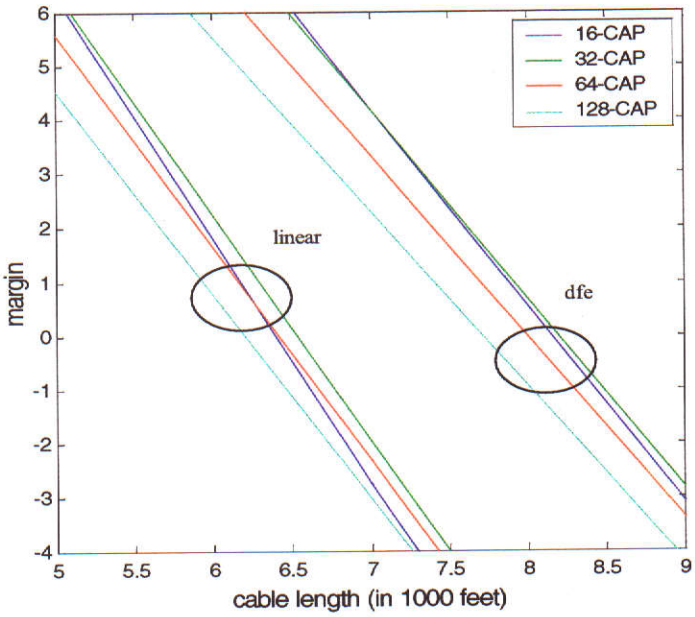

Figure 6.6: Performance margins for linear and DFE CAP receivers, test channel B, $P_e = 10^{-7}$, $\alpha = 0.15$, self-NEXT, background noise level of -140 dBm/Hz

difference in attenuation is about 7 to 8 dB at the center frequency point $f_c = 230$ kHz.

The performance margins for test channel C in the presence of stationary self-NEXT and mixed-NEXT plus background noise are shown in Table 6.2. The margin computed with the MFB is also included for comparison. From the Table, we notice that both the linear and DFE receivers have negative performance margins. In the case of stationary self-NEXT, the best margin is -2.28 dB achieved by a DFE receiver using the 16–CAP scheme. In comparison, from Fig. 6.6, the DFE receiver with the same CAP scheme achieves a 1 to 2 dB performance margin for the same cable but without bridge tap. The 3 to 4 dB performance drop is due to the bridge tap which causes a deep null near 250 kHz as shown in Fig. 6.3.

Table 6.2: Performance margins (dB) for test channel C and noise spectrum of -140 dBm/Hz

	mixed NEXT + noise			self NEXT + noise		
	MF	Linear	DFE	MF	Linear	DFE
16–CAP	-2.0	-10.73	-7.34	16.7	-10.13	-2.28
32–CAP	-2.49	-12.24	-8.01	15.7	-11.36	-2.37
64–CAP	-3.49	-13.65	-8.94	14.16	-12.31	-2.74
128–CAP	-4.49	-13.90	-9.53	12.64	-11.61	-2.89

Also from Table 6.2, we observe that in the presence of self-NEXT, the performance achieved by the linear and DFE receiver is well below that computed with the MFB. For the same channel, but in the presence of mixed-NEXT, the performance gap is much smaller. Our explanations for the performance gaps are given as follows.

First, recall in Chapter 3 that a MF maximises the SNR at the slicer without taking into consideration the channel ISI, whereas the linear or DFE receivers try to achieve a balance between minimising noise enhancement and at the same time equalising ISI. Therefore, the performance margins for the linear and DFE receivers are bounded by that computed with the MFB. Second, from Fig. 6.4, we observe that in the passband, the spectra of mixed-NEXT and self-NEXT are significantly different. That means that in terms of SNR loss due to the equalisation of the channel ISI, the equalising methods are much more effective in the presence of mixed-NEXT than self-NEXT.

6.2 MMSE Results – Data-like Cross-Talk

The MMSE performance results are now examined for the linear and DFE receivers in the presence of a single data-like cross-talk. In contrast to the case of the stationary cross-talk, the performance results are highly dependent on the system excess bandwidth, among the other system parameters. For this reason, we use a different approach to compare of the two receivers. In the following, We show the performance margin vs data rate for various CAP schemes, while keeping the length of the cable and system bandwidth the same.

6.2.1 System Model

A 2–D CAP system model with a single data-like self-NEXT is shown in Fig. 6.7. The transmitter consists of a 2–D encoder (not shown) and I and Q RRC shaping filters. The output power of the transmitter is fixed to 1 Watt. The DFE receiver consists of a pair of FF analog filters and an infinite-length FB cross-connected matrix filter. For the linear receiver, we simply set the feedback paths to zero.

The transmission channel is 100 m of UTP–3 wire pair. The channel transfer function is described by the worst-case propagation loss model which was discussed in detail in Chapter 3. The pair-to-pair NEXT loss for the same UTP cable is also discussed in Chapter 3. Fig. 6.8 shows the worst case propagation loss and pair-to-pair NEXT loss for the cable, based on the parameters given in Table 3.2 and 3.3. For a given input SNR, the background AWGN spectrum at the receiver input can be computed by assuming the signal spectrum is uniform over 30 MHz bandwidth of the transmission channel and zero outside the bandwidth.

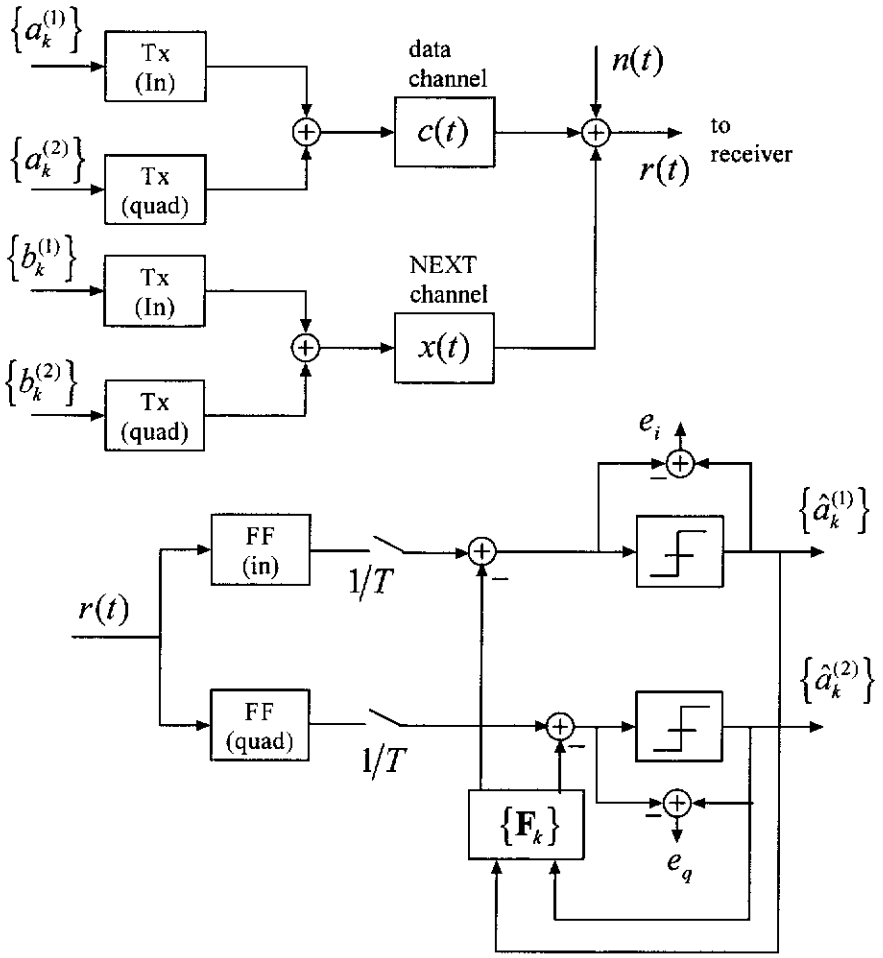

Figure 6.7: System model of DFE CAP receiver with one data-like NEXT

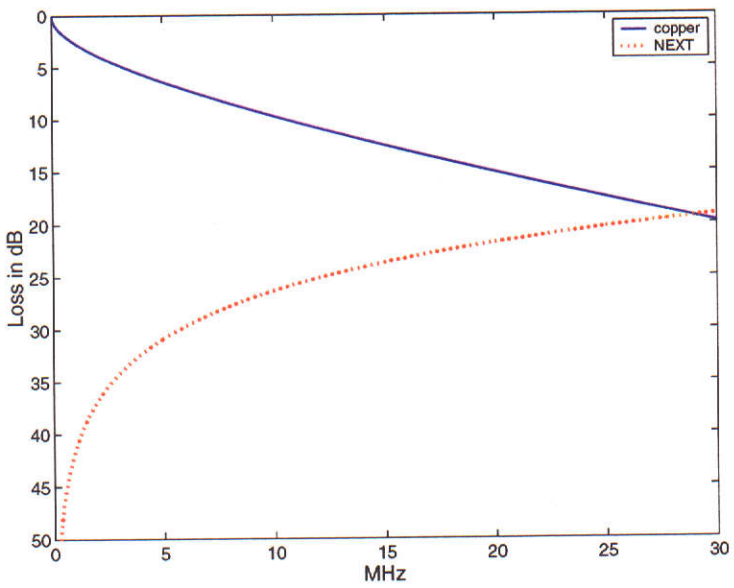

Figure 6.8: Worst-case propagation loss and pair-to-pair NEXT loss for 100 m of UTP-3 cable

6.2.2 SNR Calculation

The normalised MMSE expressions for the linear and DFE receivers operating in the presence of data-like cross-talks are derived in Chapter 4 and 5. For convenience, we repeat the corresponding MMSE for each dimension of the receivers below. For the linear receiver,

$$\varepsilon'_{min} = T \int_{-\frac{1}{2T}}^{\frac{1}{2T}} \frac{1}{R(f) + b(f)}\, df \tag{6.9}$$

and for the DFE receiver,

$$\varepsilon'_{\min} = \exp\left\{-T \int_{-\frac{1}{2T}}^{\frac{1}{2T}} \ln\left[R(f) + b(f)\right] df\right\}. \tag{6.10}$$

where

$$R(\bar{f}) \triangleq \frac{1}{T}\mathbf{P}^H\mathbf{W}^{-1}\mathbf{P} + 1 \qquad \text{and} \qquad b(\bar{f}) \triangleq \frac{1}{T}\,\mathrm{Im}\left\{\mathbf{P}^H\mathbf{W}^{-1}\tilde{\mathbf{P}}\right\}$$

and where $-\frac{1}{2T} \leq \bar{f} \leq \frac{1}{2T}$,

$$\mathbf{P}(\bar{f}) \triangleq \begin{bmatrix} P(\bar{f} - \frac{K}{T}) \\ P(\bar{f} - \frac{K-1}{T}) \\ \vdots \\ P(\bar{f} + \frac{K}{T}) \end{bmatrix} \quad \text{and} \quad \tilde{\mathbf{P}}(\bar{f}) \triangleq \begin{bmatrix} \tilde{P}(\bar{f} - \frac{K}{T}) \\ \tilde{P}(\bar{f} - \frac{K-1}{T}) \\ \vdots \\ \tilde{P}(\bar{f} + \frac{K}{T}) \end{bmatrix}.$$

where $P(f)$ and $\tilde{P}(f)$ are the transfer functions of the equivalent I and Q channels, respectively. The matrix $\mathbf{W}(\bar{f}) \triangleq [W_{k,l}]$ for $-K \leq k, l \leq K$ can be computed from

$$W_{k,l}(\bar{f}) \triangleq \frac{1}{T}\mathbf{Q}^H(\bar{f} + \frac{k}{T})\mathbf{Q}(\bar{f} + \frac{l}{T}) + S_{n'}(\bar{f} + \frac{k}{T})\delta_{kl}$$

where $\mathbf{Q}(f)$ consists of the transfer functions of all the equivalent cross-talk channels and $S_{n'}(f)$ is the normalised spectrum of the background noise.

From the normalised MMSE expressions in (6.9) and (6.10), the SNR at the slicer is given by

$$\text{SNR}_o = \frac{1}{\varepsilon'_{min}} \tag{6.11}$$

From (6.11) we can compute the performance margin using (6.8) in the same way as we did in the stationary cross-talk case.

6.2.3 Maximum Data Rate

In Chapter 3, we briefly discussed the maximum data rate of an uncoded system in an ideal bandlimited Gaussian channel. To this author's best knowledge, the maximum data rate under interferences such as data-like cross-talk is still an open issue. However, it is reasonable to assume that the maximum data rate is loosely bounded by a pair of bounds which can be computed depending on how the sum of cross-talks is treated. Using (3.33), the lower

bound is computed by treating the total data-like interference as another additive Gaussian noise source which has the same average power spectrum as the sum of all interference spectra. The upper bound is computed, assuming that data like interference has no effect on the achievable rate. Table 6.3 shows the data rate bounds vs input SNR (SNR_{in}) using the receive signal and noise spectra, given the targeted BER of $P_e = 10^{-10}$, as specified in the ATM LAN application [12].

Table 6.3: Upper and lower bounds for the maximum data rate of an uncoded system in presence of one data-like NEXT, given BER = 10^{-10}

SNR_{in} (dB)	lower bound	upper bound
20	37.12 Mbps	66.00 Mbps
30	51.22 Mbps	148.83 Mbps
40	57.47 Mbps	244.03 Mbps

6.2.4 Numerical Results

First, from Fig. 6.9a, it can been seen that the negative performance margins means that in general the uncoded system can not satisfy the BER requirement of 10^{-10} unless coding techniques are also utilised; CAP receiver with DFE performs marginally better than LE. The gap is small at the lower end of data rates and is getting larger at the other end of data rates. This indicates that as data rate increases, receivers with DFE tend to hold the performance better than with LE; Under the channel condition, 16–CAP scheme has the highest performance margin which is 2 dB over 32–CAP and 4-5 dB over 64–CAP. A clear indication of this is that one should optimise symbol rate so as to achieve the best performance;

Next, in Fig. 6.9b where $SNR_{in} = 30$ dB, we see quite a different picture compared to that in Fig. 6.9a where the performance curves for different CAP schemes are almost parallel to each other. For the DFE receiver, at data rates below 80 Mb/s, the 32–CAP scheme has the best performance margin, while the 64–CAP scheme is the best scheme at rates above 80 Mb/s. For the linear receiver, the best schemes are now the 64– and 128–CAP schemes at the lower and upper range of data rates with the cross-over rate at around 88 Mb/s. More importantly, at SNR of 30 dB, the 16–CAP scheme now has the worst or next worst performance margin. This is somewhat quite unexpected result. An additional plot where $SNR_{in} = 40$ dB is shown in Fig 6.11.

In summary, for linear Gaussian channel, CAP receivers based on equalisation techniques perform significantly different with or without data-like cross-talks. In the latter case, suppression of the data-like cross-talk by the receivers is just as important as conventional channel equalisation. In the next section, we investigate in detail how to achieve an effective suppression of the cross-talk by judicious selection of system parameters.

6.3 NEXT Equalisation vs System Parameters

In this section, using the DFE CAP receiver as an example, we investigate the relationship between data-like NEXT suppression and the system parameters which include excess bandwidth, data rate, CAP scheme, and relative phase between the received signal and the NEXT signal. Our choice of the DFE CAP receiver is due mainly to the extra degree of freedom it has over a linear CAP receiver. In terms of the equalisation of data-like NEXT, the behaviours of the linear receiver and the FF filters in the DFE receiver are similar, as indicated by the simulation results in Chapter 4 and 5. We expect the conclusions drawn here are also useful in the design of linear receivers in

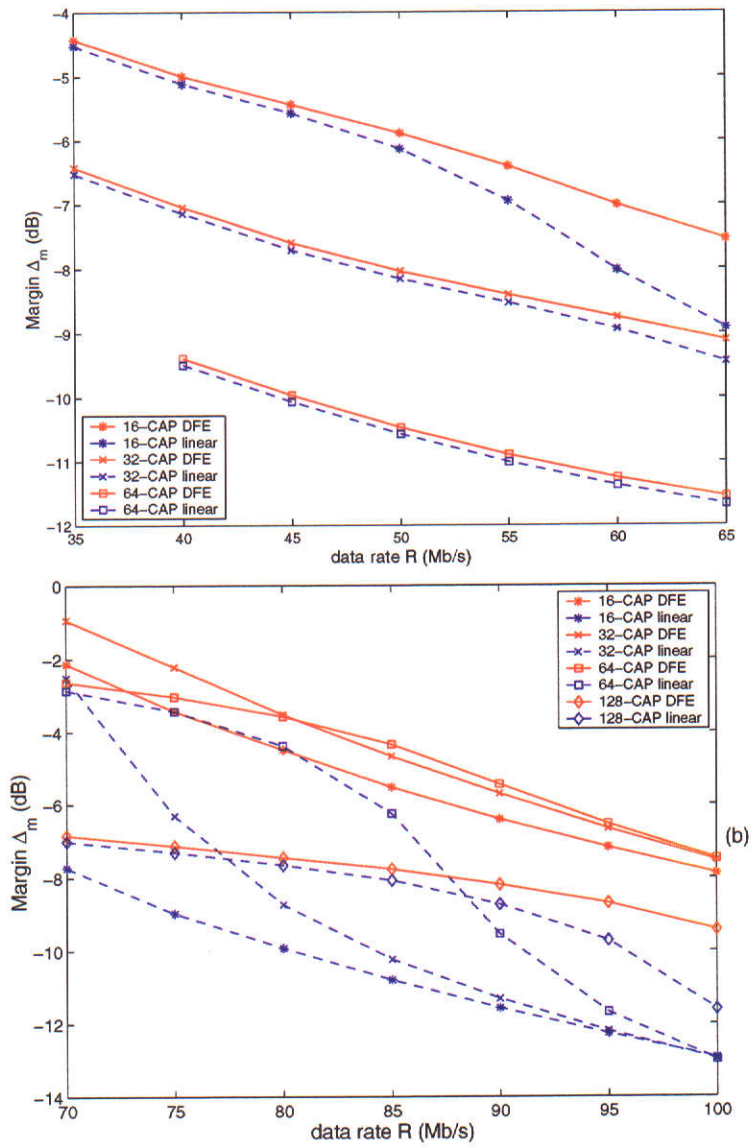

Figure 6.9: Performance margin vs data rates, for system bandwidth of 30 MHz, 100 m of UTP–3 cable, and one data-like NEXT, (a) $\mathrm{SNR}_{in} = 20$ dB, (b) $\mathrm{SNR}_{in} = 30$ dB

the same NEXT environment.

6.3.1 Performance vs Excess Bandwidth

Fig. 6.10 plots three sets of SNR_o curves against roll-off factor α, under three different input SNRs (SNR_{in}), for a system bandwidth of 30 MHz and

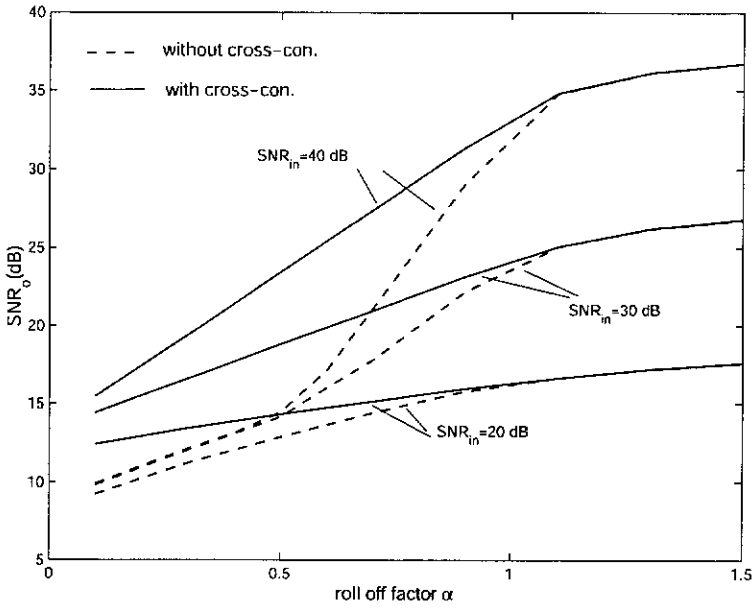

Figure 6.10: SNR at slicer vs roll-off factor α, for system bandwidth of 30 MHz, 16–CAP, 100 m of UTP–3 cable, and one data-like NEXT

the 16–CAP scheme. Note that since the bandwidth is fixed, larger α means smaller system data rate. This figure also compares the performance between a DFE with a cross-connected FB matrix filter and a DFE with a non-cross-connected FB matrix filter. In the later case, we simply set the respective coefficients of the FB matrix filter to zero.

From these curves, it can be seen that high values of SNR_o can be achieved by using relatively large roll-off factor (≥ 1). The slopes of these curves indicates that the optimum α is around 1.2 in the sense that moving away from this point will result in either little performance gain or a large drop in the SNR at the slicer. This is particularly true for high SNR_{in}. At low SNR_{in}, it is less obvious, because of the high input noise level.

We next compare the solid curves with the dotted curves. One prominent feature in the comparison is that at large α, the performances of the two DFE

structures are almost indistinguishable. The explanation for this is that the FF filters alone almost completely suppress the cross-talk and the CCI. In the implementation of such systems, this result can mean significant hardware savings.

6.3.2 Performance vs Data Rate

Fig. 6.11 plots the performance margin against data rate for rates from 70 to 100 Mb/s and for a desired BER of $P_e = 10^{-10}$ and SNR_{in} of 40 dB. From the figure, we see that positive performance margins can be achieved for the range of data rates studied and the CAP scheme with the highest performance margin depends on the data rate. Between 75 and 98 Mb/s, 64–CAP has better performance whereas 32–CAP and 128–CAP are better at lower and higher data rates, respectively.

For each of the given data rates, the roll-off factors for the various CAP schemes are listed in Table 6.4. The number in bold corresponds to the CAP scheme which gives the best performance under the system condition. It can be seen that in a data-like NEXT dominant environment, the choice of CAP schemes depends strongly on the roll-off factor α.

Table 6.4: Roll-off factors α vs data rates R in Mb/s, given a bandwidth of 30 MHz, input SNR of 40 dB, 100 m of UTP–3 cable and one NEXT; bold font indicates the CAP scheme achieving the best performance margin

	R=70	R=75	R=80	R=85	R=90	R=95	R=100
16–CAP	0.71	0.60	0.50	0.41	0.33	0.26	0.20
32–CAP	**1.14**	**1.00**	0.88	0.76	0.67	0.58	0.5
64–CAP	1.5	1.4	**1.25**	**1.12**	**1.00**	**0.89**	0.8
128–CAP	2.00	1.80	1.63	1.47	1.33	1.21	**1.1**

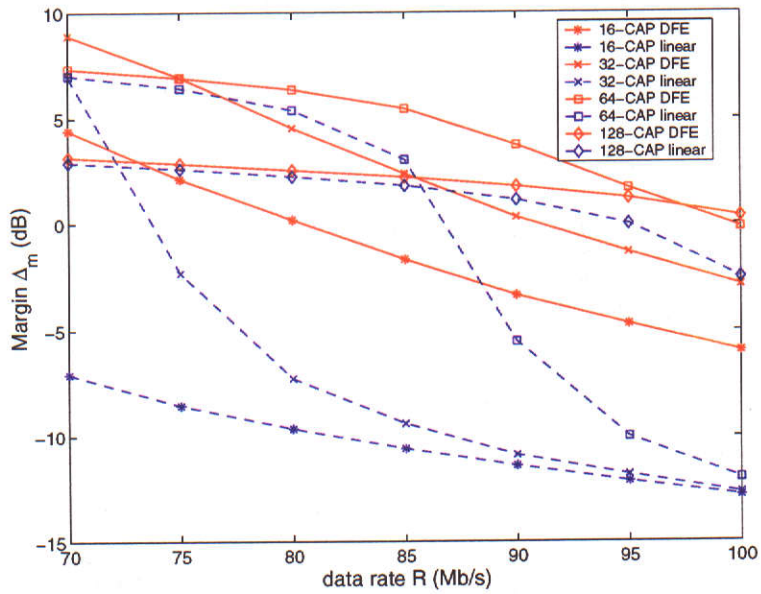

Figure 6.11: Performance margin vs data rates, for system bandwidth of 30 MHz, input SNR of 40 dB, 100 m of UTP–3 cable, and one data-like NEXT

6.3.3 Performance vs Input Noise

Fig. 6.12 shows SNR_o versus data rate, for $\alpha = 1.2$, 16-CAP, and 2 different values of SNR_{in}. We notice that for the same SNR_{in}, the two SNR curves for the systems with and without NEXT are approximately parallel to each other. This suggests that the performance drop due to the addition of data-like NEXT is independent of the system data rate.

From Fig. 6.10, we see that data-like NEXT can be suppressed by choosing a large excess bandwidth. The question is then whether we should choose a large excess bandwidth in order to suppress data-like NEXT or a small bandwidth to reduce noise enhancement. Numerical studies on this issue are shown in Fig. 6.13 where we plot the difference in SNR_o between systems with $\alpha = 1.2$ and 0.2 as a function of input SNR, for 16–CAP and data rates of $R = 20$,

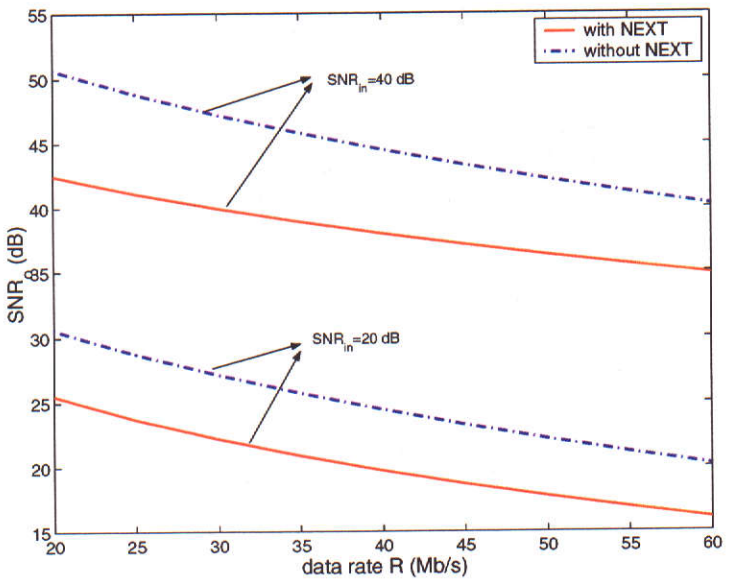

Figure 6.12: SNR at slicer versus data rate, 16–CAP, roll-off factor $\alpha = 1.2$ with and without data-like NEXT

40 and 60 Mb/s. This figure shows that in the presence of data-like NEXT, it is not always advantageous to use large excess bandwidth, especially at low SNR_{in}. However, in data-like NEXT dominant environment (high SNR_{in}), there is a clear advantage in using large excess bandwidths.

6.3.4 Performance vs Relative Phase

In the final study, we investigate the effect of the relative phase between the received signal and the data-like cross-talk on the system performance. The whole data symbol period is equally divided into 8 time slots which represent 8 relative phases, denoted by ϕ_k for $0 \leq k \leq 7$. The first phase ϕ_0 indicates that the peaks of the impulse responses of the equivalent channel and the NEXT channel are aligned; For the second phase ϕ_1, the impulse responses of the equivalent NEXT channel is shifted by $\frac{1}{8}$ of a symbol period T, relative to the equivalent channel; and so on. The performance margin vs relative phase is

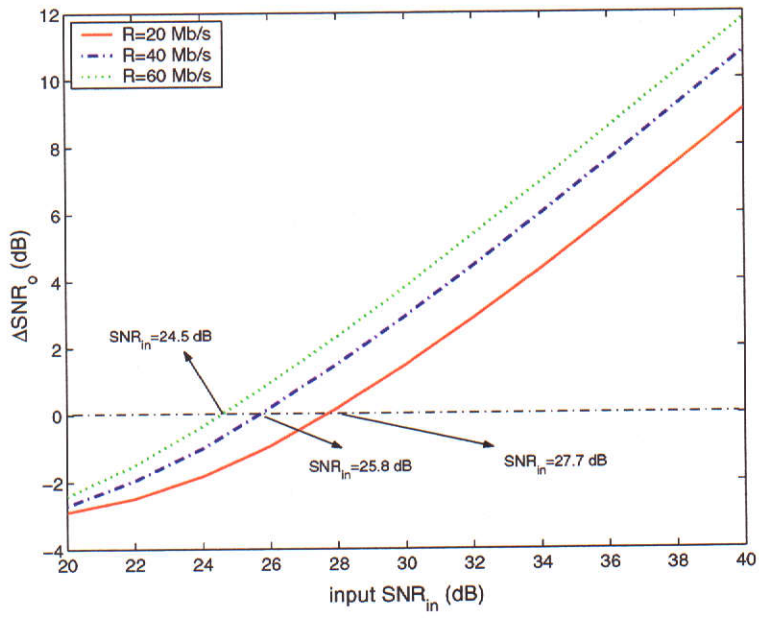

Figure 6.13: Difference in SNR_o between systems with $\alpha = 1.2$ and 0.2 versus SNR_{in}, 16–CAP

Table 6.5: Performance margin in dB vs relative phase, given $R = 51.84$ Mb/s, $B_{sys} = 30$ MHz, $\alpha = 1.3$ and 16–CAP

	ϕ_0	ϕ_1	ϕ_2	ϕ_3	ϕ_4	ϕ_5	ϕ_6	ϕ_7
$\triangle_m$	26.3	27.0	28.3	29.3	29.6	29.2	28.2	26.9

shown in Table 6.5.

The results in Table 6.5 clearly show that the difference in performance margin is about 3.3 dB between the best and worst phases. This feature is unique in a sense that it shows the nature of the interference signal. It was suggested in [55] that we adjust the relative phase of the signals transmitted in adjacent pairs of wires in order to achieve the optimum performance.

6.4 Summary

In this chapter, we conducted a number of numerical studies for linear and DFE CAP receivers. First, we concentrated on the MMSE performance over three different test channels in the presence of stationary cross-talks. The results showed that as expected, the DFE receiver always performs better than the linear receiver, because of its extra degree of freedom in spectral shaping; Amongst the CAP schemes under consideration, we found that the 16–CAP scheme achieves the best performance result. The 32–CAP scheme is only marginally worse off than 16–CAP scheme; The performance gaps between the MFB and linear/DFE receiver were also shown, which suggest that the receiver structures based on equalisation are more effective in the presence of white noise-like interference spectrum than self-NEXT interference spectrum.

Second, we studied the performance of the two receiver structures over a fixed length channel in the presence of a single data-like cross-talk. The results suggested that at relatively low input SNRs, in terms of performance margin, the CAP schemes follow the same order as in the stationary cross-talk case. However, at relatively high input SNRs, the suppression of data-like NEXT plays a key role in system performance which leads to the next study.

Following the previous study, the objective of the third and final study was to investigate the relationship between the performance margin and various design parameters in the presence of a single data-like cross-talk. The results showed that data-like NEXT can be effectively suppressed by the use of large excess bandwidth ($\alpha \geq 1$); As a result, symbol rate is also reduced by a factor of 2.

It should be pointed out that for the same bandwidth, a carefully designed TDMA or FDMA scheme will also virtually eliminate interference from

another user. These schemes have different design philosophy from cross-talk suppression by large excessive bandwidth. In theory, TDMA or FDMA scheme guarantees each user a interference free time slot or frequency band. In contrast, large excess bandwidth technique relies on the assumption that among the multiple users, there is only one dominant data-like interferer, and receiver performs joint optimisation on noise filtering, channel equalisation, and interference suppression.

In the NEXT dominated and high SNR environment, system performance improvement is dependent on the effective suppression of data-like NEXT. In a low SNR environment, care needs to be taken in the choice of excess bandwidth, since it is possible that noise enhancement resulting from large excess bandwidth outweighs the benefit of the NEXT suppression; The system performance is also affected by the relative phase between the data and the cross-talk signals. The results indicated that the performance gap between the best and the worst phase is about 3.3 dB. This suggests that one way of improving the system performance is to optimise the relative phase between the transmitted signals on adjacent wire pairs as suggested in [55].

CHAPTER 7
ADAPTIVE EQUALISERS

7.1 Introduction

In this chapter, we propose a new adaptive linear CAP receiver and study its convergence characteristics. The new receiver structure is based on the existing receiver discussed in Chapter 2. We show that the I and Q finite-length FSEs of the new receiver have identical MMSE solutions. This particular feature enables the implementation of a improved adaptive algorithm based on the standard LMS algorithm. For this reason, we call the new algorithm the *modified LMS*. Theoretical analysis and simulation results show that the modified LMS algorithm more than doubles the performance of the standard LMS algorithm in terms of initial convergence rate or misadjustment.

7.2 Derivation of the New Receiver

The proposed receiver is motivated by the transfer functions of the optimum I and Q receivers given by (4.35) and (4.36), which we reproduce below for convenience

$$G_{io}(f) = \frac{S_{n'}^{-1}(f)P^*(f)}{\frac{2}{T}\sum_{k=0}^{K}\Gamma(\bar{f}^+ + \frac{k}{T}) + 1} \tag{7.1}$$

$$G_{qo}(f) = \frac{S_{n'}^{-1}(f)\tilde{P}^*(f)}{\frac{2}{T}\sum_{k=0}^{K}\Gamma(\bar{f}^+ + \frac{k}{T}) + 1} \tag{7.2}$$

where $S_n(f)$ is the spectrum of channel noise, $P(f)$ is the transfer function of the inphase equivalent channel, and $\Gamma(f) \triangleq \frac{|P(f)|^2}{S_n(f)}$. The summation in the denominator represents spectrum folding of $\Gamma(f)$ as discussed in Chapter 4.

The above equations can be re-written in the following form

$$G_{io}(f) = G_t^*(f)W(f) \tag{7.3}$$

$$G_{qo}(f) = \tilde{G}_t^*(f)W(f) \tag{7.4}$$

where $W(f)$ is defined by

$$W(f) \triangleq \frac{\sigma^2 S_n^{-1}(f)C^*(f)}{\frac{2}{T}\sum_{l=0}^{L}\Gamma\left(\bar{f}^+ + \frac{l}{T}\right) + 1}$$

and where $C(f)$ is the transfer function of the transmission channel.

From (7.3), we may view the transfer function $G_{io}(f)$ of the optimum inphase filter as the cascade of the transfer functions, $G_t^*(f)$ and $W(f)$. Similarly, $G_{qo}(f)$ for the optimum quadrature filter is the cascade of $\tilde{G}_t(f)$ and the same $W(f)$. Note that $G_t^*(f)$ and $\tilde{G}_t^*(f)$ are simply filters that are matched to the transmit filter pair $G_t(f)$ and $\tilde{G}_t(f)$ and therefore they are known, whereas the filter represented by $W(f)$ is channel dependent and hence is unknown.

Based on the above observations, we propose a new receiver structure as shown in Fig. 7.1. The main difference between the new and existing receiver shown in Chapter 2 is the addition of two fixed front-end analog filters that are matched to the transmit filter pair. It is clear that this structure change does not effect the MMSE of the original linear receiver provided the sampling rate before the FSEs is sufficiently high such that there is no aliasing, and the FSEs have infinite number of taps. However, in the following, we prove that as a result of the two fixed filters, both equalisers have the same MMSE solutions.

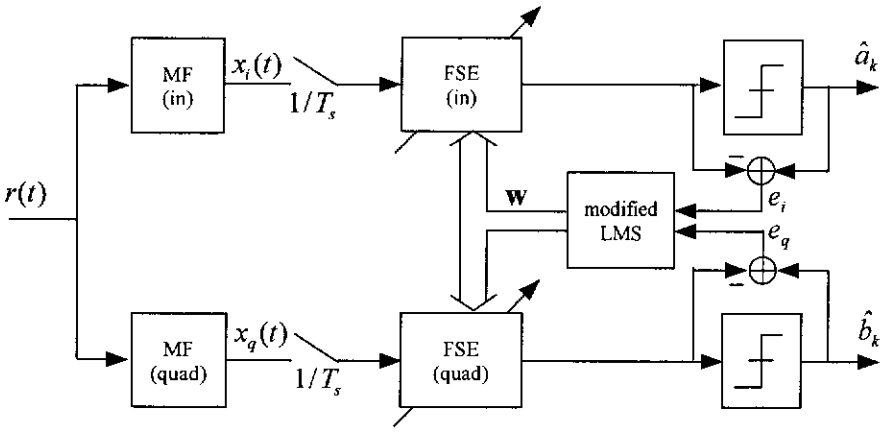

Figure 7.1: Proposed adaptive linear CAP receiver

7.2.1 MMSE Solution

Define $h_{ii}(t) \triangleq g_t(t) \otimes c(t) \otimes g_t(-t)$ where $h_{ii}(t)$ is the equivalent channel from the input of the inphase shaping filter to the output of the inphase receive, filter, and $c(t)$, $g_t(t)$ and $\tilde{g}_t(t)$ denote the transmission channel, inphase transmit filter and receive filter, respectively. Similarly, the equivalent channels resulting from the other combinations of the I and Q inputs and outputs can be defined in the same way as follows

$$h_{iq}(t) \triangleq g_t(t) \otimes c(t) \otimes \tilde{g}_t(-t)$$

$$h_{qi}(t) \triangleq \tilde{g}_t(t) \otimes c(t) \otimes g_t(-t)$$

$$h_{qq}(t) \triangleq \tilde{g}_t(t) \otimes c(t) \otimes \tilde{g}_t(-t)$$

Note, both the transmission channel and transmit filters are not shown in Fig. 7.1. Let $H_{ii}(f)$, $H_{iq}(f)$, $H_{qi}(f)$, and $H_{qq}(f)$ be the Fourier transforms of the corresponding equivalent channels. In the frequency domain, it can readily

be shown from the above definitions that

$$H_{ii}(f) = H_{qq}(f) = |G_{rc}(f)|C(f) \tag{7.5a}$$

$$H_{qi}(f) = -H_{iq}(f) = (-j)\,\mathrm{sgn}(f)|G_{rc}(f)|C(f) \tag{7.5b}$$

where $G_{rc}(f)$ is the transfer function of the RC filter defined in Chapter 2.

Define $H(f) \triangleq H_{ii}(f)$ and $\tilde{H}(f) \triangleq H_{qi}(f)$ and denote the corresponding impulse responses by $h(t)$ and $\tilde{h}(t)$. The input signals to the I and Q equalisers are given then by

$$x_i(t) \triangleq x_{si}(t) + z(t)$$

$$x_q(t) \triangleq x_{sq}(t) + \tilde{z}(t)$$

where

$$x_{si}(t) \triangleq \sum_{l=-\infty}^{\infty} \left[a_l h(t - lT) + b_l \tilde{h}(t - lT)\right]$$

$$x_{sq}(t) \triangleq \sum_{l=-\infty}^{\infty} \left[b_l h(t - lT) - a_l \tilde{h}(t - lT)\right]$$

and

$$z(t) \triangleq \int n(\tau) g_t(\tau - t)\, d\tau \qquad \text{and} \qquad \tilde{z}(t) \triangleq \int n(\tau) \tilde{g}_t(\tau - t)\, d\tau$$

Let $\mathbf{w}_i$ and $\mathbf{w}_q$ denote the weight vectors of the I and Q equalisers. Suppose both equalisers have the same length N such that

$$\mathbf{w}_i \triangleq \left[w_0^i, w_1^i, \ldots, w_{N-1}^i\right]^T$$

$$\mathbf{w}_q \triangleq \left[w_0^q, w_1^q, \ldots, w_{N-1}^q\right]^T$$

At the sampling instants $t_s = kT$[1] where k is an integer, the outputs of the

[1]The sampling phase is absorbed into the channel $c(t)$

equalisers, denoted by $y_i(kT)$ and $y_q(kT)$ are given by

$$y_i(kT) \triangleq \mathbf{w}_i^T \mathbf{x}_i(kT) \qquad \text{and} \qquad y_q(kT) \triangleq \mathbf{w}_q^T \mathbf{x}_q(kT)$$

where $\mathbf{x}_i(kT)$ and $\mathbf{x}_q(kT)$ are vectors consisting of the input samples to the FSEs. We can express $\mathbf{x}_i(kT)$ and $\mathbf{x}_q(kT)$ as follows

$$\mathbf{x}_i(kT) \triangleq \mathbf{x}_{si}(kT) + \mathbf{z}(kT) \qquad \text{and} \qquad \mathbf{x}_q(kT) \triangleq \mathbf{x}_{sq}(kT) + \tilde{\mathbf{z}}(kT)$$

where $\mathbf{x}_{si}(kT)$, $\mathbf{x}_{sq}(kT)$, $\mathbf{z}(kT)$ and $\tilde{\mathbf{z}}(kT)$ are defined by

$$\begin{aligned}
\mathbf{x}_{si}^T(kT) &\triangleq \left[x_{si}(kT), x_{si}(kT - T_s), \ldots, x_i(kT - (N-1)T_s)\right] \\
\mathbf{x}_{sq}^T(kT) &\triangleq \left[x_{sq}(kT), x_q(kT - T_s), \ldots, x_{sq}(kT - (N-1)T_s)\right] \\
\mathbf{z}^T(kT) &\triangleq \left[z(kT), z(kT - T_s), \ldots, z(kT - (N-1)T_s)\right] \\
\tilde{\mathbf{z}}^T(kT) &\triangleq \left[\tilde{z}(kT), \tilde{z}(kT - T_s), \ldots, \tilde{z}(kT - (N-1)T_s)\right]
\end{aligned}$$

where T_s is the tap delay of the FSEs. It is selected such that there is no aliasing in the samples of the input signals. Typically, T/T_s equals some integer such that the output sequence can be easily decimated.

The MSEs at the slicers are defined by

$$\varepsilon_i \triangleq E\left[|a_{k-\Delta_i} - y_i(kT)|^2\right] \tag{7.6a}$$

$$\varepsilon_q \triangleq E\left[|b_{k-\Delta_q} - y_q(kT)|^2\right] \tag{7.6b}$$

where Δ_i and Δ_q are the I and Q system delays in units of T and $a_{k-\Delta_i}$ and $b_{k-\Delta_q}$ are the desired symbols. We seek the optimum solutions, denoted by $\mathbf{w}_{io}$ and $\mathbf{w}_{qo}$ to the following minimisation problems

$$\mathbf{w}_{io} = \arg \min_{(\Delta_i, \mathbf{w}_i)} E\left[|a_{k-\Delta_i} - y_i(kT)|^2\right] \tag{7.7a}$$

$$\mathbf{w}_{qo} = \arg \min_{(\Delta_q, \mathbf{w}_q)} E\left[|b_{k-\Delta_q} - y_q(kT)|^2\right] \tag{7.7b}$$

Assuming the transmission channel is time-invariant and channel noise $n(t)$ is stationary, the MSEs at the slicer are independent of time $t_s = kT$. For convenience, we set $k = 0$. Keeping Δ_i and Δ_q fixed for the time being, we firstly find the optimum solutions denoted by $\mathbf{w}_{iod}$ and $\mathbf{w}_{qod}$, by minimising the MSEs with respect to the equaliser weight vectors $\mathbf{w}_i$ and $\mathbf{w}_q$. This is a well known problem, e.g., [56] and $\mathbf{w}_{iod}$ and $\mathbf{w}_{qod}$ satisfy the following equations

$$\mathbf{A}_i\mathbf{w}_{iod} = \mathbf{d}_i \qquad \text{and} \qquad \mathbf{A}_q\mathbf{w}_{qod} = \mathbf{d}_q \tag{7.8}$$

where

$$\mathbf{A}_i \triangleq E[\mathbf{x}_i(0T)\mathbf{x}_i^T(0T)], \qquad \mathbf{A}_q \triangleq E[\mathbf{x}_q(0T)\mathbf{x}_q^T(0T)]$$

$$\mathbf{d}_i \triangleq E[a_{-\Delta_i}\mathbf{x}_i(0T)], \qquad \mathbf{d}_q \triangleq E[b_{-\Delta_q}\mathbf{x}_q(0T)]$$

Assuming that the input symbols are independent of channel noise, $\mathbf{A}_i$ and $\mathbf{A}_q$ may be written as

$$\mathbf{A}_i = \mathbf{A}_{si} + \mathbf{A}_z \tag{7.9}$$

$$\mathbf{A}_q = \mathbf{A}_{sq} + \mathbf{A}_{\tilde{z}} \tag{7.10}$$

where

$$\mathbf{A}_{si} \triangleq E[\mathbf{x}_{si}(0T)\mathbf{x}_{si}^T(0T)], \qquad \mathbf{A}_{sq} \triangleq E[\mathbf{x}_{sq}(0T)\mathbf{x}_{sq}^T(0T)]$$

and

$$\mathbf{A}_z \triangleq E[\mathbf{z}(0T)\mathbf{z}^T(0T)], \qquad \mathbf{A}_{\tilde{z}} \triangleq E[\tilde{\mathbf{z}}(0T)\tilde{\mathbf{z}}^T(0T)]$$

From the above definitions, the elements of $\mathbf{A}_{si}$ and $\mathbf{A}_{sq}$ are given by

$$\mathbf{A}_{si}[i,j] = E[x_{si}(-iT_s)x_{si}(-jT_s)]$$

$$\mathbf{A}_{sq}[i,j] = E[x_{sq}(-iT_s)x_{sq}(-jT_s)]$$

for $0 \leq i, j \leq N-1$. Assuming the I and Q symbol sequences consist of i.i.d data symbols and expanding the RHS, it can be shown that

$$\begin{aligned}\mathbf{A}_{si}[i,j] &= \mathbf{A}_{sq}[i,j] \\ &= \sigma^2 \sum_l \left[h(-iT_s - lT)h(-jT_s - lT) + \tilde{h}(-iT_s - lT)\tilde{h}(-jT_s - lT)\right] \quad (7.11)\end{aligned}$$

where σ^2 is the symbol variance.

Similarly, the elements of $\mathbf{A}_z$ and $\mathbf{A}_{\tilde{z}}$ are given by

$$\begin{aligned}\mathbf{A}_z[i,j] &= E[z(-iT_s)z(-jT_s)] \\ \mathbf{A}_{\tilde{z}}[i,j] &= E[\tilde{z}(-iT_s)\tilde{z}(-jT_s)]\end{aligned}$$

Now, since

$$\begin{aligned}z(-kT_s) &= \int n(\tau)g_t(kT_s + \tau)\,d\tau \\ \tilde{z}(-kT_s) &= \int n(\tau)\tilde{g}_t(kT_s + \tau)\,d\tau\end{aligned}$$

it follows that

$$\mathbf{A}_z[i,j] = \iint R_n(\tau_1 - \tau_2)g_t(iT_s + \tau_1)g_t(jT_s + \tau_2)\,d\tau_1\,d\tau_2$$

where $R_n(\tau_1 - \tau_2) \triangleq E[n(\tau_1)n(\tau_2)]$. Let $u = iT_s + \tau_1$ and $s = jT_s + \tau_2$. Then

$$\mathbf{A}_z[i,j] = \iint R_n(mT_s + u - s)g_t(u)g_t(s)\,du\,ds$$

where $m \triangleq j - i$. Define

$$R_z(t) \triangleq \iint R_n(t + u - s)g_t(u)g_t(s)\,du\,ds$$

Note that the RHS of the above expression represents the convolution of $g_t(-t)$, $g_t(t)$ and $R_n(t)$, i.e., $R_z(t) = g_t(-t) \otimes g_t(t) \otimes R_n(t)$. Let $S_z(f) \triangleq \mathcal{F}[R_z(t)]$ and

$S_n(f) \triangleq \mathcal{F}[R_n(t)]$. Then, in the frequency domain, we have

$$S_z(f) = |G_t(f)|^2 S_n(f) \tag{7.12}$$

Using (7.12), we may express the elements of the $\mathbf{A}_z$ as follows

$$\mathbf{A}_z[i,j] = R_z(mT_s) = \int |G_t(f)|^2 S_n(f) e^{jmT_s 2\pi f}\, df \tag{7.13}$$

Using the same procedure, it can be shown that

$$\mathbf{A}_{\tilde{z}}[i,j] = R_{\tilde{z}}(mT_s) = \int |\tilde{G}_t(f)|^2 S_n(f) e^{jmT_s 2\pi f}\, df \tag{7.14}$$

Now, since $|G_t(f)| = |\tilde{G}_t(f)|$, from (7.13) and (7.14) we have

$$\mathbf{A}_z[i,j] = \mathbf{A}_{\tilde{z}}[i,j] \tag{7.15}$$

and from (7.11) and (7.15), we conclude that

$$\mathbf{A}_i = \mathbf{A}_q \triangleq \mathbf{A} \tag{7.16}$$

Note that $\mathbf{A}$ is not a Toeplitz matrix, due to the fractionally-spaced sampling at the equaliser. Following the same arguments as in [57], it can be shown that $\mathbf{A}$ is always invertible, regardless of the input noise condition, provided the roll-off factor is less than 100%. Accordingly, from (7.8), the optimum solutions may be written as

$$\mathbf{w}_{iod} = \mathbf{A}^{-1}\mathbf{d}_i \tag{7.17a}$$

$$\mathbf{w}_{qod} = \mathbf{A}^{-1}\mathbf{d}_q \tag{7.17b}$$

where $\mathbf{d}_i$ and $\mathbf{d}_q$ are given by

$$\mathbf{d}_i[i] = E[a_{-\Delta_i} x_{si}(-iT_s)] \tag{7.18a}$$

$$\mathbf{d}_q[i] = E[b_{-\Delta_q} x_{sq}(-iT_s)] \tag{7.18b}$$

for $0 \leq i \leq N-1$. Expanding the RHS of (7.18), it is readily shown that

$$\mathbf{d}_i[i] = \sigma^2 h(\Delta_i T - iT_s) \tag{7.19a}$$

$$\mathbf{d}_q[i] = \sigma^2 h(\Delta_q T - iT_s) \tag{7.19b}$$

We next optimise the MSE at the slicer with respect to the system delays Δ_i and Δ_q. Substituting (7.17) into (7.6) and after simplification, the I and Q MMSEs denoted by $\varepsilon_{i,min}$ and $\varepsilon_{q,min}$, are given by

$$\varepsilon_{i,min} = \sigma^2 \min_{\Delta_i}(1 - \mathbf{d}_i^T \mathbf{A}^{-1} \mathbf{d}_i) \tag{7.20a}$$

$$\varepsilon_{q,min} = \sigma^2 \min_{\Delta_q}(1 - \mathbf{d}_q^T \mathbf{A}^{-1} \mathbf{d}_q) \tag{7.20b}$$

Substituting (7.19) into (7.20), by inspection, it is clear that the expressions in the RHS of both (7.20a) and (7.20b) are equal, provided $\Delta_i = \Delta_q$. Thus, assuming the global optimum solution exists, we have

$$\Delta_{io} = \Delta_{qo} \triangleq \Delta_o \tag{7.21}$$

and

$$\varepsilon_{i,min} = \varepsilon_{q,min} \tag{7.22}$$

Let $\mathbf{d}_o \triangleq \mathbf{d}_{io} = \mathbf{d}_{qo}$ denote the vectors corresponding to the optimum system delay Δ_o. Since $\mathbf{w}_{iod}$ and $\mathbf{w}_{qod}$ are functions of system delay only, we finally have

$$\mathbf{w}_{io} = \mathbf{w}_{qo} = \mathbf{A}^{-1} \mathbf{d}_o \tag{7.23}$$

7.2.2 Proposed Adaptive Algorithm

By adding two fixed front-end filters to the standard CAP linear receiver, we have shown that the optimum I and Q finite-length FSEs are identical. In

this subsection, we show how this feature of the receiver structure can be exploited to improve the performance of *stochastic-gradient* adaptive algorithms, such as the standard LMS algorithm [47] and its variants.

In the standard LMS algorithm, the gradient of the quadratic error surface is estimated by a one-point sample mean. Thus, the estimate is far from being accurate or, simply 'noisy'. In the proposed CAP receiver, in order to improve the accuracy of this estimate, we propose a modified LMS algorithm, based on the standard LMS algorithm. The modified LMS algorithm is given by

$$\mathbf{w}(n+1) = \mathbf{w}(n) + \mu_m[e_i(n)\mathbf{x}_i(n) + e_q\mathbf{x}_q(n)] \tag{7.24}$$

where as shown in Fig. 7.1, $\mathbf{w}(n)$ is the common weight vector for both I and Q equalisers, μ_m is the algorithm step size. Note that (7.24) is updated at the symbol rate and for clarity we omit T in the equation.

The basic idea of the new algorithm is that we force the I and Q equalisers to have the same convergence in the mean and to get a better estimate of the true gradient, we use both the I and Q errors at the slicers. Such an idea is similar to the block LMS algorithm [58]. The main difference is that compared to the standard LMS algorithm, our algorithm approximately doubles the convergence performance as will be shown shortly, whereas the block LMS algorithm maintains similar performance level.

For comparison purpose, the standard LMS algorithm for the existing receiver is shown below.

$$\mathbf{w}_i(n+1) = \mathbf{w}_i(n) + \mu\, e^i(n)\mathbf{x}(n) \tag{7.25a}$$

$$\mathbf{w}_q(n+1) = \mathbf{w}_q(n) + \mu\, e^q(n)\mathbf{x}(n) \tag{7.25b}$$

where, in order to differentiate the errors at the slicer, we now use $e^i(n)$ and

$e^q(n)$ to denote the inphase and quadrature errors for the standard LMS algorithm.

7.3 Convergence Analysis

In this section, we derive the learning curves for both the modified LMS and standard LMS adaptive algorithms defined by (7.24) and (7.25). These adaptive algorithms are then compared in terms of their *initial convergence rates* and *misadjustment*, which will be defined shortly. Simulation results are also given to confirm our theoretical analysis.

7.3.1 Independence Assumptions

As with common practice, we make use of the well known *independence assumption* (IA) e.g., [59, 60, 56] in order to make the analysis mathematically tractable. However, it should be pointed out that although IA has little relationship with the underlying physical scenario, it is known to lead to reasonable results in many scenarios as is in the case presented below. In fact, recent studies show that it is not necessary to use IA in order to perform convergence analysis. Detailed discussions on convergence without IA can be found in [61, 62].

Without going details, IA simply states that the sequence $\{\mathbf{x}(n)\}$ for all n is treated as an iid sequence; the minimum (in the least mean square sense) I and Q symbol estimation error, denoted by e_o^i and e_o^q are independent of $\mathbf{x}(n)$. From the IA, we can deduce the following two results.

First, since $\mathbf{x}(n)$ is correlated with the desired symbol denoted by a_n, then $\mathbf{x}(n)$ is independent of all the previously transmitted symbols, $a_1, a_2, \ldots, a_{n-1}$, where the starting symbol is a_1. The same arguments also holds for b_n and $b_1, b_2, \ldots, b_{n-1}$. Second, it will be shown that the I and Q weight-error vectors

$\delta\mathbf{w}_i(n)$ and $\delta\mathbf{w}_q(n)$ (defined shortly) depend only on all the $\mathbf{x}(1), \mathbf{x}(2), \ldots, \mathbf{x}(n-1)$, and therefore, $\delta\mathbf{w}_i(n)$ and $\delta\mathbf{w}_q(n)$ are independent of $\mathbf{x}(n)$.

IA is also applicable to the modified LMS algorithm. In this case, we assume that the sequences $\{\mathbf{x}_i(n)\}$ and $\{\mathbf{x}_q(n)\}$ are iid sequences; the minimum (in the least mean square sense) I and Q symbol estimation error, denoted by $e_{io}(n)$ and $e_{qo}(n)$, are independent of $\{\mathbf{x}_i(n)\}$ and $\{\mathbf{x}_q(n)\}$, respectively. Note that $\mathbf{x}_i(n)$ and $\mathbf{x}_q(n)$ are correlated. Again, like the standard LMS case, the relationships between $\mathbf{x}_i(n)$ ($\mathbf{x}_q(n)$) and inphase (quadrature) data symbols, and between $\mathbf{x}_i(m)$ or $\mathbf{x}_q(m)$ for $1 \leq m \leq n$ and the weight-error vector $\delta\mathbf{w}(n)$, also hold.

7.3.2 Standard LMS

The convergence analysis for the FSEs has already been shown in [63]. Here, using the inphase FSE as an example, we give an outline of the key steps and the main results. Let $\mathbf{w}_{io}$ be the weight vector of the optimum inphase FSE. At the sampling time $t_s = nT$, the FSE tap weight vector is expressed as

$$\mathbf{w}_i(n) = \mathbf{w}_{io} + \delta\mathbf{w}_i(n) \tag{7.26}$$

where $\delta\mathbf{w}_i(n)$ is called the *weight-error vector*. The estimation error at the slicer is given by

$$e^i(n) \triangleq a_n - \mathbf{w}_i^T(n)\mathbf{x}(n)$$

Note this error is zero-mean, since the symbol and hence the equaliser input vector, are zero-mean. Using (7.26), it is easily shown that

$$e^i(n) = e_o^i(n) - \delta\mathbf{w}_i^T(n)\mathbf{x}(n) \tag{7.27}$$

where $e_o^i(n) \triangleq a(n) - \mathbf{w}_{io}^T \mathbf{x}(n)$. The inphase MSE at the slicer is defined as

$$\varepsilon_i \triangleq E\big[|e^i(n)|^2\big]$$

Using (7.27) and the IA, and expanding the RHS of the above equation, it can be shown that

$$\varepsilon_i(n) = \varepsilon_{io} + E\big[\delta\mathbf{w}_i^T(n)\mathbf{A}_x\delta\mathbf{w}_i(n)\big] \tag{7.28}$$

where $\varepsilon_{io} \triangleq E[(e_o^i)^2(n)]$ is the MMSE of the existing receiver structure and $\mathbf{A}_x \triangleq E[\mathbf{x}^T(n)\mathbf{x}(n)]$.

The second term in (7.28) may be viewed as the *excess MSE* denoted by $\varepsilon_{ex}^i \triangleq E\big[\delta\mathbf{w}_i^T(n)\mathbf{A}_x\delta\mathbf{w}_i(n)\big]$. Let $\mathbf{P}$ be the *unitary matrix* which diagonalises the matrix $\mathbf{A}_x$, i.e., $\mathbf{A}_x = \mathbf{P}\mathbf{D}_x\mathbf{P}^T$, then the excess MSE may be written as

$$\varepsilon_{ex}^i(n) = E\big[\mathbf{v}^T(n)\mathbf{D}_x\mathbf{v}(n)\big] \tag{7.29}$$

where $\mathbf{v}(n) \triangleq \mathbf{P}^T\delta\mathbf{w}_i(n)$. Also, applying $\mathbf{P}$ to the input data vector $\mathbf{x}(n)$, we denote the transformed vector by $\mathbf{s}(n) \triangleq \mathbf{P}^T\mathbf{x}(n)$. Substituting (7.27) into the LMS algorithm of (7.25), and then pre-multiplying both side by $\mathbf{P}^T$ and after some simplification, we obtain

$$\mathbf{v}(n+1) = [\mathbf{I} - \mu\mathbf{s}(n)\mathbf{s}^T(n)]\mathbf{v}(n) + \mu e_o^i\mathbf{s}(n) \tag{7.30}$$

It can be seen that the weight-error vector $\mathbf{v}(n)$ (or $\mathbf{w}_i(n)$) is correlated with all the previous $\mathbf{s}(m)$ (or $\mathbf{x}(m)$) for $1 \leq m \leq n-1$, assuming $\mathbf{x}(1)$ is the first data vector and therefore, from IA, it is independent of $\mathbf{s}(n)$ (or $\mathbf{x}(n)$).

Substituting (7.30) into (7.29) and expanding the RHS, we get

$$\begin{aligned}\varepsilon_{ex}^{i}(n+1) = E\big[&\mathbf{v}^T\mathbf{D}_x\mathbf{v} - \mu\mathbf{v}^T\mathbf{D}_x\mathbf{s}\mathbf{s}^T\mathbf{v} - \mu\mathbf{v}^T\mathbf{s}\mathbf{s}^T\mathbf{D}_x\mathbf{v} + \mu^2\mathbf{v}^T\mathbf{s}\mathbf{s}^T\mathbf{D}_x\mathbf{s}\mathbf{s}^T\mathbf{v} \\ &+ \mu e_o^i\mathbf{v}^T\mathbf{D}_x\mathbf{s} - \mu^2 e_o^i\mathbf{v}^T\mathbf{s}\mathbf{s}^T\mathbf{D}_x\mathbf{s} \\ &+ \mu e_o^i\mathbf{s}^T\mathbf{D}_x\mathbf{v} - \mu^2 e_o^i\mathbf{s}^T\mathbf{D}_x\mathbf{s}\mathbf{s}^T\mathbf{v} \\ &+ (\mu e_o^i)^2\mathbf{s}^T\mathbf{D}_x\mathbf{s}\big]\end{aligned}$$

where we have omitted the time index (n) on the RHS for clarity. Using again the IA, the expectation of the terms inside the bracket are given by

$$E[\mathbf{v}^T\mathbf{D}_x\mathbf{v}] = \varepsilon_{ex}^{i}(n)$$

$$E[\mathbf{v}^T\mathbf{D}_x\mathbf{s}\mathbf{s}^T\mathbf{v}] = E[\mathbf{v}^T\mathbf{s}\mathbf{s}^T\mathbf{D}_x\mathbf{v}] = E[\mathbf{v}^T\mathbf{D}_x^2\mathbf{v}]$$

$$E[(e_o^i)^2\mathbf{s}^T\mathbf{D}_x\mathbf{s}]\,\varepsilon_{io} = \mathrm{tr}\,E[\mathbf{s}\mathbf{s}^T\mathbf{D}_x]\,\varepsilon_{io} = \mathrm{tr}[\mathbf{D}_x^2]\,\varepsilon_{io}$$

$$E[e_o^i\mathbf{v}^T\mathbf{D}_x\mathbf{s}] = E[e_o^i]E[\mathbf{v}^T\mathbf{D}_x\mathbf{s}] = 0,$$

and,

$$E[e_o^i\mathbf{v}^T\mathbf{s}\mathbf{s}^T\mathbf{D}_x\mathbf{s}] = E[e_o^i\mathbf{s}^T\mathbf{D}_x\mathbf{v}] = E[e_o^i\mathbf{s}^T\mathbf{D}_x\mathbf{s}\mathbf{s}^T\mathbf{v}] = 0$$

To simplify the derivations further, the authors in [63] assumed that the elements in $\mathbf{s}$ are iid random variables such that they have the same *kurtosis* $\kappa \triangleq E[s_i^4]/(E[s_i^2])^2$ where s_i is the ith element of the vector $\mathbf{s}$. By expanding $\mathbf{v}^T\mathbf{s}\mathbf{s}^T\mathbf{D}_x\mathbf{s}\mathbf{s}^T\mathbf{v}$, it can be shown that [63]

$$E[\mathbf{v}^T\mathbf{s}\mathbf{s}^T\mathbf{D}_x\mathbf{s}\mathbf{s}^T\mathbf{v}] \approx \varepsilon_{ex}(n)N_s\lambda_{rms}^2 + (\kappa - 1)E[\mathbf{v}^T\mathbf{D}_x^3\mathbf{v}] \qquad (7.31)$$

where N_s is the number of significant eigenvalues in $\mathbf{A}_x$ (or $\mathbf{D}_x$), λ_i is the ith largest eigenvalue, and $\lambda_{rms}^2 \triangleq \frac{1}{N_s}\sum_{i=1}^{N_s}\lambda_i^2$. Summarising all the expectation

terms, we obtain

$$\varepsilon_{ex}^{i}(n+1) = \varepsilon_{ex}^{i}(n) - 2\mu E[\mathbf{v}^T\mathbf{D}_x^2\mathbf{v}] + \mu^2\varepsilon_{ex}^{i}(n)N_s\lambda_{rms}^2 + \mu^2(\kappa-1)E[\mathbf{v}^T\mathbf{D}_x^3\mathbf{v}] + \mu^2\,\mathrm{tr}[\mathbf{D}_x^2]\varepsilon_{io} \tag{7.32}$$

In order to obtain a more mathematically tractable formula, the authors further assume that

$$E[\mathbf{v}^T\mathbf{D}_x^3\mathbf{v}] \approx \lambda_{rms}^2 E[\mathbf{v}^T\mathbf{D}_x\mathbf{v}] = \lambda_{rms}^2\varepsilon_{ex}^{i}(n) \tag{7.33a}$$

$$E[\mathbf{v}^T\mathbf{D}_x^2\mathbf{v}] \approx \bar{\lambda}E[\mathbf{v}^T\mathbf{D}_x\mathbf{v}] = \bar{\lambda}\varepsilon_{ex}^{i}(n) \tag{7.33b}$$

where $\bar{\lambda}$ is defined as $\bar{\lambda} \triangleq \frac{1}{N_s}\sum_{i=1}^{N_s}\lambda_i$. Note that the approximations become exact when all the eigenvalues in $\mathbf{D}_x$ are equal. Then, (7.32) becomes

$$\varepsilon_{ex}^{i}(n+1) = \gamma\varepsilon_{ex}^{i}(n) + \mu^2\,\mathrm{tr}[\mathbf{D}_x^2]\varepsilon_{io} \tag{7.34}$$

where $\gamma \triangleq 1-2\mu\bar{\lambda}+\mu^2\lambda_{rms}^2(N_s+\kappa-1)$. Solving the difference equation (7.34), we obtain

$$\varepsilon_{ex}^{i}(n) = \gamma^n\varepsilon_{ex}^{i}(0) + \mu^2\,\mathrm{tr}[\mathbf{D}_x^2]\varepsilon_{io}\frac{1-\gamma^n}{1-\gamma} \tag{7.35}$$

for the excess MSE. In terms of the normalised MSE, it can be shown from (7.35) that

$$\varepsilon_i(n) = \gamma^n\varepsilon_i(0) + (1-\gamma^n)\varepsilon_{io} + \mu^2\,\mathrm{tr}[\mathbf{D}_x^2]\varepsilon_{io}\frac{1-\gamma^n}{1-\gamma} \tag{7.36}$$

Note that in order for (7.35) and (7.36) to converge, it is necessary that $|\gamma| < 1$. Thus, from the definition of γ, we obtain

$$0 < \mu < \frac{2\bar{\lambda}}{\lambda_{rms}^2(N_s+\kappa-1)} \tag{7.37}$$

The learning curve described by (7.36) is often characterised by its *initial convergence rate* and *misadjustment*. The initial convergence rate for the

inphase learning curve is defined by

$$\frac{1}{\tau_i} \triangleq \ln\left\{\frac{\varepsilon_i(0)-\varepsilon_i(\infty)}{\varepsilon_i(1)-\varepsilon_i(\infty)}\right\}$$

where τ_i is called the *time constant*, and $\varepsilon_i(0)$, $\varepsilon_i(1)$ and $\varepsilon_i(\infty)$ are computed from (7.36). The corresponding misadjustment is defined by

$$\mathcal{M}_i \triangleq \frac{\varepsilon_{ex}^i(\infty)}{\varepsilon_{io}}$$

where $\varepsilon_{ex}^i(\infty)$ is computed from (7.35).

7.3.3 Modified LMS

The common weight vector $\mathbf{w}$ for the I and Q equalisers in Fig. 7.1 can be written in the following form

$$\mathbf{w}(n) = \mathbf{w}_o + \delta\mathbf{w}(n) \tag{7.38}$$

where $\mathbf{w}_o$ is the optimum weight vector and $\delta\mathbf{w}(n)$ is the weight-error vector. The I and Q errors $e_i(nT)$ and $e_q(nT)$ at the slicer are defined by

$$e_i(n) \triangleq a_n - \mathbf{w}^T(n)\mathbf{x}_i(n)$$

$$e_q(n) \triangleq b_n - \mathbf{w}^T(n)\mathbf{x}_q(n)$$

Using (7.38), we have

$$e_i(n) = e_{io}(n) - \delta\mathbf{w}^T(n)\mathbf{x}_i(n) \tag{7.39a}$$

$$e_q(n) = e_{qo}(n) - \delta\mathbf{w}^T(n)\mathbf{x}_q(n) \tag{7.39b}$$

where $e_{io}(n)$ and $e_{qo}(n)$ are given by

$$e_{io}(n) \triangleq a_n - \mathbf{w}_o^T\mathbf{x}_i(n)$$

$$e_{qo}(n) \triangleq b_n - \mathbf{w}_o^T\mathbf{x}_q(n)$$

The inphase MSE at the slicer is defined by

$$\varepsilon(n) \triangleq E[(e_i)^2(n)]$$

Expanding the RHS, using (7.39) and the orthogonality principle, it can be shown that

$$\varepsilon(n) = \varepsilon_o + E[\delta\mathbf{w}^T(n)\mathbf{A}\delta\mathbf{w}(n)] \tag{7.40}$$

where $\varepsilon_o \triangleq E[e_{io}^2(n)] = E[e_{qo}^2(n)]$ and $\mathbf{A}$ is defined as $\mathbf{A} \triangleq E[\mathbf{x}_i\mathbf{x}_i^T] = E[\mathbf{x}_q\mathbf{x}_q^T]$, as derived previously. The second term in (7.40) can be thought as the excess MSE which we denote by

$$\varepsilon_{ex}(n) \triangleq E[\delta\mathbf{w}^T(n)\mathbf{A}\delta\mathbf{w}(n)]$$

Similarly, we can derive the same expression as the RHS of (7.40) for the quadrature MSE at the slicer. This result shows that the I and Q equalisers not only have the same MMSE solutions, but also the same MSE at any sampling time.

Let $\mathbf{Q}$ be the unitary matrix such that

$$\mathbf{Q}^T\mathbf{A}\mathbf{Q} = \mathbf{D}$$

where $\mathbf{D}$ is a diagonal matrix which contains the eigenvalues $\{\theta_l\}$ of $\mathbf{A}$. Linear transformations of $\delta\mathbf{w}(n)$, $\mathbf{x}_i(n)$ and $\mathbf{x}_q(n)$ by $\mathbf{D}^T$ give

$$\mathbf{u}(n) \triangleq \mathbf{Q}^T\delta\mathbf{w}(n), \qquad \mathbf{t}_i(n) \triangleq \mathbf{Q}^T\mathbf{x}_i(n), \qquad \mathbf{t}_q(n) \triangleq \mathbf{Q}^T\mathbf{x}_q(n)$$

Now, substituting (7.38) into the modified LMS algorithm (7.24) and after some simplification, we get

$$\delta\mathbf{w}(n+1) = \delta\mathbf{w} - \mu_m[\mathbf{x}_i\mathbf{x}_i^T + \mathbf{x}_q\mathbf{x}_q^T]\delta\mathbf{w} + \mu_m[e_{io}\mathbf{x}_i + e_{qo}\mathbf{x}_q] \tag{7.41}$$

where for clarity we have omitted (n) on the RHS of the equation. Pre-multiplying both side of (7.41) by $\mathbf{Q}^T$ and using the definitions for $\mathbf{u}(n)$, $\mathbf{t}_i(n)$, and $\mathbf{t}_q(n)$, we have

$$\mathbf{u}(n+1) = \mathbf{u}(n) - \mu_m \mathbf{T}(n)\mathbf{u}(n) + \mu_m \mathbf{r}_t(n) \tag{7.42}$$

where $\mathbf{T}(n)$ and $\mathbf{r}_t(n)$ are defined by

$$\mathbf{T}(n) \triangleq \mathbf{Q}^T[\mathbf{x}_i\mathbf{x}_i^T + \mathbf{x}_q\mathbf{x}_q^T]\mathbf{Q} = \mathbf{t}_i\mathbf{t}_i^T + \mathbf{t}_q\mathbf{t}_q^T$$

$$\mathbf{r}_t(n) \triangleq \mathbf{Q}^T(e_{io}\mathbf{x}_i + e_{qo}\mathbf{x}_q) = e_{io}\mathbf{t}_i + e_{qo}\mathbf{t}_q$$

Substituting (7.42) into $\varepsilon_{ex}(n)$ and expanding the result, it is shown in Appendix E that $\varepsilon_{ex}(n)$ satisfies

$$\varepsilon_{ex}(n+1) = \varepsilon_{ex}(n)\gamma_m + 2\mu_m^2 \varepsilon_o \operatorname{tr}[\mathbf{D}^2] \tag{7.43}$$

where γ_m is given by

$$\gamma_m \triangleq 1 - 4\mu_m\bar{\theta} + 2\mu_m^2\theta_{rms}^2\big(N_{ms} + \kappa_m + 1\big)$$

in which κ_m is the kurtosis defined by $\kappa_m \triangleq E[x_i^4]/(E[x_i^2])^2$, N_{ms} is the number of significant eigenvalues in $\{\theta_l\}$, and $\bar{\theta}$ and θ_{rms}^2 are the average and RMS average of the significant eigenvalues, i.e.,

$$\bar{\theta} \triangleq \frac{1}{N_{ms}}\sum_{l=1}^{N_{ms}}\theta_l \qquad \text{and} \qquad \theta_{rms}^2 \triangleq \frac{1}{N_{ms}}\sum_{l=1}^{N_{ms}}\theta_l^2$$

where the eigenvalues $\{\theta_l\}$ are arranged in descending order, i.e., $\theta_1 \geq \theta_2 \geq \cdots \geq \theta_N$.

Solving the first order difference equation (7.43), we have

$$\varepsilon_{ex}(n) = \gamma_m^n \varepsilon_{ex}(0) + 2\mu_m^2 \operatorname{tr}[\mathbf{D}^2]\varepsilon_o \frac{1-\gamma_m^n}{1-\gamma_m} \tag{7.44}$$

Finally, from (7.44) the learning curve of the modified LMS is given by

$$\varepsilon(n) = \gamma_m^n \varepsilon(0) + (1 - \gamma_m^n)\varepsilon_o + 2\mu_m^2 \,\mathrm{tr}[\mathbf{D}^2]\varepsilon_o \frac{1 - \gamma_m^n}{1 - \gamma_m} \tag{7.45}$$

Again, for (7.44) and (7.45) to converge, it is necessary that $|\gamma_m| < 1$, or from the definition of $|\gamma_m|$,

$$0 < \mu_m < \frac{2\bar{\theta}}{\theta_{rms}^2(N_{ms} + \kappa_m + 1)} \tag{7.46}$$

As in the previous case for the standard LMS algorithm, the initial convergence rate and misadjustment for the modified LMS algorithm are given by

$$\frac{1}{\tau} \triangleq \ln\left\{\frac{\varepsilon(0) - \varepsilon(\infty)}{\varepsilon(1) - \varepsilon(\infty)}\right\} \qquad \text{and} \qquad \mathcal{M} \triangleq \frac{\varepsilon_{ex}(\infty)}{\varepsilon_o}$$

where $\varepsilon(0)$, $\varepsilon(1)$, and $\varepsilon(\infty)$ are computed from (7.45); $\varepsilon_{ex}(\infty)$ and ε_o from (7.44) and (7.20), respectively.

7.4 Simulation Results

Our simulation consists of 100 m of UTP-3 cable, the SNR at the input to the CAP receiver set to 30 dB, 16–CAP scheme with a symbol rate of 12.96 Mbaud, and a RRC filter with a roll-off factor of 1.0. For convenience, the starting frequency of the passband shaping filter is at DC and the centre frequency is at 12.96 MHz. The FSEs have 25 taps with an over sampling rate of 4. In addition, the fixed front-end receive filters of the new receiver is treated as part of the transmission channel.

We assume that the equalisers are sufficiently long such that the MMSEs for both standard and proposed receivers are the same, i.e., $\varepsilon_{io} = \varepsilon_o$. This is a valid assumption, as indicated in Section 7.2. We compare the modified

LMS algorithm with the standard LMS algorithm in terms of their initial convergence rates and misadjustments. Since these two parameters are generally inter-dependent [56], we compare either the initial convergence rates or the misadjustments while forcing the others parameters to be the same. In this way, we make the comparison as fair as possible.

In the evaluation of (7.36) and (7.45), we assume that $\kappa = \kappa_m \approx 1.64$ where κ_m is computed from the symbol sequence of the 16–CAP scheme, and $N_s = N_{ms} \approx 12$ for the channel which is found by inspecting the calculated results.

Comparison of initial convergence rates

As indicated above, in order to maintain the same misadjustment, we first select the step size μ for the standard LMS algorithm and then use (7.35) to find the misadjustment. From this misadjustment, we then compute the step size for the modified algorithm. Alternatively, we can merge these two step into a single equation which is given by

$$\mu_m = \frac{2\mu^2 \operatorname{tr}[\mathbf{D}_x^2]\,\bar{\theta}}{\mu^2 \operatorname{tr}[\mathbf{D}_x^2]\theta_{rms}^2\,(N_s + \kappa + 1) - \operatorname{tr}[\mathbf{D}^2](1-\gamma)} \tag{7.47}$$

Fig. 7.2 plots the normalised MSE against time in units of symbol period. The 'noisy' lines show the MSE learning curves of the adaptive algorithms, whereas the smooth lines are the predicted learning curves as given by (7.36) and (7.45) for the standard and modified LMS, respectively. It can be seen that both algorithms have as expected, the same misadjustment, but at different convergence rates. The calculated initial convergence rates for the standard and modified LMS are $\tau^{-1} = 0.03$ and $\tau_m^{-1} = 0.058$, respectively for a misadjustment of 10%. The convergence rate of the proposed adaptive algorithm is thus approximately double that of the standard LMS algorithm.

We obtain similar results for other values of misadjustment.

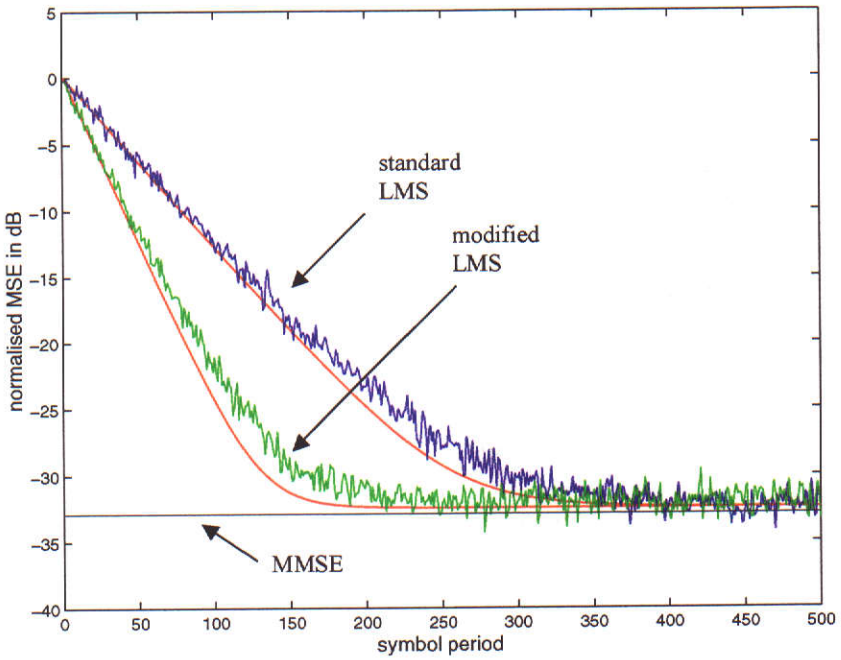

Figure 7.2: Comparison of initial convergence rates with same misadjustment, averaged over 60 trials

Comparison of misadjustments

In the second simulation, we fix the convergence rate while comparing the misadjustments. But first, we would like to simplify the convergence calculation. The simplification is illustrated through the convergence rate of the modified LMS algorithm. Since $\varepsilon(0) > \varepsilon(1) \gg \varepsilon(\infty)$, the initial convergence rate can be approximated by

$$\frac{1}{\tau} \approx \ln \frac{\varepsilon(0)}{\varepsilon(1)} \tag{7.48}$$

For the normalised learning curves ($\varepsilon(0) = 1$), it can be seen from (7.48), that in order to achieve the same convergence rates for both algorithms, we

have $\varepsilon_i(1) = \varepsilon(1)$. Using (7.36) and (7.45), we can write

$$2(\mathrm{tr}[D^2]\varepsilon_o + \theta_{rms}^2(N_s + \kappa + 1))\mu_m^2 - 4\bar{\theta}\mu_m + 2\mu\bar{\lambda} - \mu^2\lambda_{rms}^2(N_s + \kappa - 1) - \mu^2\,\mathrm{tr}[D_x^2]\varepsilon_o = 0 \tag{7.49}$$

where $1 - \varepsilon_o \approx 1$. Therefore, the initial convergence rates of the standard and modified LMS algorithms can be made the same by first selecting a step size μ then using (7.49) to find the corresponding μ_m.

Fig. 7.3 plots the simulated and predicated learning curves. We observe that both algorithms have approximately the same initial convergence rates while the misadjustments differ. The calculated values of the misadjustment for the standard and modified LMS algorithms are 0.67 and 0.17, respectively. In other words, the misadjustment of the proposed algorithm is less than half of that of the standard LMS algorithm.

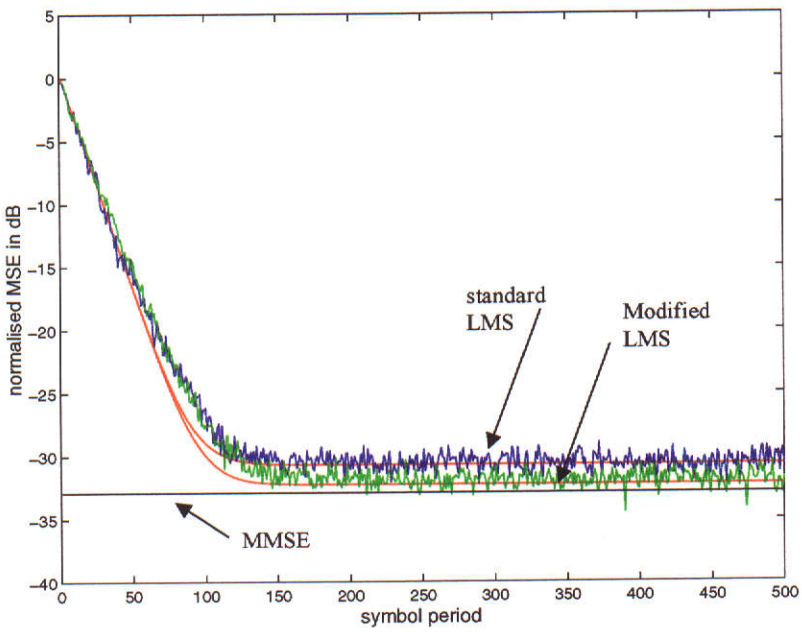

Figure 7.3: Comparison of misadjustments with same initial convergence rate, averaged over 60 trials

7.5 Summary

In this chapter, we considered an alternative linear CAP receiver structure based an existing linear CAP receiver using two parallel FSEs. The main difference between the two receivers is that the new receiver has two fixed analog filters which are matched to the transmit filter pair, followed by a pair of FSEs. The MMSE for finite-length FSEs was then derived. Results showed that the equalisers in the new receiver have the same MMSE solutions. Using this feature, we proposed a modified LMS algorithm which was then analysed. We showed that compared with the standard LMS algorithm, the new algorithm approximately doubles the initial convergence rate for the same misadjustment, or alternatively, it more than halves the misadjustment for the same initial convergence rate. Simulation results were also given.

CHAPTER 8
CONCLUSIONS

8.1 Concluding Remarks

The key driving force behind the current research on CAP systems is that they have the same bandwidth efficiency as their corresponding QAM systems, but with a transceiver structure that is surprisingly simple to implement. This feature alone makes CAP the ideal replacement line code for many communication systems, in particular xDSL systems using QAM/PAM line codes.

With the target xDSL systems in mind, we studied the channel and interference models for the types of cables commonly found in existing PSTNs. Apart from the usual channel impairments such as time dispersion and background noise, cross-talks from adjacent copper wire pairs can also limit the data throughput of these systems. In our system analysis, we considered two types of cross-talk models, namely, the stationary model and data-like model. The choice of cross-talk models depends on the cable of interests. If there is a large number of (unsynchronised) interferers and none of them is dominant, then, by invoking the central limit theorem, their total effect can be modelled as an additive Gaussian noise source. On the other hand, if there is only a very limited number of interferers and one or two of them are dominant, then the data-like model is more appropriate. The former interference model is often applicable in xDSL systems, whereas the latter model is applicable in applications such as ATM LAN over UTP-3 cables. It should be pointed that the

two aforesaid cross-talk models represent the two extreme cases in an actual system.

In recent years, significant research efforts around the world have been directed towards an understanding of the CAP line code. As part of this world wide research effort, our focus is on the MMSE performance of linear and DFE CAP receivers, operating in the presence of stationary and/or data-like cross-talks and additive Gaussian channel noise. The study of linear CAP receivers could have been approached by specialising the existing results for a general linear MIMO system, but to the author's best knowledge, this approach has not produced any more meaningful solutions that offer further insights into the performance of the CAP systems than what has already been shown. Treating both linear and DFE CAP receivers as new problems, we reconsidered these MMSE problems with special consideration of the Hilbert pair relationship between the transmit filter pairs.

Our new results provide better understanding of both receiver structures. To be more specific, in the linear receiver case when both data-like cross-talks and noise are present, the derived transfer functions of the optimum receive filter pair are given in frequency intervals of $1/T$ Hz where the contribution of the cross-talk in each interval is clearly represented. And when only channel noise is present, the derived expressions can be further simplified to a form similar to that found in a QAM system.

In the DFE case, we provided a method of computing the transfer functions of the optimum feed-forward and feed-back filters, provided the channel spectral matrix can be factorised into a product of minimum and maximum phase terms. The MMSE expression for the DFE receiver provides an important performance bound in the engineering design of such systems. Apart from

these immediate applications, the derived results also give further insights into some of the known engineering issues such as the effects of the relative phase of the cross-talk signals on the system performance as discussed previously.

To further our understanding of the CAP line code, three sets of numerical studies were conducted, based on the derived results. In the first set of studies, we compared the MMSE performance of a linear and a DFE CAP receiver in a stationary cross-talk environment. In order to determine the effectiveness of the receiver structures based on equalisation techniques, our comparisons also included the results computed with the MFB. In the second set of studies, we compared the MMSE performance of a linear and a DFE CAP receiver in a data-like cross-talk environment. The results demonstrated the importance of NEXT equalisation in the design of a CAP transceiver system operating in data-like NEXT dominant environments. In the final set of studies, we further investigated the relationship between the performance of a DFE CAP receiver and various system parameters, in the presence of data-like NEXT. Much information on the performance of linear and DFE receiver structures has been revealed in these studies. It complements the existing knowledge on CAP receivers obtained through the use of finite length receive filters. Without the limitation imposed by the finite length of the receive filters, we were able to gain a clearer and hence better understanding of these issues.

In addition, we also considered a novel adaptive linear CAP receiver, based on an existing adaptive linear CAP receiver structure. The main feature of the proposed receiver structure is that the optimum I and Q FSEs have the same transfer functions. Based on the standard LMS algorithm, a modified LMS algorithm was proposed for the new receiver structure. Analysis and

simulation results showed that the initial convergence rate of the modified LMS algorithm is approximate twice as fast as that of the standard LMS algorithm, given the same misadjustment; alternatively, given the same initial convergence rate, the misadjustment of the modified LMS algorithm is less than half of that of the standard LMS algorithm.

8.2 Suggestions for Future Work

Although significant research efforts have been recently put into the standard 2–D CAP line code, there remain many unknowns. The purpose of our current work is twofold – to further our understanding of CAP systems, and to stimulate further researches on issues arising from this work. In the following, we summarise some of these issues which are directly related to the research work presented in this thesis.

One clear omission is research on related hardware issues. In particular, we would like to know what are the expected performance levels of the linear and DFE CAP receivers with finite-length FSEs. This issue is particularly important in the presence of data-like cross-talks. Compared to the simulation results in Fig. 4.6, the results in Fig. 4.5 indicate that the FSEs require a relatively large number of taps to approach the performance of the ideal equalisers. In another words, we can expect a significant performance drop as a result of the constraint on the number of taps. Another hardware related design issue is the implementation of the fixed front-end (analog) filters shown in Chapter 7. Since these filters are typically implemented as digital filters, an important design issue is to try to achieve simultaneously the Hilbert pair relationship and a close approximation of the passband RRC filter characteristics.

The second omission is research on the convergence characteristics of the adaptive equaliser in the presence of data-like cross-talks. The learning curves

shown in [13] which are confirmed by our simulation results, reveal that the total convergence process can be divided into two stages . The explanations given by the authors of [13] are as follows. In the first stage, the equaliser mainly 'sees' ISI, therefore it follows the same curve for the situation when there are no data-like cross-talks. After the removal of enough ISI, the equaliser starts to jointly equalise the remaining ISI and the data-like cross-talk. The convergence rate in the second stage is much slower than that in the first stage, due to this joint equalisation. Theoretical analysis on the convergence characteristics is required in order to fully understand this observation.

Finally, from the above discussions, we see that the performance of CAP receivers based on the conventional linear and DFE receiver structures will be severely degraded due to the limitation on system bandwidth or the number of equaliser taps, or both, in the presence of data-like cross-talk. This indicates that research on new CAP receiver structures are required to effectively combat this type of interference.

APPENDIX A
PROOF OF $\mathbf{\Lambda}^H\mathbf{W}^{-1}\mathbf{\Lambda} = \mathbf{W}^{-1}$

let $Q_m(\bar{f})$ and $\tilde{Q}_m(\bar{f})$ be the inphase and quadrature equivalent channels of the mth interferer which uses the same 2–D CAP line code. Then

$$W_{k,l}(\bar{f}) = \frac{1}{T}\left\{\sum_{m=1}^{L_b/2}\left[Q_m^*(\bar{f}+\frac{k}{T})Q_m(\bar{f}+\frac{l}{T}) + \tilde{Q}_m^*(\bar{f}+\frac{k}{T})\tilde{Q}_m(\bar{f}+\frac{l}{T})\right]\right\} + N_o'\delta_{kl} \tag{A.1}$$

where $-K \le k,l \le K$ are the row and column indices, respectively, and $\bar{f} \in [-\frac{1}{2T}, \frac{1}{2T}]$. Without loss of generality, in the equation we assume that channel noise is white. The upper triangle of matrix $\mathbf{W}$ may be divided into 6 regions depending on the values of k and l as shown below

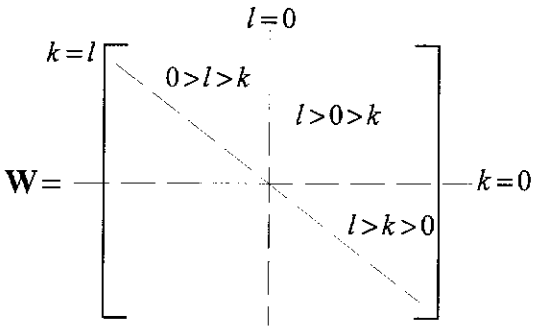

Consider the matrix elements in each region. From (A.1) and recall that $\tilde{x}(f) = (-j)\,\mathrm{sgn}(f)x(f)$, we have

1. $k = l$ case

$$W_{k,l} = \frac{1}{T}\left\{\sum_{m=1}^{L_b/2}\left[\left|Q_m(\bar{f}+\frac{l}{T})\right|^2 + \left|\tilde{Q}_m(\bar{f}+\frac{l}{T})\right|^2\right]\right\} + N_o'\delta_{lk} \neq 0$$

2. $0 > l > k$ case

$$W_{k,l} = \frac{1}{T}\sum_{m=1}^{L_b/2}\Big[Q_m^*(\bar{f}+\frac{k}{T})Q_m(\bar{f}+\frac{l}{T}) + (j)(-1)Q_m^*(\bar{f}+\frac{k}{T})(-j)(-1)Q_m(\bar{f}+\frac{l}{T})\Big] = \frac{2}{T}\sum_{m=1}^{L_b/2} Q_m^*(\bar{f}+\frac{k}{T})Q_m(\bar{f}+\frac{l}{T}) \neq 0$$

3. $l > 0 > k$ case

$$W_{k,l} = \frac{1}{T}\sum_{m=1}^{L_b/2}\Big[Q_m^*(\bar{f}+\frac{k}{T})Q_m(\bar{f}+\frac{l}{T}) + (j)(-1)Q_m^*(\bar{f}+\frac{k}{T})(-j)(1)Q_m(\bar{f}+\frac{l}{T})\Big] = 0$$

4. $k > l > 0$ case

$$W_{k,l} = \frac{1}{T}\sum_{m=1}^{L_b/2}\Big[Q_m^*(\bar{f}+\frac{k}{T})Q_m(\bar{f}+\frac{l}{T}) + (j)Q_m^*(\bar{f}+\frac{k}{T})(-j)Q_m(\bar{f}+\frac{l}{T})\Big] = \frac{2}{T}\sum_{m=1}^{L_b/2} Q_m^*(\bar{f}+\frac{k}{T})Q_m(\bar{f}+\frac{l}{T}) \neq 0$$

5. $k < 0,\ l = 0$ case

$$W_{k,l} = \frac{1}{T}\sum_{m=1}^{L_b/2}\Big[Q_m^*(\bar{f}+\frac{k}{T})Q_m(\bar{f}) + (j)(-1)Q_m^*(\bar{f}+\frac{k}{T})(-j)\,\mathrm{sgn}(\bar{f})Q_m(\bar{f})\Big] = \frac{1}{T}[1-\mathrm{sgn}(\bar{f})]\sum_{m=1}^{L_b/2} Q_m^*(\bar{f}+\frac{k}{T})Q_m(\bar{f}).$$

6. $k = 0,\ l > 0$ case

$$\begin{aligned} W_{k,l} &= \frac{1}{T}\sum_{m=1}^{L_b/2}\big[Q_m^*(\bar{f})Q_m(\bar{f}+\frac{l}{T}) \\ &\quad + (j)\,\mathrm{sgn}(\bar{f})Q_m^*(\bar{f})(-j)Q_m(\bar{f}+\frac{l}{T})\big] \\ &= \frac{1}{T}[1+\mathrm{sgn}(\bar{f})]\sum_{m=1}^{L_b/2} Q_m^*(\bar{f})Q_m(\bar{f}+\frac{l}{T}). \end{aligned}$$

Since $\mathbf{W}$ is Hermitian, the elements in the lower triangle region follows immediately.

Now, consider the situation where $\bar{f} > 0$ and $K = 3$ (for other values of K, the steps are very similar), then $\mathbf{W}$ can be written as follows

$$\mathbf{W} = \begin{bmatrix} \mathbf{A}_{11}^{(3\times3)} & \mathbf{0}^{(3\times4)} \\ \mathbf{0}^{(4\times3)} & \mathbf{A}_{22}^{(4\times4)} \end{bmatrix}$$

where $\mathbf{A}_{11}^{(3\times3)} \triangleq [W_{k,l}]$ for $-3 \le k,l \le -1$ and $\mathbf{A}_{22}^{(4\times4)} \triangleq [W_{k,l}]$ for $0 \le k,l \le 3$. Then

$$\mathbf{W}^{-1} = \begin{bmatrix} [\mathbf{A}_{11}^{(3\times3)}]^{-1} & \mathbf{0}^{(3\times4)} \\ \mathbf{0}^{(4\times3)} & [\mathbf{A}_{22}^{(4\times4)}]^{-1} \end{bmatrix}.$$

For $\bar{f} > 0$, $\mathbf{\Lambda}(\bar{f}) = \mathrm{diag}[\underbrace{j,\ldots,j}_{3},\underbrace{-j,\ldots,-j}_{4}]$. Therefore,

$$\mathbf{\Lambda}^H\mathbf{W}^{-1}\mathbf{\Lambda} = \mathbf{W}^{-1}. \tag{A.2}$$

For $\bar{f} < 0$, it is easily shown that $\mathbf{W}$ has the following form

$$\mathbf{W} = \begin{bmatrix} \mathbf{A}_{11}^{(4\times4)} & \mathbf{0}^{(4\times3)} \\ \mathbf{0}^{(3\times4)} & \mathbf{A}_{22}^{(3\times3)} \end{bmatrix}$$

and $\mathbf{\Lambda}(\bar{f}) = \mathrm{diag}[\underbrace{j,\ldots,j}_{4},\underbrace{-j,\ldots,-j}_{3}]$. Hence, (A.2) is also true.

APPENDIX B
SOLUTION TO $X(f)$

Define $f^+ \in [0,\ \infty)$ and the related notation $f^- \in (-\infty,\ 0)$. We write $f^+ = \bar{f} + \frac{m^+}{T}$. Then, for $f > 0$, $X(f)$ may be expressed as

$$\begin{aligned} X(f^+) &= \left[1 - K_T(\bar{f} + \frac{m^+}{T}) - j\,\tilde{K}_T(\bar{f} + \frac{m^+}{T})\right] \\ &= 1 - K_T(\bar{f}) - j\,\tilde{K}_T(\bar{f}) \\ &\triangleq X_T^+(\bar{f}) \end{aligned} \tag{B.1}$$

Similarly, for $f < 0$, we have

$$\begin{aligned} X(-f^+) &= 1 - K_T(-\bar{f}) + j\,\tilde{K}_T(-\bar{f}) \\ &\triangleq X_T^-(-\bar{f}) \end{aligned} \tag{B.2}$$

Now, we express $K_T(\bar{f})$ and $\tilde{K}_T(\bar{f})$ in terms of the folded spectrum of $K(f)$ and $\tilde{K}(f)$ respectively, i.e.,

$$K_T(\bar{f}) = \frac{1}{T}\sum_{k=-K}^{K} K\big(\bar{f} + \frac{k}{T}\big) \tag{B.3a}$$

$$\tilde{K}_T(\bar{f}) = \frac{1}{T}\sum_{k=-K}^{K} \tilde{K}\big(\bar{f} + \frac{k}{T}\big) \tag{B.3b}$$

Substituting (4.33) into (B.3) and expanding the RHS, we get

$$\begin{aligned} K_T(\bar{f}) = \frac{1}{T}\Big\{ &\Gamma(\bar{f})X(\bar{f}) + X_T^+(\bar{f})\sum_{k=1}^{K}\Gamma(\bar{f} + \frac{k}{T}) \\ &+ X_T^-(\bar{f})\sum_{k=1}^{K}\Gamma(\bar{f} - \frac{k}{T})\Big\} \end{aligned} \tag{B.4}$$

and

$$\tilde{K}_T(\bar{f}) = \frac{-j}{T}\Big\{\mathrm{sgn}(\bar{f})\Gamma(\bar{f})X(\bar{f}) + X_T^+(\bar{f})\sum_{k=1}^{K}\Gamma(\bar{f}+\frac{k}{T}) - X_T^-(\bar{f})\sum_{k=1}^{K}\Gamma(\bar{f}-\frac{k}{T})\Big\} \tag{B.5}$$

Next, substituting (B.4) and (B.5) and back into (B.1) and (B.2), and solving for $X_T^+(\bar{f})$ and $X_T^-(\bar{f})$, we obtain

$$X(f^+) = X(-f^+) = X_T^+(\bar{f}) = X_T^-(-\bar{f}) = \frac{1}{\frac{1}{T}\Big\{2\sum_{k=1}^{L}\Gamma(\bar{f}+\frac{k}{T}) + [1+\mathrm{sgn}(\bar{f})]\Gamma(\bar{f})\Big\} + 1} \tag{B.6}$$

From the above equation, we notice first that $X(f)$ is an even function of f, and secondly the denominator on the RHS is the same as $S_{rb}(\bar{f})$ in (4.24). Finally, using the same technique as for $S_{rb}(\bar{f})$, we get

$$X(f) = \frac{1}{\frac{2}{T}\sum_{k=0}^{K}\Gamma\big(\bar{f}^+ + \frac{k}{T}\big) + 1} \tag{B.7}$$

where $\bar{f}^+ = |f| - \frac{m^+}{T}$ for some suitable integer m^+.

APPENDIX C
EXPANSION OF MSE

For convenience, we repeat (5.2) below

$$\varepsilon = E\left[\mathbf{e}^T(kT)\mathbf{e}(kT)\right] = trE\left[\mathbf{e}(kT)\mathbf{e}^T(kT)\right]. \tag{C.1}$$

The term of $\mathbf{e}(kT)\mathbf{e}^T(kT)$ can be expanded as follows

$$\begin{aligned}
&\mathbf{e}(kT)\mathbf{e}^T(kT) \\
&= [\mathbf{w}(kT) - \mathbf{a}(kT)][\mathbf{w}^T(kT) - \mathbf{a}^T(kT)] \\
&= \mathbf{w}(kT)\mathbf{w}^T(kT) - \mathbf{w}(kT)\mathbf{a}^T(kT) \\
&- \mathbf{a}(kT)\mathbf{w}^T(kT) + \mathbf{a}(kT)\mathbf{a}^T(kT).
\end{aligned} \tag{C.2}$$

Expanding each term on the RHS of (C.2) further and taking their expectations with respect to all symbols, we get

$$\begin{aligned}
&E[\mathbf{w}(kT)\mathbf{w}^T(kT)] \\
&= \iint [\sigma^2 \sum_{m=-\infty}^{\infty} \mathbf{g}_t^T(-\tau_1 - mT)\mathbf{g}_t(-\tau_2 - mT) + r_n(\tau_1 - \tau_2)] \\
&\qquad\qquad \mathbf{g}_r(\tau_1)\mathbf{g}_r^T(\tau_2)d\tau_1 d\tau_2 \\
&- \sigma^2 \sum_{l=1}^{\infty} \int \mathbf{g}_r(\tau)\mathbf{p}^T(-\tau + lT)\mathbf{F}_l^T d\tau \\
&- \sigma^2 \sum_{l=1}^{\infty} \int \mathbf{F}_l\mathbf{p}(-\tau + lT)\mathbf{g}_r^T(\tau)d\tau \\
&+ \sigma^2 \sum_{l=1}^{\infty} \mathbf{F}_l\mathbf{F}_l^T
\end{aligned} \tag{C.3}$$

where $r_n(\tau) \triangleq E[n(t-\tau)n(t)]$,

$$E[\mathbf{w}(kT)\mathbf{a}^T(kT)] = \sigma^2 \int \mathbf{g}_r(\tau)\mathbf{p}^T(-\tau)d\tau$$

and

$$E[\mathbf{a}(kT)\mathbf{a}^T(jT)] = \sigma^2\delta_{jk}\mathbf{I}.$$

In summary, the expectation of (C.2) can be written as

$$\begin{aligned}
\mathbf{E}_e = & \\
& \iint [\sum_{m=-\infty}^{\infty} \mathbf{g}_t^T(-\tau_1 - mT)\mathbf{g}_t(-\tau_2 - mT) + \sigma^{-2} r_n(\tau_1 - \tau_2)] \\
& \qquad\qquad \mathbf{g}_r(\tau_1)\mathbf{g}_r^T(\tau_2)d\tau_1 d\tau_2 \\
& - \sum_{l=1}^{\infty} \int \mathbf{g}_r(\tau)\mathbf{p}^T(-\tau + lT)\mathbf{F}_l^T d\tau \\
& - \sum_{l=1}^{\infty} \int \mathbf{F}_l\mathbf{p}(-\tau + lT)\mathbf{g}_r^T(\tau)d\tau + \sum_{l=1}^{\infty} \mathbf{F}_l\mathbf{F}_l^T \\
& - \int \mathbf{g}_r(\tau)\mathbf{p}^T(-\tau)d\tau - \int \mathbf{p}(-\tau)\mathbf{g}_r^T(\tau)d\tau + \mathbf{I}
\end{aligned} \tag{C.4}$$

where $\mathbf{E}_e \triangleq E[\mathbf{e}(kT)\mathbf{e}^T(kT)]/\sigma^2$.

We now re-write summation term $\sum_m \mathbf{g}_t^T\mathbf{g}_t$ in the above equation as follows

$$\sum_{m=-\infty}^{\infty} \mathbf{g}_t^T\mathbf{g}_t = \sum_{m=-\infty}^{\infty} \mathbf{q}^T\mathbf{q} + \sum_{m=-\infty}^{0} \mathbf{p}^T\mathbf{p} + \sum_{m=1}^{\infty} \mathbf{p}^T\mathbf{p}. \tag{C.5}$$

Substituting (C.5) into (C.4), we define the matrix $\mathbf{E}_f$ as follows

$$\begin{aligned}
&\mathbf{E}_f \triangleq \\
&\sum_{l=1}^{\infty} \iint \mathbf{p}^T(-\tau_1 - lT)\mathbf{p}(-\tau_2 - lT)\mathbf{g}_r(\tau_1)\mathbf{g}_r^T(\tau_2)d\tau_1 d\tau_2 \\
&- \sum_{l=1}^{\infty} \int \mathbf{g}_r(\tau)\mathbf{p}^T(-\tau + lT)\mathbf{F}_l^T d\tau - \sum_{l=1}^{\infty} \int \mathbf{F}_l \mathbf{p}(-\tau + lT)\mathbf{g}_r^T(\tau)d\tau \\
&+ \sum_{l=1}^{\infty} \mathbf{F}_l \mathbf{F}_l^T.
\end{aligned}$$

Note $\mathbf{E}_f$ can be factorised into the following form

$$\begin{aligned}
&\mathbf{E}_f = \\
&\sum_{l=1}^{\infty} \Big(\int \mathbf{g}_r(\tau)\mathbf{p}^T(-\tau + lT)d\tau - \mathbf{F}_l \Big) \Big(\int \mathbf{g}_r(\tau)\mathbf{p}^T(-\tau + lT)d\tau - \mathbf{F}_l \Big)^T. \qquad \text{(C.6)}
\end{aligned}$$

Next, we define

$$\begin{aligned}
A(\tau_1, \tau_2) \triangleq &\sum_{m=-\infty}^{\infty} \mathbf{q}^T(-\tau_1 - mT)\mathbf{q}(-\tau_2 - mT) \\
&+ \sum_{m=-\infty}^{0} \mathbf{p}^T(-\tau_1 - mT)\mathbf{p}(-\tau_2 - mT) + \sigma^{-2} r_n(\tau_1 - \tau_2).
\end{aligned}$$

Note that A is symmetric, i.e., $A(\tau_1, \tau_2) = A(\tau_2, \tau_1)$. Then, equation (C.4) can be written as

$$\mathbf{E}_e(\mathbf{g}_r, \mathbf{F}) = \mathbf{E}_f(\mathbf{g}_r, \mathbf{F}) + \mathbf{E}_g(\mathbf{g}_r) \qquad \text{(C.7)}$$

where the matrix $\mathbf{E}_g$ is given by

$$\begin{aligned}
\mathbf{E}_g \triangleq &\iint A(\tau_1, \tau_2)\mathbf{g}_r(\tau_1)\mathbf{g}_r^T(\tau_2)d\tau_1 d\tau_2 \\
&- \int \mathbf{g}_r(\tau)\mathbf{p}^T(-\tau)d\tau - \int \mathbf{p}(-\tau)\mathbf{g}_r^T(\tau)d\tau + \mathbf{I}.
\end{aligned}$$

APPENDIX D
PROOF THAT $\mathbf{E}_\gamma$ IS A SCALAR MATRIX

The matrix $\mathbf{\Phi}(z) \triangleq \mathbf{I} + \mathbf{M}(z)$ can be diagonalised by the unitary matrix

$$\mathbf{\Psi} \triangleq \frac{1}{2}\begin{bmatrix} 1 & j \\ j & 1 \end{bmatrix}.$$

That is

$$\mathbf{\Psi}^H \mathbf{\Phi} \mathbf{\Psi} = \begin{bmatrix} R-b & 0 \\ 0 & R+b \end{bmatrix}. \tag{D.1}$$

But $\mathbf{\Phi}(e^{j\theta})$ is positive definite since $\mathbf{M}(e^{j\theta})$ is positive definite. Therefore, the diagonal entries of $\mathbf{\Psi}^H \mathbf{\Phi} \mathbf{\Psi}$ are positive real functions of $\bar{f}$.

Now, since $\int_{-\pi}^{\pi} \ln(R \pm b)\, d\theta > -\infty$, then from one-dimensional factorisation theory, e.g. [5], there exist sequences $\alpha(z)$ and $\beta(z)$

$$\alpha(e^{j\theta}) \triangleq \sum_{m=0}^{\infty} \alpha_m e^{-jm\theta} \quad \text{and} \quad \beta(e^{j\theta}) \triangleq \sum_{m=0}^{\infty} \beta_m e^{-jm\theta}$$

with α_0 and β_0 being real and positive, such that $\mathbf{\Psi}^H \mathbf{\Phi} \mathbf{\Psi} = \mathbf{V}\mathbf{V}^H$ where $\mathbf{V}$ is defined as

$$\mathbf{V} \triangleq \begin{bmatrix} \alpha & 0 \\ 0 & \beta \end{bmatrix}.$$

Thus,

$$\begin{aligned} \mathbf{\Phi} &= (\mathbf{\Psi}\mathbf{V}\mathbf{\Psi}^H)(\mathbf{\Psi}\mathbf{V}^H\mathbf{\Psi}^H) \\ &= \mathbf{U}\mathbf{U}^H \end{aligned} \tag{D.2}$$

where

$$\mathbf{U} \triangleq \mathbf{\Psi V \Psi}^H = \begin{bmatrix} \alpha+\beta & -j(\alpha-\beta) \\ j(\alpha-\beta) & \alpha+\beta \end{bmatrix} \tag{D.3}$$

Let $\mathbf{U}_0$ denote the DC term in $\mathbf{U} = \sum_{m=-\infty}^{\infty} \mathbf{U}_m e^{-jm\theta}$. It follows from (D.3) that

$$\mathbf{U}_0 = \begin{bmatrix} \alpha_0+\beta_0 & -j(\alpha_0-\beta_0) \\ j(\alpha_0-\beta_0) & \alpha_0+\beta_0 \end{bmatrix} \tag{D.4}$$

Now, the matrix $\mathbf{E}_\gamma$ can also be written as

$$\mathbf{E}_\gamma = [\mathbf{U}_0 \mathbf{U}_0^H]^{-1} = \begin{bmatrix} x & jy \\ -jy & x \end{bmatrix}$$

where x and y are some real values. But, from the definition, $\mathbf{E}_\gamma$ cannot be complex, we thus conclude that $y = 0$, or $\mathbf{E}_\gamma$ is a scalar matrix.

APPENDIX E
CONVERGENCE OF THE MODIFIED LMS ALGORITHM

For convenience, the equation (7.42) is repeated below

$$\mathbf{u}(n+1) = \mathbf{u}(n) - \mu_m \mathbf{T}(n)\mathbf{u}(n) + \mu_m \mathbf{r}_t(n) \tag{E.1}$$

Using (E.1) and expanding ε_{ex}, we get

$$\begin{aligned}\varepsilon_{ex}(n+1) = E\big[&\mathbf{u}^T\mathbf{D}\mathbf{u} - \mu_m \mathbf{u}^T\mathbf{D}\mathbf{T}\mathbf{u} + \mu_m \mathbf{u}^T\mathbf{D}\mathbf{r}_t \\ &- \mu_m \mathbf{u}^T\mathbf{T}\mathbf{D}\mathbf{u} + \mu_m^2 \mathbf{u}^T\mathbf{T}\mathbf{D}\mathbf{T}\mathbf{u} - \mu_m^2 \mathbf{u}^T\mathbf{T}\mathbf{D}\mathbf{r}_t \\ &+ \mu_m \mathbf{r}_t^T\mathbf{D}\mathbf{u} - \mu_m^2 \mathbf{r}_t^T\mathbf{D}\mathbf{T}\mathbf{u} + \mu_m^2 \mathbf{r}_t^T\mathbf{D}\mathbf{r}_t\big]\end{aligned} \tag{E.2}$$

Now, using IA, each of the expectation terms in the above equation can be evaluated as follows

$$\begin{aligned}E\big[\mathbf{u}^T\mathbf{D}\mathbf{u}\big] &= \varepsilon_{ex}(n) \\ E\big[\mathbf{u}^T\mathbf{D}\mathbf{T}\mathbf{u}\big] &= E\big[\mathbf{u}^T\mathbf{D}(\mathbf{t}_i\mathbf{t}_i^T + \mathbf{t}_q\mathbf{t}_q^T)\mathbf{u}\big] \\ &\quad + E\big[\mathbf{u}^T\mathbf{D}\mathbf{t}_i\mathbf{t}_i^T\mathbf{u}\big] + E\big[\mathbf{u}^T\mathbf{D}\mathbf{t}_q\mathbf{t}_q^T\mathbf{u}\big] \\ &= 2E\big[\mathbf{u}^T\mathbf{D}^2\mathbf{u}^T\big]\end{aligned}$$

where we have used $E[\mathbf{t}_i\mathbf{t}_i^T] = E[\mathbf{t}_q\mathbf{t}_q^T] = \mathbf{D}$

$$\begin{aligned}E\big[\mathbf{u}^T\mathbf{D}\mathbf{r}_t\big] &= E\big[\mathbf{u}^T\mathbf{D}(e_{io}\mathbf{t}_i + e_{qo}\mathbf{t}_q)\big] = 0 \\ E\big[\mathbf{u}^T\mathbf{T}\mathbf{D}\mathbf{u}\big] &= E\big[\mathbf{u}^T(\mathbf{t}_i\mathbf{t}_i^T + \mathbf{t}_q\mathbf{t}_q^T)\mathbf{D}\mathbf{u}\big] = 2E\big[\mathbf{u}^T\mathbf{D}^2\mathbf{u}\big] \\ E\big[\mathbf{u}^T\mathbf{T}\mathbf{D}\mathbf{r}_t\big] &= E\big[\mathbf{u}^T\mathbf{T}\mathbf{D}(e_{io}\mathbf{t}_i + e_{qo}\mathbf{t}_q)\big] = 0 \\ E\big[\mathbf{r}_t^T\mathbf{D}\mathbf{u}\big] &= 0, \qquad E\big[\mathbf{r}_t^T\mathbf{D}\mathbf{T}\mathbf{u}\big] = 0\end{aligned}$$

and

$$E\left[\mathbf{r}_t^T\mathbf{D}\mathbf{r}_t\right] = E\left[(e_{io}\mathbf{t}_i^T + e_{qo}\mathbf{t}_t^T)\mathbf{D}(e_{io}\mathbf{t}_i + e_{qo}\mathbf{t}_t)\right]$$
$$= 2\varepsilon_o \,\mathrm{tr}[\mathbf{D}^2]$$

The evaluation of the term $E\left[\mathbf{u}^T\mathbf{T}\mathbf{D}\mathbf{T}\mathbf{u}\right]$ is not straight forward, as will be shown below.

First, we expand the expectation

$$E\left[\mathbf{u}^T\mathbf{T}\mathbf{D}\mathbf{T}\mathbf{u}\right] = E\left[\mathbf{u}^T(\mathbf{t}_i\mathbf{t}_i^T + \mathbf{t}_q\mathbf{t}_q^T)\mathbf{D}(\mathbf{t}_i\mathbf{t}_i^T + \mathbf{t}_q\mathbf{t}_q^T)\mathbf{u}\right]$$
$$= 2E\left[\mathbf{u}^T\mathbf{t}_i\mathbf{t}_i^T\mathbf{D}\mathbf{t}_i\mathbf{t}_i^T\mathbf{u}\right] + 2E\left[\mathbf{u}^T\mathbf{t}_i\mathbf{t}_i^T\mathbf{D}\mathbf{t}_q\mathbf{t}_q^T\mathbf{u}\right] \qquad \text{(E.3)}$$

Note that the first term on the RHS of (E.3) is identical to (7.31), except that the corresponding quantities are now for the modified LMS. Therefore, we can immediately write

$$E\left[\mathbf{u}^T\mathbf{t}_i\mathbf{t}_i^T\mathbf{D}\mathbf{t}_i\mathbf{t}_i^T\mathbf{u}\right] \approx \varepsilon_{ex}(n)N_s\,\theta_{rms}^2 + (\kappa_m - 1)E\left[\mathbf{u}^T\mathbf{D}^3\mathbf{u}\right] \qquad \text{(E.4)}$$

where N_s is the number of significant eigenvalues $\{\theta_i\}$ of $\mathbf{D}$, and θ_{rms}^2 is the RMS average of the significant eigenvalues, i.e., $\theta_{rms}^2 \triangleq \frac{1}{N_s}\sum_{l=1}^{N_s}\theta_l^2$, assuming the eigenvalues are arranged in descending order. A related quantities $\bar{\theta}$ is defined by $\bar{\theta} \triangleq \frac{1}{N_s}\sum_{l=1}^{N_s}\theta_l$

We now evaluate the second expectation term $E[\mathbf{u}^T\mathbf{t}_i\mathbf{t}_i^T\mathbf{D}\mathbf{t}_q\mathbf{t}_q^T\mathbf{u}]$. Expressing the I and Q vectors $\mathbf{t}_i$ and $\mathbf{t}_q$ as follows

$$\mathbf{t}_i = \mathbf{t}_{11} + \mathbf{t}_{21} + \mathbf{z}_t \qquad \text{(E.5a)}$$

$$\mathbf{t}_q = \mathbf{t}_{12} + \mathbf{t}_{22} + \tilde{\mathbf{z}}_t \qquad \text{(E.5b)}$$

where the transformed vectors $\mathbf{t}_{11}$, $\mathbf{t}_{12}$, $\mathbf{t}_{21}$, $\mathbf{t}_{22}$, $\mathbf{z}_t$ and $\tilde{\mathbf{z}}_t$ correspond to the original vectors which consist of samples from their respective signals $x_{11}(t)$,

$x_{12}(t)$, $x_{21}(t)$, $x_{22}(t)$, $z(t)$ and $\tilde{z}(t)$ which are defined by

$$x_{11}(t) \triangleq \sum_{l=-\infty}^{\infty} a_l h(t-lT), \qquad x_{12} \triangleq -\sum_{l=-\infty}^{\infty} a_l \tilde{h}(t-lT)$$

$$x_{21}(t) \triangleq \sum_{l=-\infty}^{\infty} b_l \tilde{h}(t-lT), \qquad x_{22} \triangleq \sum_{l=-\infty}^{\infty} b_l h(t-lT)$$

and, $z(t)$ and $\tilde{z}(t)$ are the filtered I and Q noise components, which have been defined previously. Using (E.5), we can expand $\mathbf{t}_i\mathbf{t}_i^T$ and $\mathbf{t}_q\mathbf{t}_q^T$ in the following form

$$\begin{aligned}\mathbf{t}_i\mathbf{t}_i^T &= \mathbf{t}_{11}\mathbf{t}_{11}^T + \mathbf{t}_{11}\mathbf{t}_{21}^T + \mathbf{t}_{11}\mathbf{z}_t^T + \mathbf{t}_{21}\mathbf{t}_{11}^T + \mathbf{t}_{21}\mathbf{t}_{21}^T + \mathbf{t}_{21}\mathbf{z}_t^T \\ &\quad + \mathbf{z}_t\mathbf{t}_{11}^T + \mathbf{z}_t\mathbf{t}_{21}^T + \mathbf{z}_t\mathbf{z}_t^T \qquad \text{(E.6a)} \\ \mathbf{t}_q\mathbf{t}_q^T &= \mathbf{t}_{12}\mathbf{t}_{12}^T + \mathbf{t}_{12}\mathbf{t}_{22}^T + \mathbf{t}_{12}\tilde{\mathbf{z}}_t^T + \mathbf{t}_{22}\mathbf{t}_{12}^T + \mathbf{t}_{22}\mathbf{t}_{22}^T + \mathbf{t}_{22}\tilde{\mathbf{z}}_t^T \\ &\quad + \tilde{\mathbf{z}}_t\mathbf{t}_{21}^T + \tilde{\mathbf{z}}_t\mathbf{t}_{22}^T + \tilde{\mathbf{z}}_t\tilde{\mathbf{z}}_t^T \qquad \text{(E.6b)}\end{aligned}$$

Before expanding $E[\mathbf{t}_i\mathbf{t}_i^T\mathbf{D}\mathbf{t}_q\mathbf{t}_q^T]$, we consider the following two expressions.

First, consider

$$E[z(t)\tilde{z}(t+\tau)] = N_0 \int g_t(s)\tilde{g}_t(s-\tau)ds \qquad \text{(E.7)}$$

It can be seen that for $\tau = 0$, $E[z(t)\tilde{z}(t)] = 0$, which means that the diagonal elements in $E[\mathbf{z}\tilde{\mathbf{z}}^T] = 0$. Based on this observation, we can assume that compared with the other terms in (E.6), the contribution by $E[\mathbf{z}\tilde{\mathbf{z}}^T]$ is negligible, i.e.,

$$E[\mathbf{z}\tilde{\mathbf{z}}^T] \approx \mathbf{0} \qquad \text{(E.8)}$$

Second, consider the (m,n)th elements of $E[\mathbf{t}_{11}\tilde{\mathbf{t}}_{12}^T]$ which can be written as

$$E[\mathbf{t}_{11}\tilde{\mathbf{t}}_{12}^T][m,n] = \sigma^2 \sum_{l=-\infty}^{\infty} h(-mT_s - lT)\tilde{h}(-nT_s - lT) \qquad \text{(E.9)}$$

We assume that the transmission channel has a linear phase. For the UTP cables, this is a valid assumption as can be seen from the corresponding simplified channel model discussed in Chapter 3. Further, we assume that the optimum sampling phase which is absorbed into the channels, is such that for some integer k_s, $h(t - k_s T_s)$ is an even function of t and hence $\tilde{h}(t - k_s T_s)$ is an odd function of t. The validity of this assumption has been observed in our simulation studies. Under these assumptions, it is easily verified the diagonal terms of $E[\mathbf{t}_{11}\tilde{\mathbf{t}}_{12}^T]$ equal 0.

As for the non-diagonal elements of $E[\mathbf{t}_{11}\tilde{\mathbf{t}}_{12}^T]$, the overall contribution to $E[\mathbf{u}^T\mathbf{t}_i\mathbf{t}_i^T\mathbf{D}\mathbf{t}_q\mathbf{t}_q^T\mathbf{u}]$ is relatively small, compared to that from $E[\mathbf{t}_{11}\tilde{\mathbf{t}}_{11}^T]$, whose elements are given by

$$E[\mathbf{t}_{11}\tilde{\mathbf{t}}_{11}^T][m,n] = \sigma^2 \sum_l h(-mT_s - lT)h(-nT_s - lT) \tag{E.10}$$

In order to see this, using 100 m of UTP-3 cable we plot values of $E[\mathbf{t}_{11}\tilde{\mathbf{t}}_{12}^T][0,n]$ and $E[\mathbf{t}_{11}\tilde{\mathbf{t}}_{11}^T][0,n]$ for $0 \leq n \leq 30$ in Fig.E.1 where the horizontal axis corresponds to the index n. From the above discussions, we conclude that the contribution of $E[\mathbf{t}_{11}\tilde{\mathbf{t}}_{12}^T]$ is negligible, i.e.,

$$E[\mathbf{t}_{11}\tilde{\mathbf{t}}_{12}^T] \approx \mathbf{0} \tag{E.11}$$

Using IA, (E.8) and (E.11), it now follows that

$$E[\mathbf{t}_i\mathbf{t}_i^T\mathbf{D}\mathbf{t}_q\mathbf{t}_q^T] \approx \mathbf{D}^3 \tag{E.12}$$

Finally, substituting (E.4) and (E.12) into (E.3), we have

$$E\left[\mathbf{u}^T\mathbf{T}\mathbf{D}\mathbf{T}\mathbf{u}\right] \approx 2\varepsilon_{ex}(n)\theta_{rms}^2(N_s + \kappa_m + 1) \tag{E.13}$$

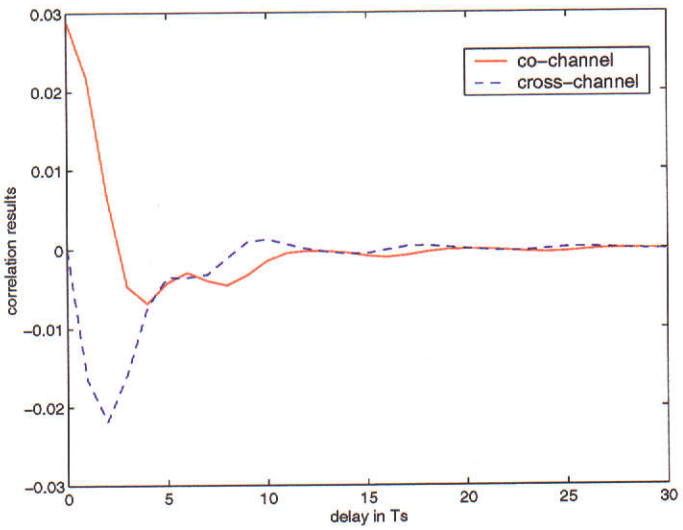

Figure E.1: Comparison of first row vectors in $E[\mathbf{t}_{11}\tilde{\mathbf{t}}_{11}^T]$ (co-channel) and $E[\mathbf{t}_{11}\tilde{\mathbf{t}}_{12}^T]$ (cross-channel)

and, summarising all the expectation terms on the RHS of (E.2), we have

$$\varepsilon_{ex}(n+1) \approx \varepsilon_{ex}(n)\left[1 - 4\mu_m\bar{\theta} + 2\mu_m^2\theta_{rms}^2(N_s + \kappa_m + 1)\right] + 2\mu_m^2\varepsilon_o \,\mathrm{tr}[\mathbf{D}^2] \quad \text{(E.14)}$$

REFERENCES

[1] ANSI Standard T.413, *Asymmetric Digital Subscriber Line Metallic Interface*, ANSI, 1995.

[2] Z. Papir and A. Simmonds, "Competing for throughput in the local loop," *IEEE Commun. Mag.*, pp. 61–66, May 1999.

[3] I. K. Czajkowski, "High-speed copper access: a tutorial overview," *Elect. & Commun. Eng. J.*, pp. 125–148, June 1999.

[4] T. Starr, J. Cioffi, and P. J. Silverman, *Understanding Digital Subscriber Line Technology*, Prentice Hall, 1999.

[5] E. A. Lee and D. G. Messerschmitt, *Digital Communication, 2nd ed.*, Kluwer Academic Publishers, 1994.

[6] D. D. Falconer, "Carrierless AM/PM," *Bell Lab. Internal Memorandum*, July 1975.

[7] N. A. Zervos and I. Kalet, "Optimized decision feedback equalization versus optimized orthogonal frequency division multiplexing for high-speed data transmission over the local cable network," *in Proc. IEEE ICC'89*, pp. 1080–1085, Sept. 1989.

[8] J. J. Werner, "Tutorial on carrierless AM/PM - Part I: Fundamentals of digital CAP transmitter," *ANSI X3T9.5 TP/PMD*, June 1992.

[9] J. J. Werner, "Tutorial on carrierless AM/PM - Part II: Performance of bandwidth efficient line codes," *ANSI X3T9.5 TP/PMD*, Feb. 1993.

[10] W. Y. Chen, G. H. Im, and J. J. Werner, "Design of digital carrierless AM/PM transceivers," *T1E1.4/92-149*, Aug. 1992.

[11] TIA/EIA-568-A Standard, *Commercial Building Telecommunications Cabling Standard*, 1994.

[12] G. H. Im, D. D. Harman, G. Huang, A. V. Mandzik, M.H. Nguyen, and J. J. Werner, "51.84 Mb/s 16-CAP ATM LAN standard," *IEEE J. Select. Areas in Commun.*, vol. 13, no. 4, pp. 620–632, May 1995.

[13] G. H. Im and J. J. Werner, "Bandwidth-efficient digital transmission over unshielded twisted-pair wiring," *IEEE J. Select. Areas in Commun.*, vol. 13, no. 9, pp. 1643–1655, Dec. 1995.

[14] V. Oksman and J. J. Werner, "Single-carrier modulation technology for very high-speed digital subscriber line," *IEEE Commun. Mag.*, pp. 82–89, May 2000.

[15] L. M. Garth, J. Yang, and J. J. Werner, "Blind equalization algorithms for dual-mode CAP-QAM reception," *IEEE Trans. Commun*, vol. 49, no. 3, pp. 455–466, Mar. 2001.

[16] I. L. Thng, A. Cantoni, and Y. H. Leung, "Low timing sensitivity receiver structure for cap," *IEEE Trans. Commun.*, vol. 48 no. 3, pp. 396–399, Mar. 2000.

[17] A. F. Shalash and K. K. Parhi, "Multidimensional carrierless AM/PM

systems for digital subscriber loops," *IEEE Trans. Commun.*, vol. 47, no. 11, pp. 1655–1667, Nov. 1999.

[18] X. Tang, I. L. Thng, and X. Li, "A new digital approach to design 3–D CAP waveforms," *IEEE Trans. Commun.*, vol. 51, no. 1, pp. 12–16, Jan. 2003.

[19] R. K. Brayton and et al, "A new algorithm for statistical circuit design based on quasinewton methods and function splitting," *IEEE Trans. Circuits Syst.*, vol. 26, pp. 784–794, Mar. 1979.

[20] J. G. Proakis, *Digital Communications*, McGraw-Hill, New York, 3rd ed., 1995.

[21] R. W. Lucky, J. Salz, and E. J. Weldon jr., *Principles of Data Communications*, McGraw-Hill, New York, 1968.

[22] A. Papoulis, *Signal Analysis*, McGraw-Hill, 1977.

[23] A. J. Viterbi, "Error bounds for convolutional codes and an asymptotically optimum decoding algorithm," *IEEE Trans. Inform. Theory*, vol. 13, pp. 260–269, Apr. 1967.

[24] R. Price, "Nonlearly feedback equalized PAM versus capacity for noisy filter channels," *Proc. Int. Conf. Commun.*, pp. 2212–2217, June 1972.

[25] G. D. Forney Jr. and M. V. Eyuboglu, "Combined equalization and coding using precoding," *IEEE Commun. Mag.*, pp. 25–34, Dec. 1991.

[26] G. D. Forney Jr. and G. Ungerboeck, "Modulation and coding for linear Gaussian channels," *IEEE Trans. on infor. theory*, vol. 44, No.6, pp.

2384–2415, Oct. 1998.

[27] J. M. Cioffi, G. P. Dudevoir, M. V. Eyuboglu, and G. D. Forney Jr., "MMSE decision-feedback equalizers and coding–part II: coding results," *IEEE Trans. Commun.*, vol. 43, no. 10, pp. 2595–2604, Oct. 1995.

[28] K. H. Mueller and J. J. Werner, "A hardware efficient passband equalizer structure for data transmission," *IEEE Trans. Commun.*, vol. 30, pp. 538–541, Mar. 1982.

[29] J. Gao and Y. H. Leung, "A new adaptive equalizer for carrierless amplitude and phase receivers," *Proc. IEEE ISCAS'99*, vol. 3, pp. 90–93, May 1999.

[30] S. U. H. Qureshi, "Adaptive equalization," *Proc. IEEE*, vol. 73, no. 9, pp. 1349–1387, Sept. 1985.

[31] J. Gao and Y. H. Leung, "Minimum mean-square performance analysis and calculations for carrierless AM/PM receiver using DFE in presence of data-like cross-talk signals," *Proc. IEEE ICC'2002*, vol. 1, pp. 69–73, Apr. 2002.

[32] J. Gao and Y. H. Leung, "Minimum mean-square performance analysis and calculations for carrierless AM/PM receiver using DFE in presence of data-like cross-talk signals," *IEEE Trans. Commun. submitted*, 2002.

[33] W. Y. Chen, *DSL Simulation Techniques and Standards Development for Digital Subscriber Line Systems*, Macmillan Technical Publishing, 1998.

[34] J. J. Werner, "The HDSL environment," *IEEE J. Select. Areas in Commun.*, vol. 9, no. 6, pp. 785–800, Aug. 1991.

[35] *ETSI TS101 135 HDSL standard*, ETSI, 2000.

[36] *Midrange Physical Layer Specification for Category 3 Unshielded Twisted Pair*, ATM Forum draft standard, 1994.

[37] W. A. Gardner, *Introduction to Random Processes with Applications to Signals and Systems*, McGraw-Hill, New York, 1990.

[38] K. Cho and D. Yoon, "On the general BER expression of one and two dimensional amplitude modulations," *IEEE Trans. Commun.*, vol. 50, No.7, pp. 1074–1080, 2002.

[39] C. E. Shannon, "A mathematical theory of communications," *Bell Sys. Tech. J.*, vol. 27, Part I, pp. 379-423, Part II, pp. 623-656, Oct. 1948.

[40] M. L. Honig, P. Crespo, and K. Steiglitz, "Suppression of near- and far-end crosstalk by linear pre- and post-filtering," *IEEE J. Select. Areas in Commun.*, vol. 10, no. 3, pp. 614–629, Apr. 1992.

[41] J. Salz, "Digital transmission over cross-coupled linear channels," *AT&T Tech. Journal*, vol. 64, no. 6, pp. 1147–1159, Jul-Aug 1985.

[42] J. Yang and S. Roy, "On joint transmit and receiver optimization for multiple-input-multiple-output (MIMO) transmission systems," *IEEE Trans. Commun.*, vol. 42, no. 12, pp. 3221–3231, Dec. 1994.

[43] J. Gao, "Minimum mean-square performance of linear carrierless AM/PM receiver in presence of data-like cross-talk signals," *Internal Report, ATRI,*

Curtin University of Technology, Jan. 2002.

[44] A. E. Danese, *Advanced Calculus - An Introduction to Applied Mathematics*, Allyn and Bacon, 1965.

[45] J. Gao, Y. H. Leung, and A. Cantoni, "Minimum mean square error receiver filters for carrierless amplitude and phase modulation," *Proc. IEEE ISCAS'2000*, vol. 4, pp. 629–932, May 2000.

[46] J. M. Cioffi, G. P. Dudevoir, M. V. Eyuboglu, and G. D. Forney Jr., "MMSE decision-feedback equalizers and coding–part I: Equalizer results," *IEEE Trans. Commun.*, vol. 43, no. 10, pp. 2582–2594, Oct. 1995.

[47] B. Widrow, *Adaptive Signal Processing*, Prentice Hall, 1985.

[48] A. Duel-Hallen, "A family of multiuser decision-feedback detectors for asynchronous code-division multiple-access channels," *IEEE Trans. Commun.*, vol. 43, No.2/3/4, pp. 421–434, Feb/Mar/Apr 1998.

[49] J. Yang and S. Roy, "Joint transmitter-receiver optimization for multi-input multi-output systems with decision feedback," *IEEE Trans. Infor. Theory*, vol. 40, No.5, pp. 1334–1347, Sept. 1994.

[50] C. Tidestav, A. Ahlen, and M. Sternad, "Realizable MIMO decision feedback equalizers: structure and design," *IEEE Trans. Sig. Process.*, vol. 49, No.1, pp. 121–133, Jan. 2001.

[51] N. Al-Dhahir and A. H. Sayed, "The finite-length multi-input multi-output MMSE-DFE," *IEEE Trans. Sig. Process.*, vol. 48, No.10, pp. 2921–2936, Oct. 2000.

[52] P. R. Motyka and J. A. Cadzow, "The factorization of discrete-process spectral matrices," *IEEE Trans. Automat. Control*, vol. 12, no. 6, pp. 698–707, Dec. 1976.

[53] D. N. P. Murthy, "Factorization of discrete-process spectral matrices," *IEEE Trans. Inform. Theory*, vol. 19, no. 5, pp. 693–696, Sept. 1973.

[54] D. D. Falconer and G. J. Foschini, "Theory of minimum mean-square-error QAM systems employing decision feedback equalization," *Bell Sys. Tech. J.*, vol. 52, no. 10, pp. 1821–1849, Dec. 1973.

[55] B. R. Petersen and D. D. Falconer, "Minimum mean square equalization in cyclostationary and stationary interference - analysis and subscriber line calculations," *IEEE J. Select. Areas in Commun.*, vol. 9 no. 6, pp. 931–940, Aug. 1991.

[56] S. Haykin, *Adaptive Filter Theory*, Prentice Hall International Inc., 3rd ed., 1996.

[57] R. D. Gitlin and S. B. Weinstein, "Fractionally-spaced equalization: An improved digital transversal equalizer," *Bell Sys. Tech. J.*, vol. 60, no. 2, pp. 275–296, Feb. 1981.

[58] G. A. Clark, S. K. Mitra, and S. R. Parker, "Block implementation of adaptive digital filters," *IEEE Trans. Acousts., Speech, Signal Processing*, vol. 20, pp. 744–752, June 1981.

[59] J. E. Mazo, "On the independence theory of equalizer convergence," *Bell Sys. Tech. J.*, vol. 58, pp. 963–993, May 1979.

[60] W. A. Gardner, "Learning characteristics of stochastic-gradient-descent algorithms: A general study, analysis, and critique," *Signal Processing*, vol. 6, pp. 113–133, 1984.

[61] S. Haykin, *Adaptive Filter Theory*, Prentice Hall International Inc., 4th ed., 2002.

[62] H. J. Butterweck, "The independence assumption: A dispensable tool in adptive filter theory," *Signal Processing*, vol. 57, no. 3, pp. 305–310, 1997.

[63] F. Y. Ling and S. U. H. Qureshi, "Convergence and stead-state behaviour of a phase-splitting fractionally spaced equalizer," *IEEE Trans. Commun.*, vol. 38, no. 4, pp. 418–425, Apr. 1990.